Angewandte Chemie
Eine Zeitschrift der Gesellschaft Deutscher Chemiker

Supporting Information

Progressive Endergonic Synthesis of Diels–Alder Adducts Driven by Chemical Energy

*S. Al Shehimy, H.-D. Le, S. Amano, S. Di Noja, L. Monari, G. Ragazzon**

Supporting information for:

Progressive endergonic synthesis of Diels-Alder adducts driven by chemical energy

Shaymaa Al Shehimy,[a] Hai-Dang Le,[a] Shuntaro Amano,[a] Simone Di Noja,[a] Luca Monari,[a] Giulio Ragazzon*[a]

[a] S. Al Shehimy, H. Le, S. Di Noja, S. Amano, L. Monari, G. Ragazzon
University of Strasbourg, CNRS, Institut de Science et d'Ingénierie Supramoléculaires (ISIS) UMR 7006
8 allée Gaspard Monge, 67000 Strasbourg, France
E-mail: ragazzon@unistra.fr

Table of contents

1. Materials and methods 3

a. Reagents and Instrumentation 3

2. Synthesis and characterization 4

a. Synthesis of 1b 4

b. Synthesis of 1c 4

c. Synthesis of 1d 5

d. Synthesis of 1e 5

e. Synthesis of 1f 6

f. Synthesis of 1g 6

g. Synthesis of carbamate 4 7

h. Synthesis of diisopropylurea (DIU) 7

3. NMR Spectra 8

4. Characterization of adducts 22

a. Assignment of exo/endo adducts 22

b. Characterization of adducts 3' and 3 23

c. Confirmation of species 3 characterization 44

5. Fueling experiments 45

a. Relation to theoretical frameworks 45

b. Experimental error 45

c. Equilibration of reaction I 45

d. Fueling with 3 equivalents of DIC over 1 cycle 46

e. Fueling with 3 equivalents of DIC over 2 cycles 46

f. Fueling with 3 equivalents of DIC over 3 cycles 48

g. Fueling with 3 equivalents of DIC at 25 mM 49

h. Limit of multiple fueling experiments 49

6. Effect of waste 50

a. Effect of waste accumulation on equilibrium 1 + 2 ↔ 3 50

b. Effect of waste accumulation on fueling 50

7. Effect of carbamate group on hydrolysis of 3' 52

8. Calculation of stored energy and thermodynamic efficiency 53

a. Fueling with 3 equiv. of DIC over 1 cycle 54

b. Fueling with 3 equivalents of DIC over 2 cycles 57

c. Fueling with 3 equivalents of DIC over 3 cycles 59

9. DFT calculations 61

10. References 67

11. Appendix – Coordinates of computed structures 68

1. Materials and methods

a. Reagents and Instrumentation

Unless otherwise stated, all chemicals and solvents were used as received from commercial sources. Furan derivatives **1a** and **1h** were purchased from Merck and Fisher, respectively. Organic solutions were concentrated under reduced pressure on a Buchi rotatory evaporator. Thin-layer chromatography (TLC) was performed on silica gel TLC Al foils with fluorescent indicator 254 nm (0.25 mm thick, 60 F254, Merck, Germany) and visualized using UV light (254 and 365 nm) and standard laboratory stains (e.g. Iodine). Column chromatography was carried out either on silica gel (Merck silica gel 60 0.040-0.063 mm) or on a Buchi Pure C-810 automated chromatography system with Flash cartridges (FlashPure EcoFlex 50 µm Silica irregular 4 to 25 g), with the indicated solvent system.

NMR (^{1}H, ^{19}F, ^{13}C) spectra were collected using Bruker 500MHz NMR (Magnet: Ascend; Console: Avance Neo; Probe: Cryo-Probe Prodigy X-^{1}H 5 mm with ^{31}P < X < ^{15}N) or Bruker 400MHz NMR (Magnet: Bruker UltraShield Plus; Console: Avance III – 400 MHz; Probe: Cryo-Probe Prodigy X-^{1}H 5 mm with ^{31}P < X < ^{15}N). Chemical shifts (δ) are expressed in ppm. The abbreviations used for the multiplicity of the NMR peaks are: **s** for singlet, bs for broad singlet, **d** for doublet, **t** for triplet, **q** for quartet, **p** for quintet, **h** for septet, and **m** for multiplet. ^{1}H NMR and ^{13}C NMR spectra were referenced vs residual solvent signals. ^{19}F NMR spectra were referenced vs 1,4-difluorobenzene in chloroform-*d* (-120.05 ppm).[1] Quantitative NMR data were integrated using Mestrenova or Topspin, and integration was done either manually or automatically relative to an internal standard. We observed some minor discrepancies between the data obtained using different methods. All the kinetic plots shown in the main text and SI are obtained using Mestrenova, while all the data reported in Section 8 and used for calculating energetic properties were obtained on Topspin. The discrepancies observed do not significantly influence any of the conclusions reported.

HRMS data were collected using Thermofisher Ultimate3000 HPLC with Thermofisher RP-MS coupled to a Thermofisher Vanquish PDA Detector and Thermofisher Orbitrap: exactive plus with extend mass range (source HESI II).

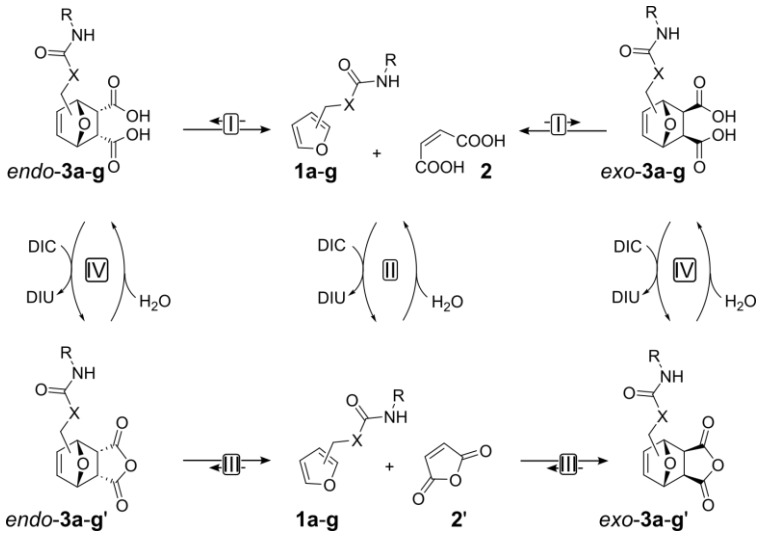

Figure S1. Reaction network studied in this work, with explicit indication of *endo* and *exo* adducts.

2. Synthesis and characterization

a. Synthesis of 1b

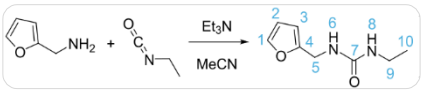

1.11 mL of 2-aminomethylfuran (furfurylamine, 12.6 mmol, 1 equiv.) and 3.84 mL of triethylamine (37.9 mmol, 3 equiv.) was added to 40 mL of anhydrous acetonitrile (CH_3CN anhydrous) in a round bottom flask connected to a condenser filled with argon. The whole solution is bubbled with argon while stirring for 15 minutes. 1.00 mL of ethyl isocyanate (12.6 mmol, 1 equiv.) is added to the mixture. The reaction is heated to 60 °C while stirring for 24 hours. After the reaction is completed, the solvent was removed under reduced pressure. The crude mixture is separated with flash column chromatography (SiO_2, cyclohexane:ethyl acetate 100:0 to 0:100 with small amount of triethylamine in the eluent). The product is obtained as a pale yellow solid (848 mg, 5 mmol, 40%).

^{1}H NMR (500 MHz, $CDCl_3$) δ (ppm): 7.33 (dd, *J* = 1.9, 0.9 Hz, 1H, 1), 6.30 (dd, *J* = 3.2, 1.9 Hz, 1H, 2), 6.21(m, 1H, 3), 4.74 (bs, 1H, 6), 4.45 (bs, 1H, 8), 4.36 (d, *J* = 5.6 Hz, 2H, 5), 3.20 (m, 2H, 9), 1.12 (t, *J* = 7.2 Hz, 3H, 10).

^{13}C NMR (126 MHz, $CDCl_3$) δ (ppm): 157.88 (s, 7), 152.58 (s, 4), 142.13 (s, 1), 110.54 (s, 2), 107.07 (s, 3), 37.65 (s, 5), 35.56 (s, 9), 15.54 (s, 10).

HRMS (ESI+) Calculated for $C_8H_{13}N_2O_2^+$, 169.0972, found 169.0967.

b. Synthesis of 1c

0.74 mL of furfurylamine (8.4 mmol, 1 equiv.) and 3.5 mL of triethylamine (25 mmol, 3 equiv.) were added to 70 mL of anhydrous acetonitrile in a round bottom flask connected to a

condenser filled with argon. The whole solution is bubbled with argon while stirring for 15 minutes. 1.3 mL of 3,5-bis(trifluroromethyl)phenyl isocyanate (7.5 mmol, 0.9 equiv.) are added to the mixture. The reaction is heated to 60 °C while stirring for 24 hours. After the reaction is completed, the solvent was removed under reduced pressure. The crude mixture is separated with flash column chromatography (SiO_2, cyclohexane:ethyl acetate 100:0 to 0:100 with small amount of triethylamine in the eluent). The product obtained is a pale yellow solid (148 mg, 5%).

^{1}H NMR (500 MHz, CD_3CN) δ (ppm): 8.00 (s, 2H, 10), 7.73 (bs, 1H, 8), 7.54 (m, 1H, 12), 7.42 (m, 1H, 1), 6.36 (m, 1H, 2), 6.26 (m, 1H, 3), 5.82 (bs, 1H, 7), 4.36 (d, *J* = 5.9, 2H, 5).

^{13}C NMR (126 MHz, CD_3CN) δ (ppm): 155.54 (s, 7), 153.85 (s, 4), 143.09 (s, 1), 142.94 (s, 9), 132.33 (q, $J^2_{C\text{-}F}$= 33.4 Hz, 11), 124.48 (q, $J^1_{C\text{-}F}$ = 274.3 Hz, 13), 118.87 (m, 12), 115.65 (p, J= 15.3 Hz, 12), 111.43 (s, 3), 107.73 (s, 2), 37,42 (s, 6).

^{19}F NMR (471 MHz, $CDCl_3$) δ (ppm): -63.43.

HRMS (ESI-) Calculated for $C_{14}H_9F_6N_2O_2^-$, 352.0574, found 352.0573.

c. Synthesis of 1d

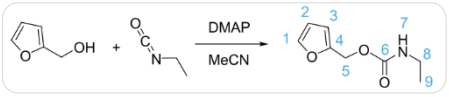

0.82 mL of 2-furanmethanol (furfuryl alcohol, 9.4 mmol, 1.5 equiv.) and 385 mg of *N*,*N*-dimethylaminopyridine (DMAP, 3.1 mmol, 0.5 equiv.) were added to 80 mL of anhydrous acetonitrile in a round bottom flask connected to a condenser filled with argon. The whole solution is bubbled with argon while stirring for 15 minutes. 0.5 mL of ethyl isocyanate (6.3 mmol, 1 equiv.) are added to the mixture. The reaction was stirred at room temperature for 24 hours. After the reaction is completed, the solvent was removed under reduced pressure. The crude mixture is separated with flash column chromatography (SiO_2, cyclohexane:ethyl acetate 90:10 to 0:100). The product obtained is a brown powder (178 mg, 13%).

^{1}H NMR (400 MHz, $CDCl_3$) δ (ppm): 7.40 (dd, *J* = 0.8, 1.8 Hz, 1H, 1), 6.39 (d, *J* = 3.2 Hz, 1H, 3), 6.34 (dd, *J* = 1.8, 3.2 Hz, 1H, 2), 5.04 (s, 2H, 5), 4.73 (bs, 1H, 7), 3.22 (p, *J* = 6.9 Hz, 2H, 8), 1.12 (p, *J* = 7.2 Hz, 3H, 9).

^{13}C NMR (ppm): (126 MHz, $CDCl_3$) δ (ppm): 156.00 (s, 6), 150.26 (s, 4), 143.28 (s, 1), 110.66 (s, 2), 110.40 (s, 3), 58.48 (s, 5), 36.07 (s, 8), 15.33 (s, 9).

HRMS (ESI+) calculated for $C_8H_{12}O_3N^+$, 170.0812, found 170.0808.

d. Synthesis of 1e

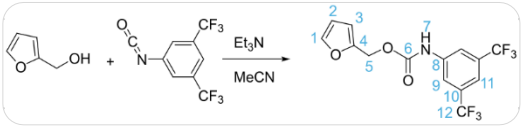

125 µL of 2-furanmethanol (1.44 mmol, 1 equiv.) and 600 µL of triethylamine (4.33 mmol, 3 equiv.) were added to 50 mL of anhydrous acetonitrile in a round bottom flask connected to a condenser filled with argon. The whole solution is bubbled with argon while stirring for 15 minutes. 250 µL of 3,5-bis(trifluroromethyl)phenyl isocyanate (1.44 mmol, 1 equiv.) are added to the mixture. The reaction is heated to 60 °C while stirring for 24 hours. After the reaction is completed, the solvent was removed under reduced pressure. The crude mixture is separated with flash

column chromatography (SiO_2, cyclohexane:ethyl acetate 100:0 to 0:100). The product is obtained as a yellowish white solid (183 mg, 1.44 mmol, 36%).

^{1}H NMR (500 MHz, $CDCl_3$) δ (ppm): 7.88 (s, 2H, 9), 7.56 (s, 1H, 11), 7.45 (dd, *J* = 1.9, 0.9 Hz, 1H, 1), 6.95 (s, 1H, 7), 6.49 (d, *J* = 3.3 Hz, 1H, 3), 6.39 (dd, *J* = 3.3, 1.9 Hz, 1H, 2), 5.19 (s, 2H, 5).

^{13}C NMR (126 MHz, $CDCl_3$) δ (ppm): 152.68 (s, 6), 149.02 (s, 4), 143.78 (s, 1), 139.36 (s, 8), 132.63 (q, $J^2_{C\text{-}F}$ = 33.5 Hz, 10), 124.26 (q, $J^1_{C\text{-}F}$ = 272.8 Hz, 12), 118.35 (bs, 9), 117.03 (m, 11), 111.41 (s, 3), 110.87 (s, 2), 59.39 (s, 5).

^{19}F NMR (471 MHz, $CDCl_3$) δ (ppm): -63.43.

HRMS (ESI-) Calculated for $C_{14}H_8F_6NO_3^-$, 352.0414, found 352.0414.

e. Synthesis of 1f

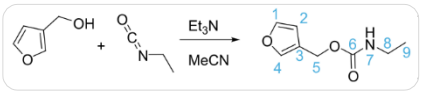

272 µL of 3-furanmethanol (3.10 mmol, 1 equiv.) and 1.3 mL of triethylamine (9.29 mmol, 3 equiv.) was added to 25 mL of anhydrous acetonitrile in a round bottom flask connected to a condenser filled with argon. The whole solution is bubbled with argon while stirring for 15 minutes. 250 µL of ethyl isocyanate (3.10 mmol, 1 equiv.) is added to the mixture. The reaction is heated to 60 °C while stirring for 24 hours. After the reaction is completed, the solvent was removed under reduced pressure. The crude mixture is separated with flash column chromatography (SiO_2, cyclohexane:ethyl acetate 100:0 to 0:100). The product is obtained as clear yellow liquid (465 mg, 2.70 mmol, 87%).

^{1}H NMR (500 MHz, CD_3CN) δ (ppm): 7.51 (bs, 1H, 4), 7.46 (t, *J* = 1.7 Hz, 1H, 1), 6.46 (bs, 1H, 2), 5.51 (bs, 1H, 7), 4.90 (s, 2H, 5), 3.10 (p, *J* = 6.25 Hz, 2H, 8), 1.06 (t, *J* = 7.5 Hz, 3H, 9).

^{13}C NMR (126 MHz, CD_3CN) δ (ppm): 157.16 (s, 6), 144.51 (s, 1), 142.38 (s, 4), 122.78 (s, 3), 111.54 (s, 2), 58.24 (s, 5), 36.38 (s, 8), 15.43 (s, 9).

HRMS (ESI+) Calculated for $C_8H_{12}NO_3^+$, 170.0812, found 170.0807.

f. Synthesis of 1g

0.2 mL of 3-furanmethanol (2.3 mmol, 1 equiv.) and 0.97 mL of triethylamine (6.9 mmol, 3 equiv.) was added to 40 mL of anhydrous acetonitrile in a round bottom flask connected to a condenser filled with argon. The whole solution is bubbled with argon while stirring for 15 min. 0.4 mL of 3,5-bis(trifluroromethyl)phenyl isocyanate (2.3 mmol, 1 equiv.) are added to the mixture. The reaction is heated to 60 °C while stirring for 24 hours. After the reaction is completed, the solvent was removed under reduced pressure. The crude mixture is separated with flash column chromatography (SiO_2, cyclohexane:ethyl acetate 100:0 to 0:100). The product is obtained as a yellowish white solid (500 mg, 1.4 mmol, 62%).

^{1}H NMR (500 MHz, $CDCl_3$) δ (ppm): 7.88 (bs, 2H, 9), 7.56 (bs, 1H, 11), 7.54 (m, 1H, 4), 7.43 (t, *J* = 1.7 Hz, 1H, 1), 6.92 (bs, 1H, 7), 6.48 (dd, *J* = 1.9, 0.8 Hz, 1H, 2), 5.11 (s, 2H, 5).

^{13}C NMR (126 MHz, $CDCl_3$) δ (ppm): 152.93 (s, 6), 143.83 (s, 1), 142.11 (s, 4), 139.44 (s, 3), 132.76 (q, $J^2_{C\text{-}F}$ = 33.6 Hz, 10), 123.19 (q, $J^1_{C\text{-}F}$ = 273.4 Hz, 12), 120.06 (s, 8), 118.33 (m, 9), 116.96 (m, 11), 110.65 (s, 2), 76.91 (s, 5).

^{19}F NMR (471 MHz, $CDCl_3$) δ (ppm): -63.43.

HRMS (ESI^-) Calculated for $C_{14}H_8F_6NO_3^-$, 352.0414, found 352.0412.

g. Synthesis of carbamate 4

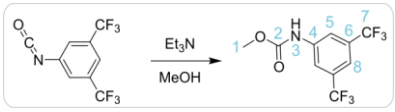

0.5 mL of 3,5-bis(trifluroromethyl)phenyl isocyanate (2.8 mmol, 1 equiv.) and 0.4 mL of triethylamine (2.8 mmol, 1 equiv.) were added to 6 mL of anhydrous methanol in a round bottom flask connected to a condenser filled with argon. The whole solution is bubbled with argon while stirring for 15 min. The reaction is then heated to 60 °C while stirring for 16 hours. After the reaction is completed, the solvent was removed under reduced pressure. The crude mixture is separated with flash column chromatography (SiO_2, cyclohexane:ethyl acetate 80:20). The product is obtained as a white crystalline powder (745 mg, 90%).

^{1}H NMR (500 MHz, CD_3CN) δ (ppm): 8.22 (bs, 1H, 3), 8.02 (bs, 2H, 5), 7.64 (bs, 1H, 8), 3.75 (s, 3H, 1).

^{13}C NMR (126 MHz, CD_3CN) δ (ppm): 154.99 (s, 2), 141.90 (s, 4), 132.56 (q, $J^2_{C\text{-}F}$ = 33.1 Hz, 7), 124.43 (q, $J^1_{C\text{-}F}$ = 271.5 Hz, 6), 119.02 (m, 4), 116.81 (m, 5), 53.24 (s, 1).

^{19}F NMR (471 MHz, CD_3CN) δ (ppm): -63.70.

HRMS (ESI^-) Calculated for $C_{10}H_7F_6NO_2^-$, 286.03082, found 286.03006.

h. Synthesis of diisopropylurea (DIU)

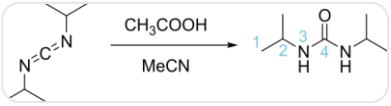

0.388 mL of diisopropylcarbodiimide **DIC** (3.2 mmol, 1 equiv.) were added to 10 mL of diethyl ether Et_2O in a round bottom flask. 0.375 mL of acetic acid (6.6 mmol, 2.6 equiv.) were added, and a white precipitate immediately formed. The reaction mixture is then stirred for 2 hours. The precipitate was eventually filtered and washed thoroughly with Et_2O, distilled water and Et_2O again. The filtrate was then dried under vacuum. It was obtained as a white crystalline powder (210 mg, 60%).

^{1}H NMR (500 MHz, CD_3CN) δ (ppm): 4.59z (bs, 2H, 3), 3.72(dh, 2H, *J*= 6.5 Hz, 1.4 Hz, 2), 1.05 (d, 12H, *J*= 6.5 Hz, 1).

^{13}C NMR (126 MHz, CD_3CN) δ (ppm): 158.01 (s, 4), 42.40 (s, 2), 23.49 (s, 1).

HRMS (ESI^+) Calculated for $C_7H_{17}N_2O^+$, 145.13354, found 145.13341.

3. NMR Spectra

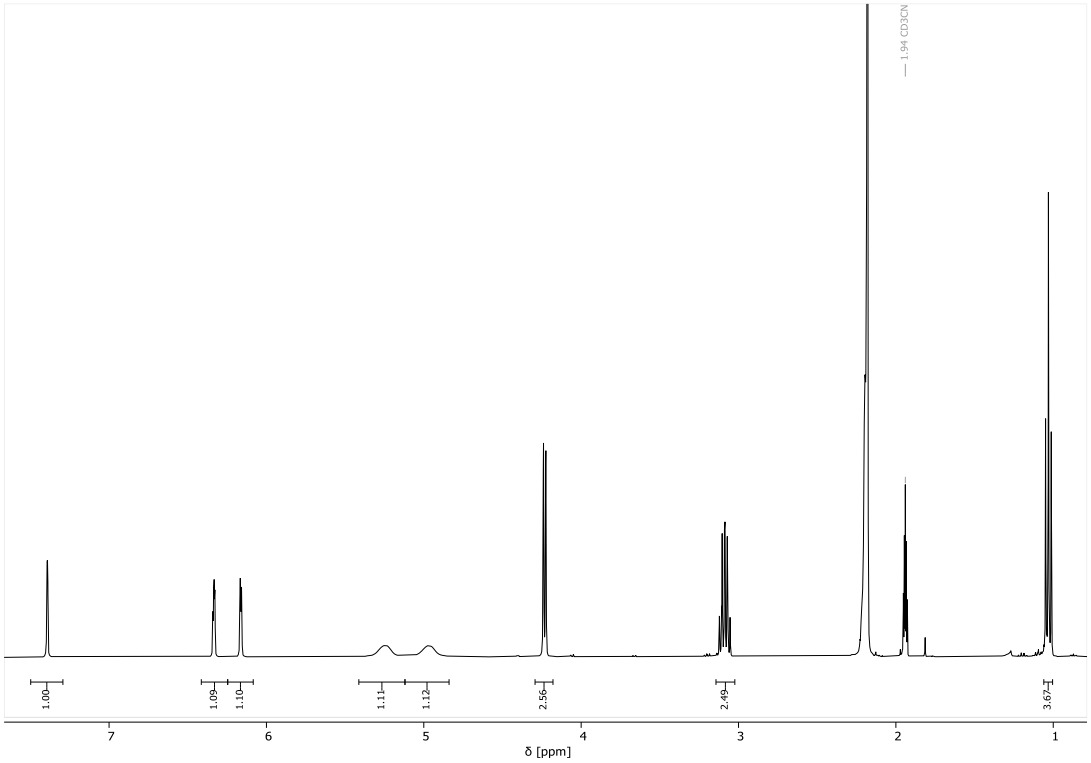

Figure S2. ^{1}H NMR (CD_3CN, 500 MHz) of **1b**.

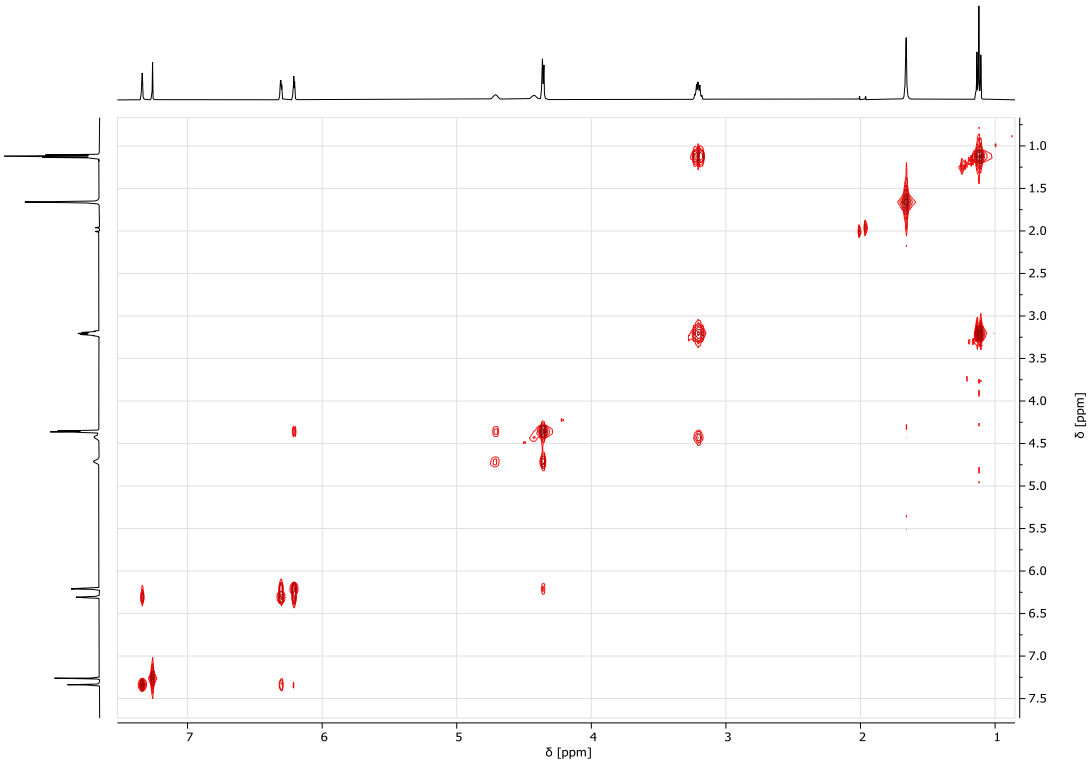

Figure S3. ^{1}H-^{1}H COSY NMR ($CDCl_3$, 500 MHz) of **1b**.

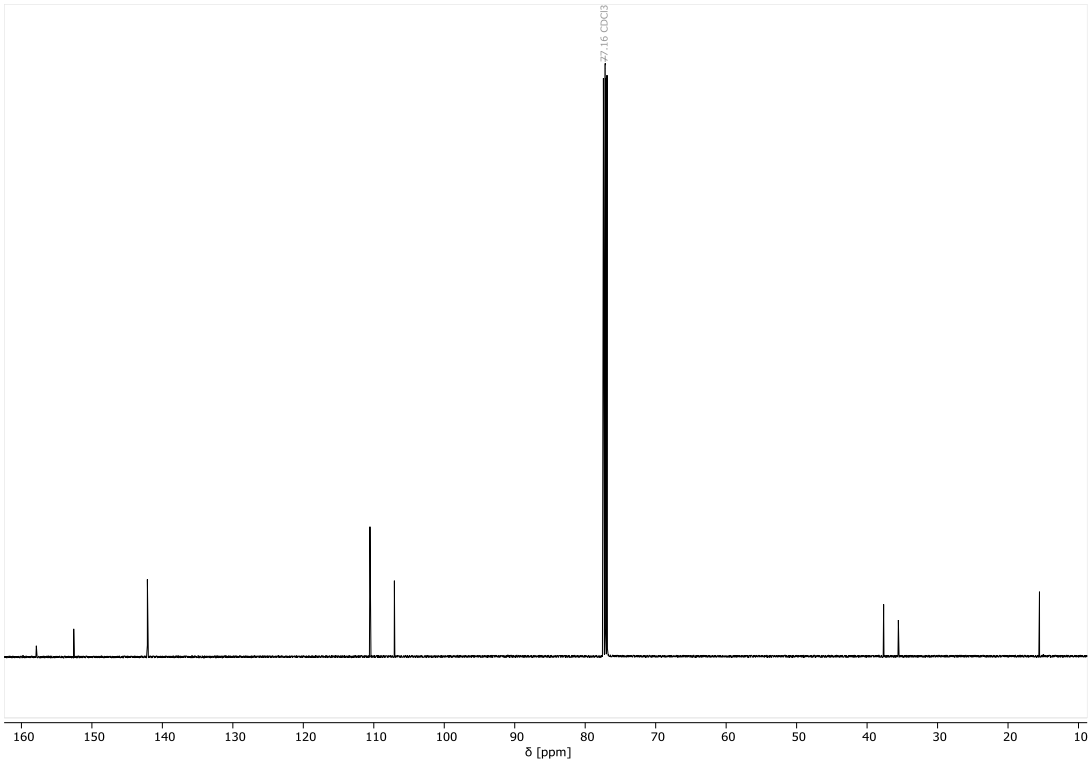

Figure S4. ^{13}C NMR ($CDCl_3$, 126 MHz) of **1b**.

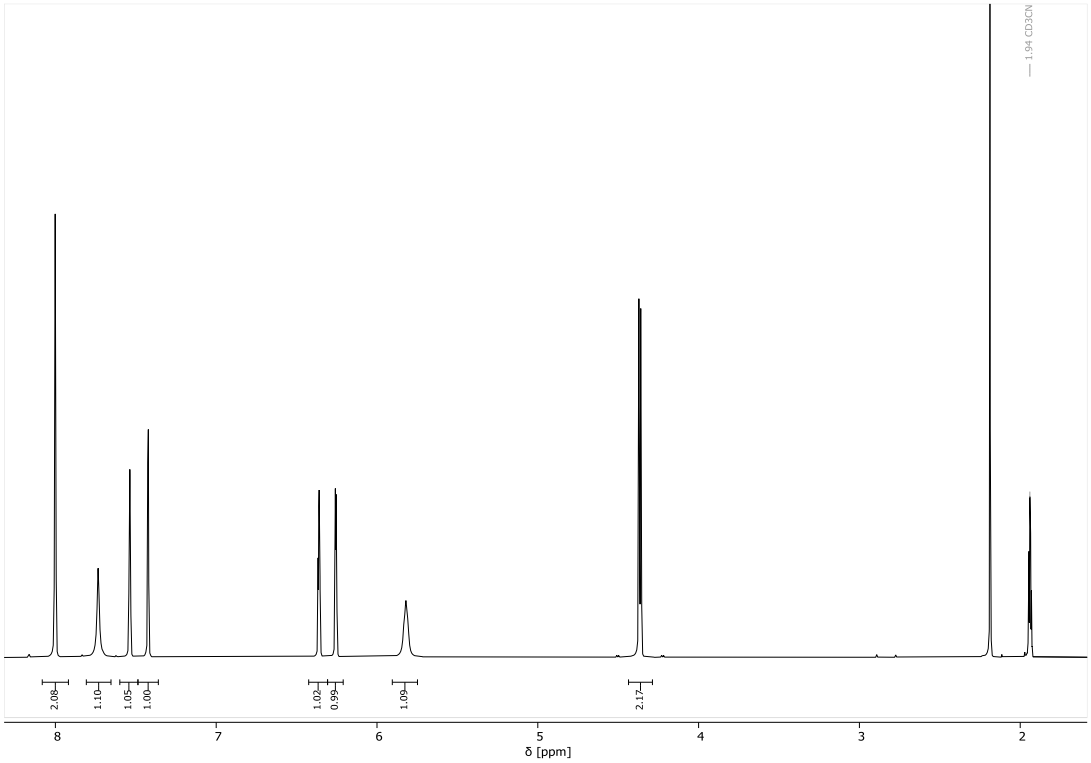

Figure S5. ^{1}H NMR (CD_3CN, 500 MHz) of **1c**.

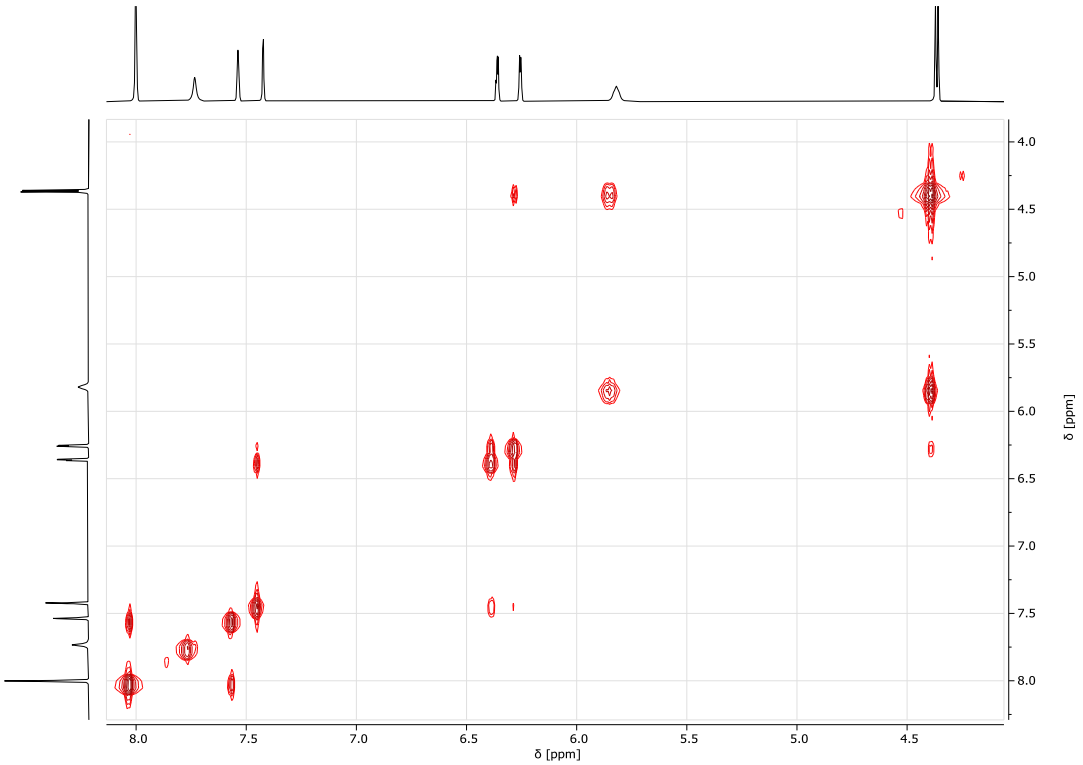

Figure S6. ^{1}H-^{1}H COSY NMR (CD_3CN, 500 MHz) of **1c**.

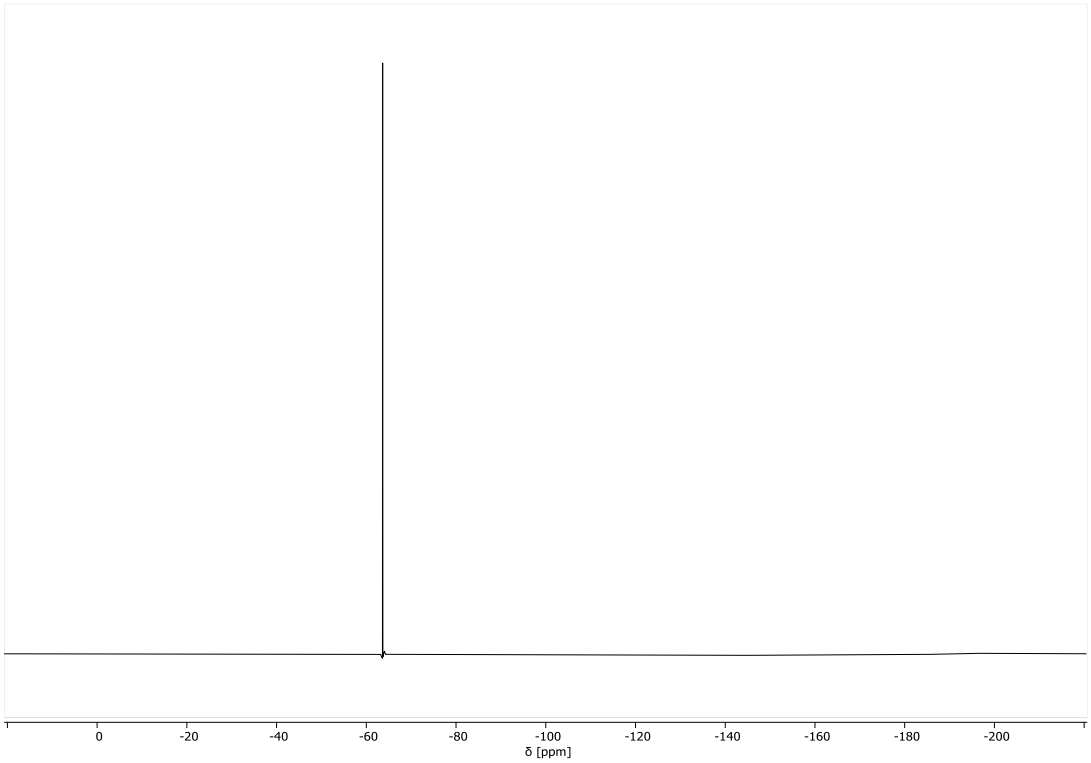

Figure S7. ^{19}F NMR (CD_3CN, 471 MHz) of **1c**.

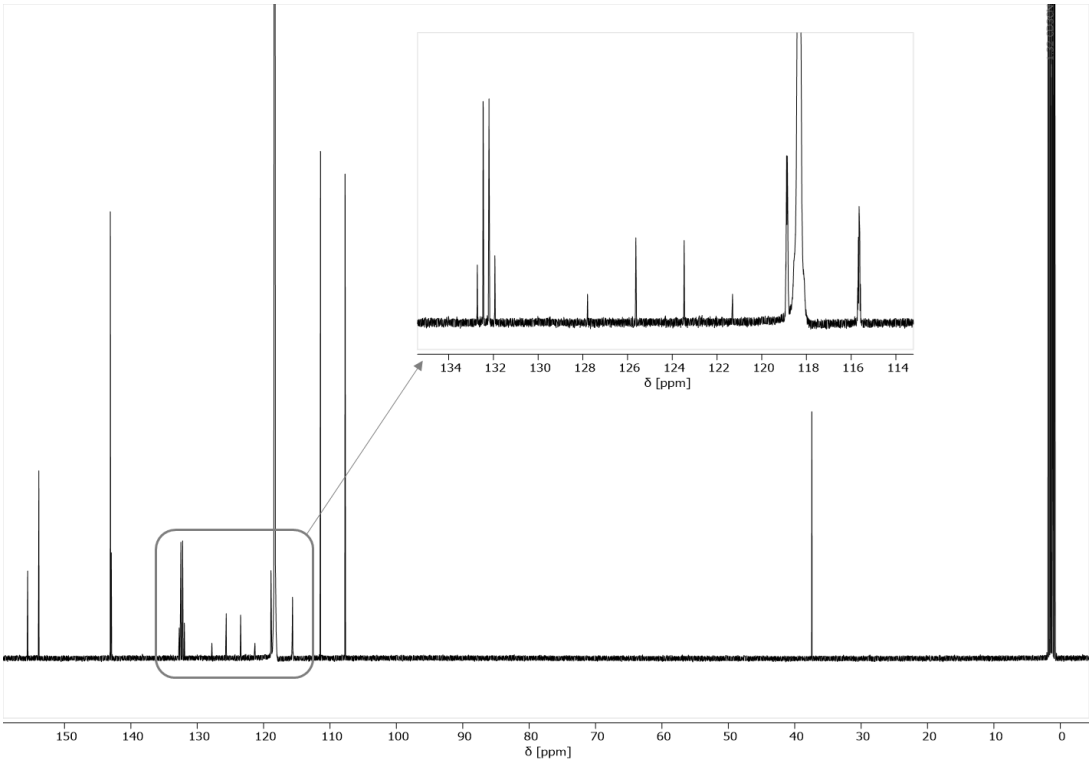

Figure S8. ^{13}C NMR (CD_3CN, 126 MHz) of **1c**.

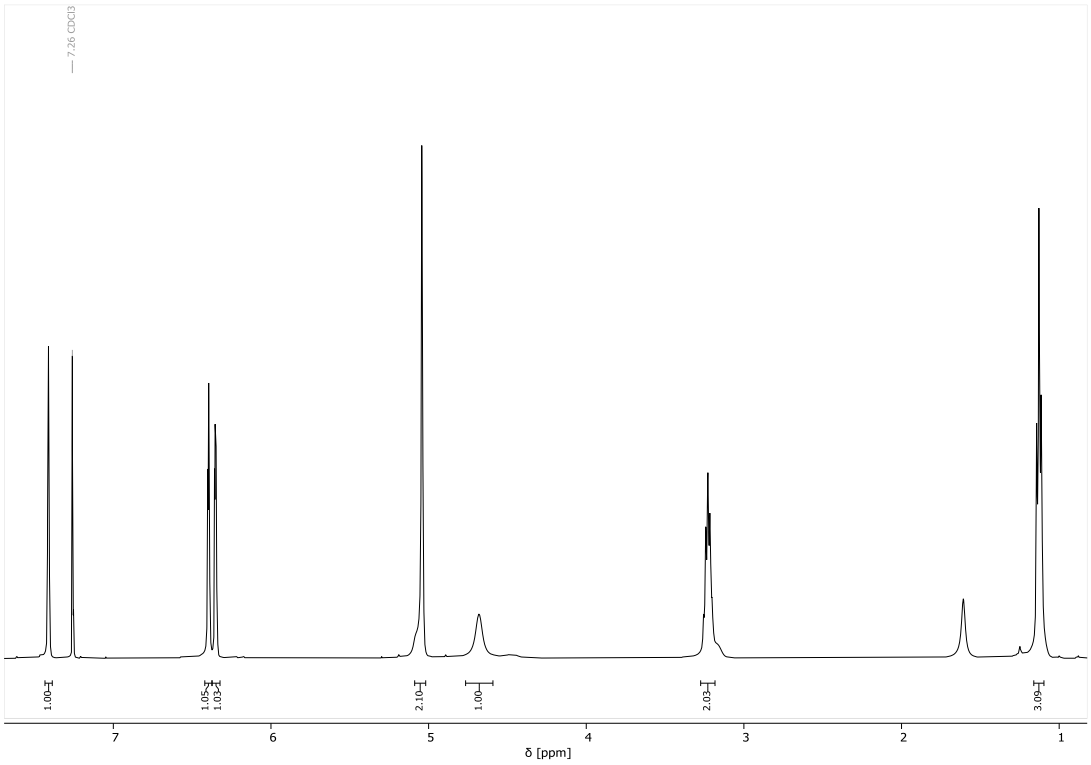

Figure S9. ^{1}H NMR ($CDCl_3$, 500 MHz) of **1d**.

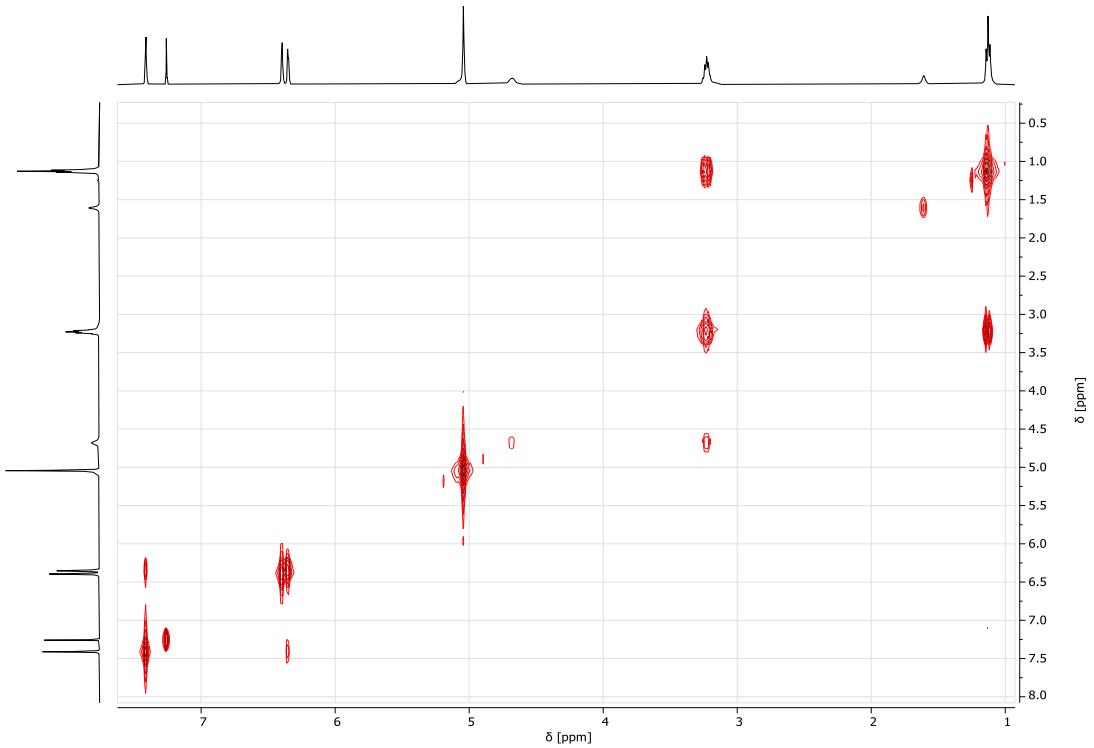

Figure S10. ^{1}H-^{1}H COSY NMR ($CDCl_3$, 500 MHz) of **1d**.

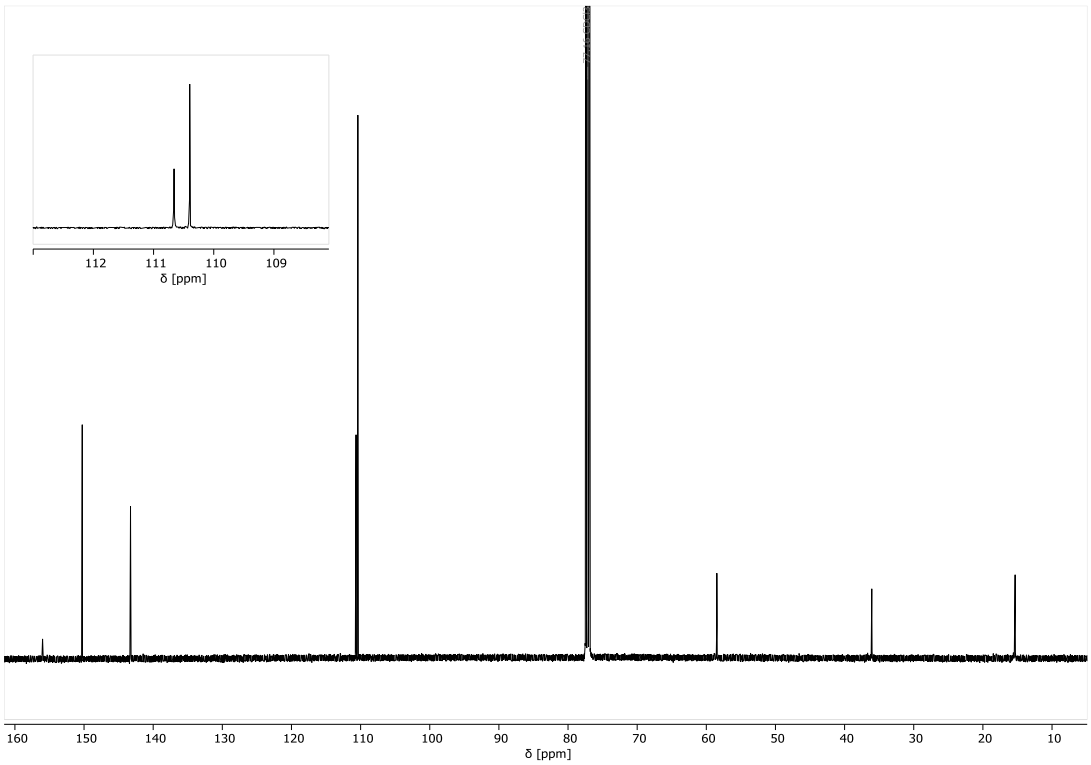

Figure S11. ^{13}C NMR ($CDCl_3$, 126 MHz) of **1d**.

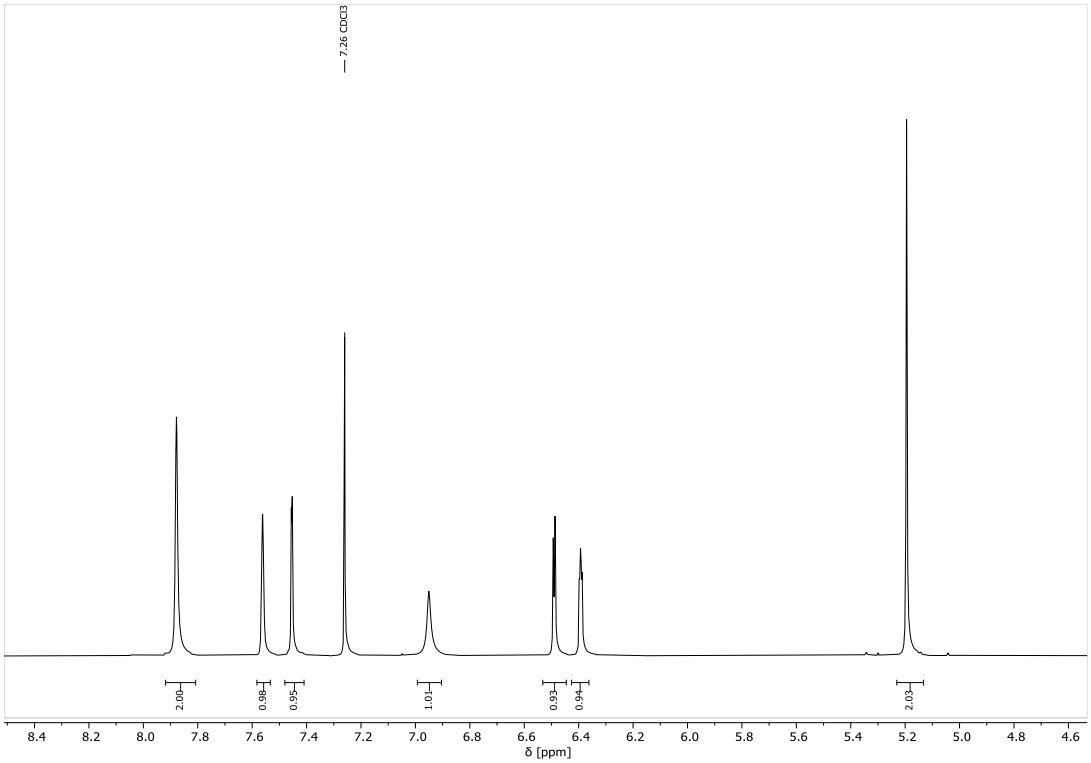

Figure S12. ^{1}H NMR ($CDCl_3$, 500 MHz) of **1e**.

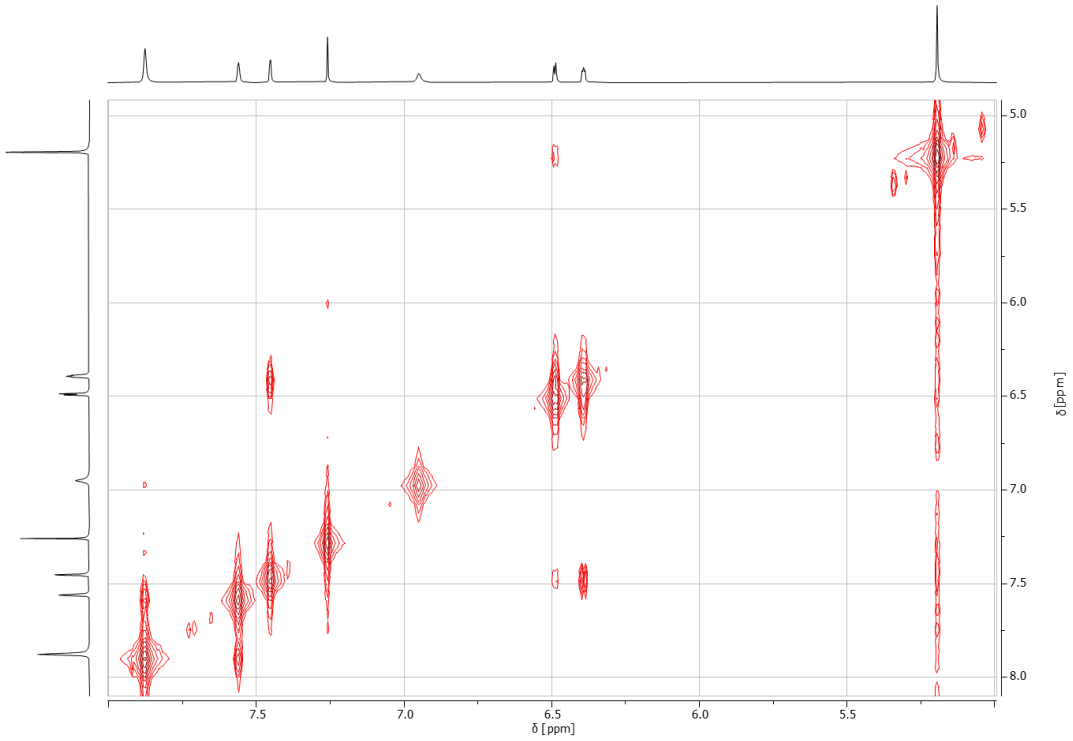

Figure S13. ^{1}H-^{1}H COSY NMR ($CDCl_3$, 500 MHz) of **1e**.

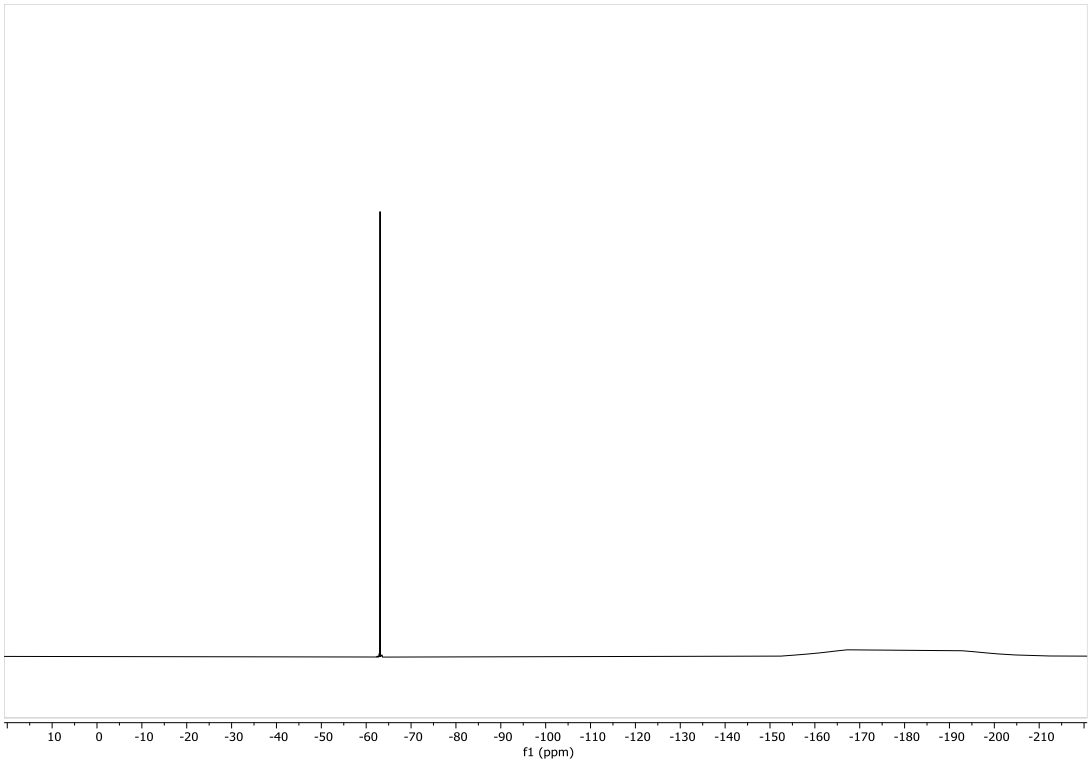

Figure S14. ^{19}F NMR ($CDCl_3$, 471 MHz) of **1e**.

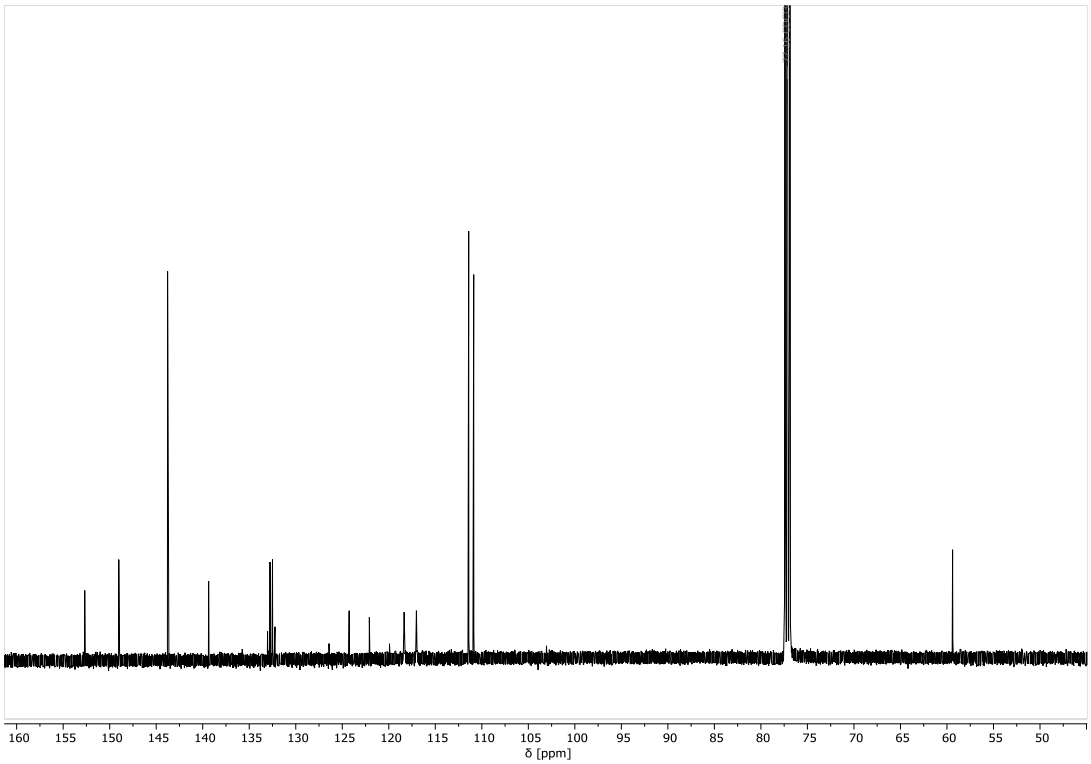

Figure S15. ^{13}C NMR ($CDCl_3$, 126 MHz) of **1e**.

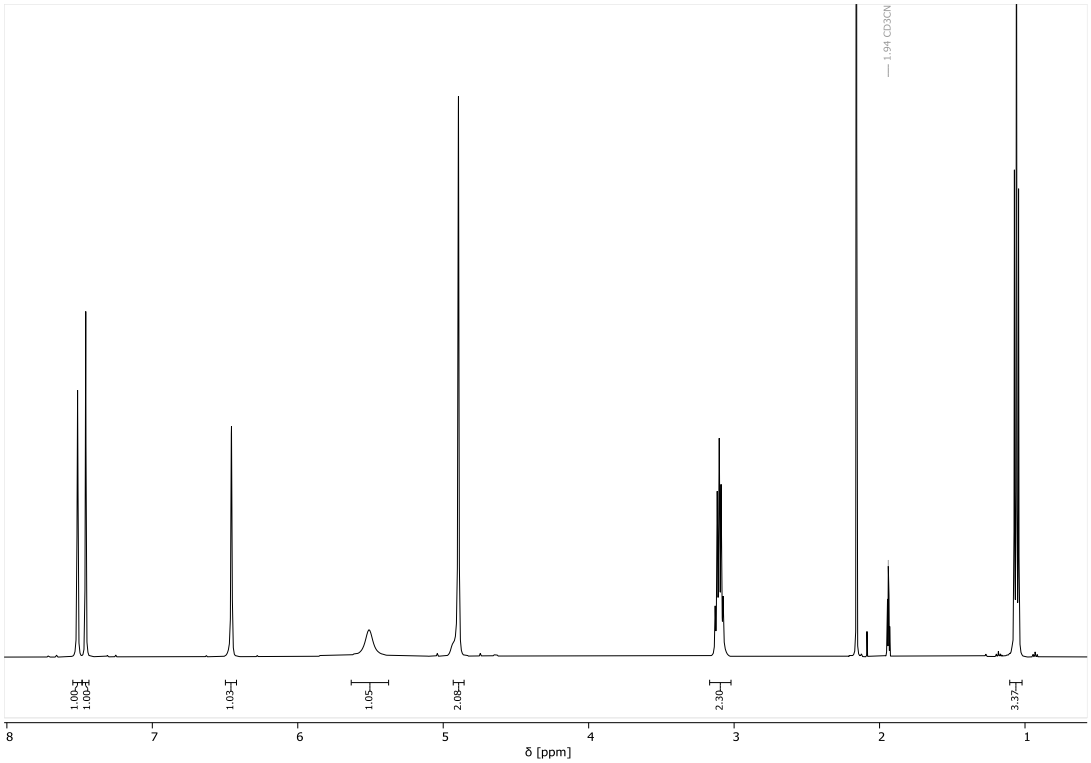

Figure S16. ^{1}H NMR (CD_3CN, 500 MHz) of **1f**.

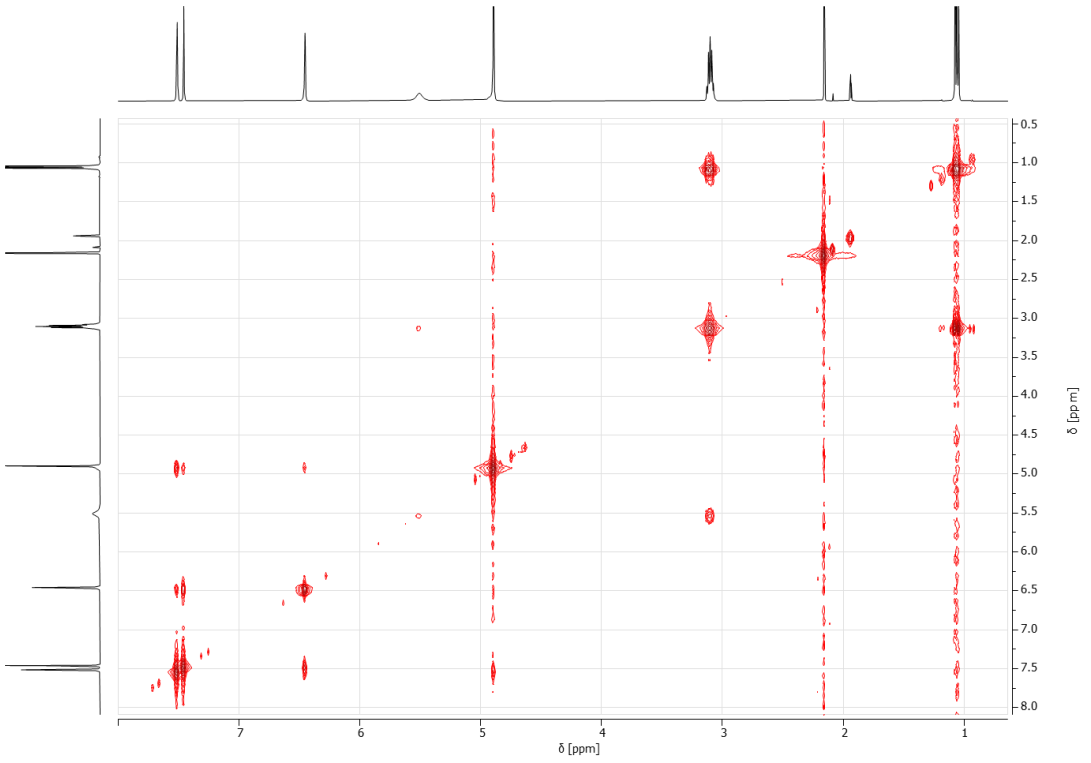

Figure S17. ^{1}H-^{1}H COSY NMR (CD_3CN, 500 MHz) of **1f**.

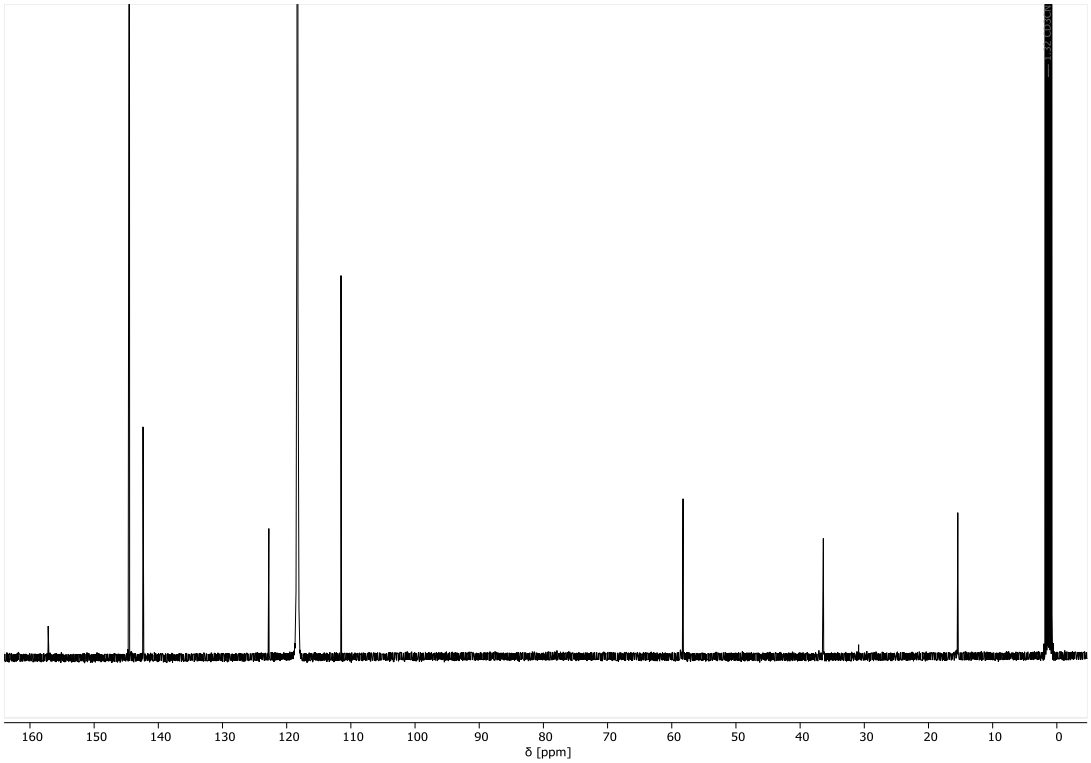

Figure S18. ^{13}C NMR (CD_3CN, 126 MHz) of **1f**.

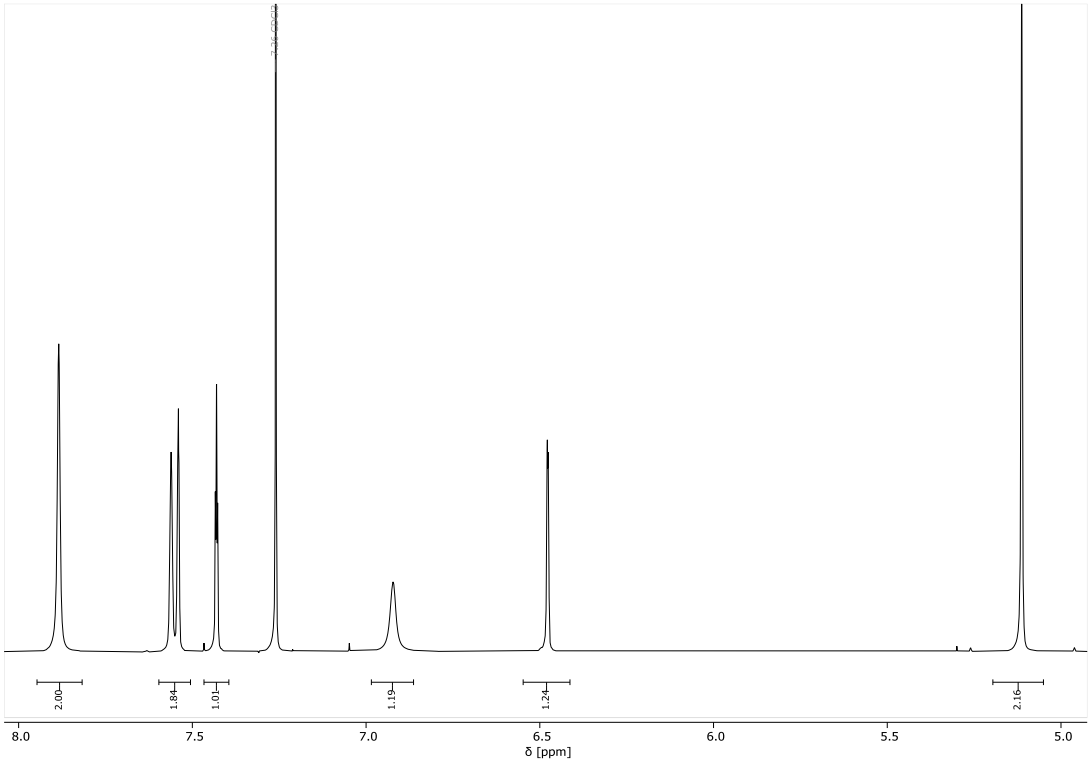

Figure S19. ^{1}H NMR ($CDCl_3$, 500 MHz) of **1g**.

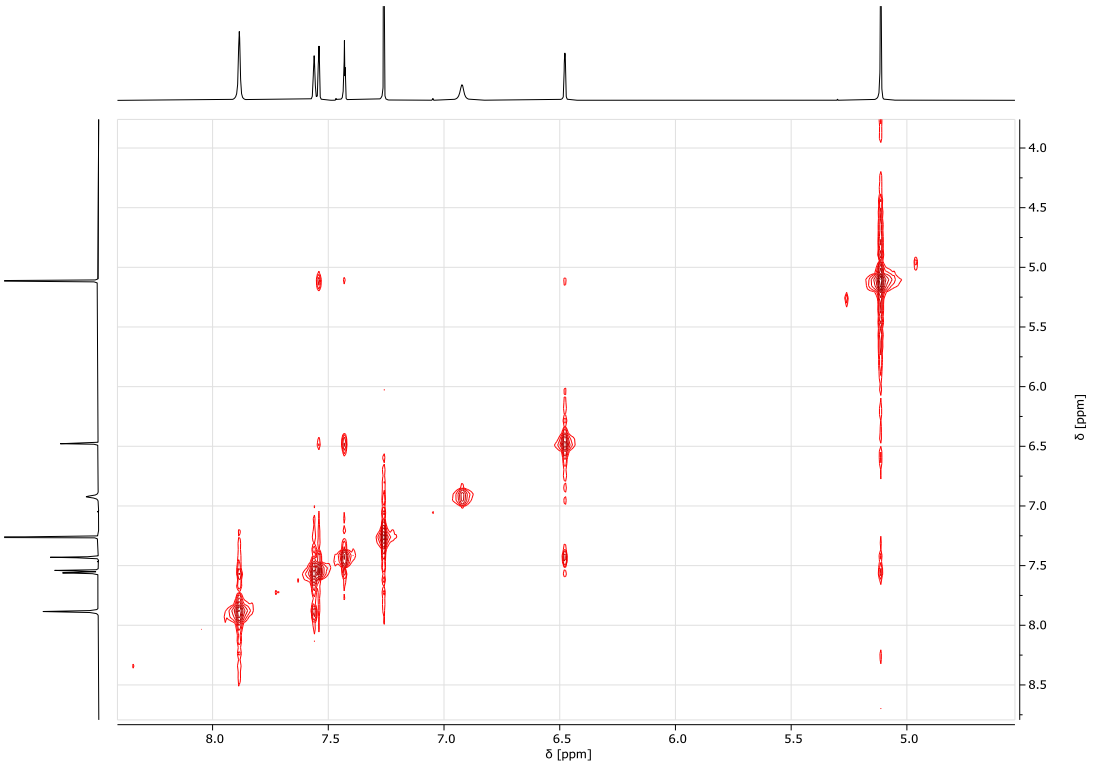

Figure S20. ^{1}H-^{1}H COSY NMR ($CDCl_3$, 500 MHz) of **1g**.

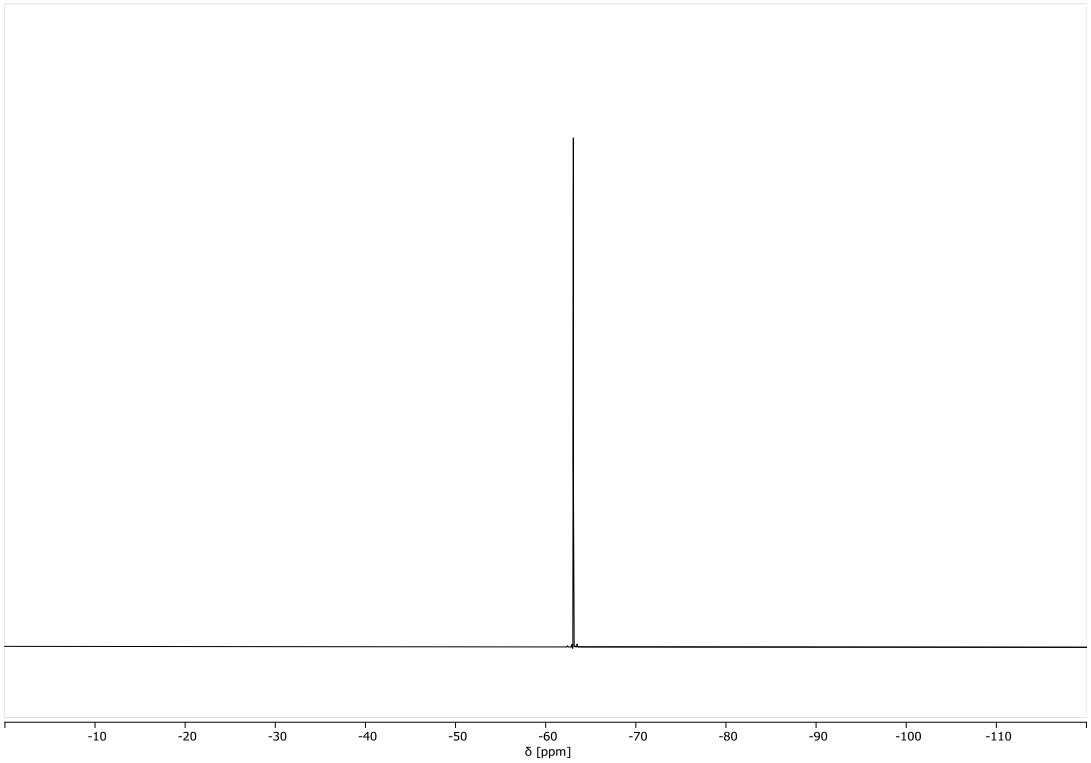

Figure S21. ^{19}F NMR ($CDCl_3$, 471 MHz) of **1g**.

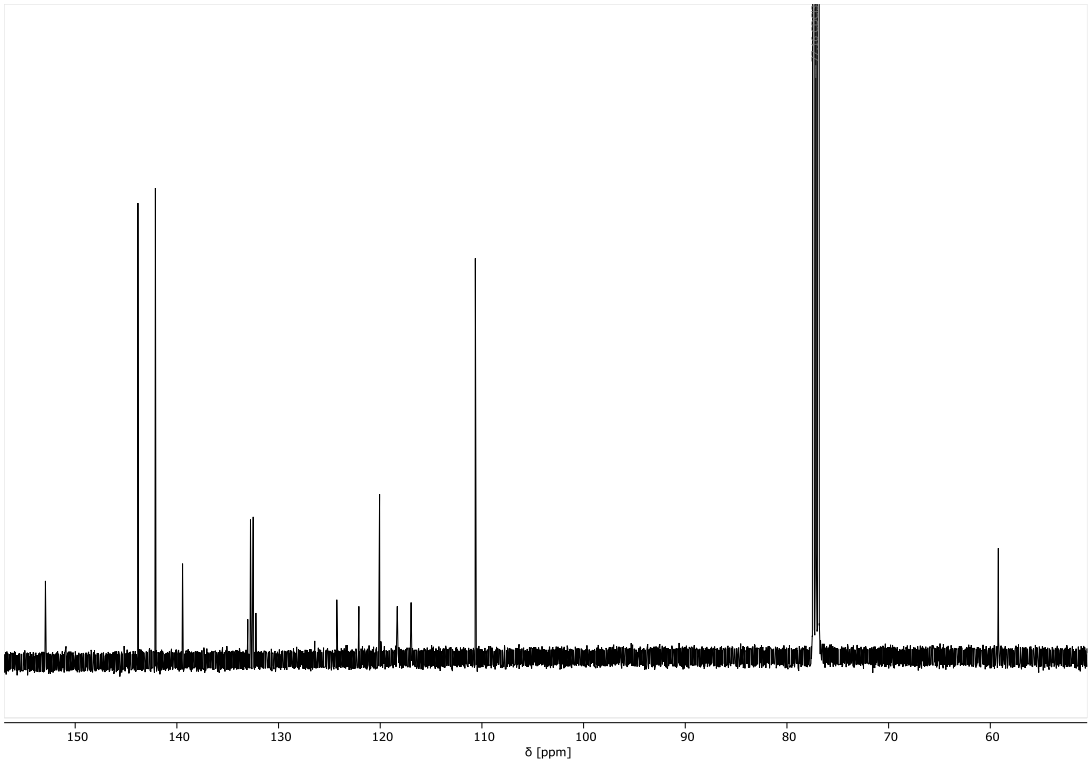

Figure S22. ^{13}C NMR ($CDCl_3$, 126 MHz) of **1g**.

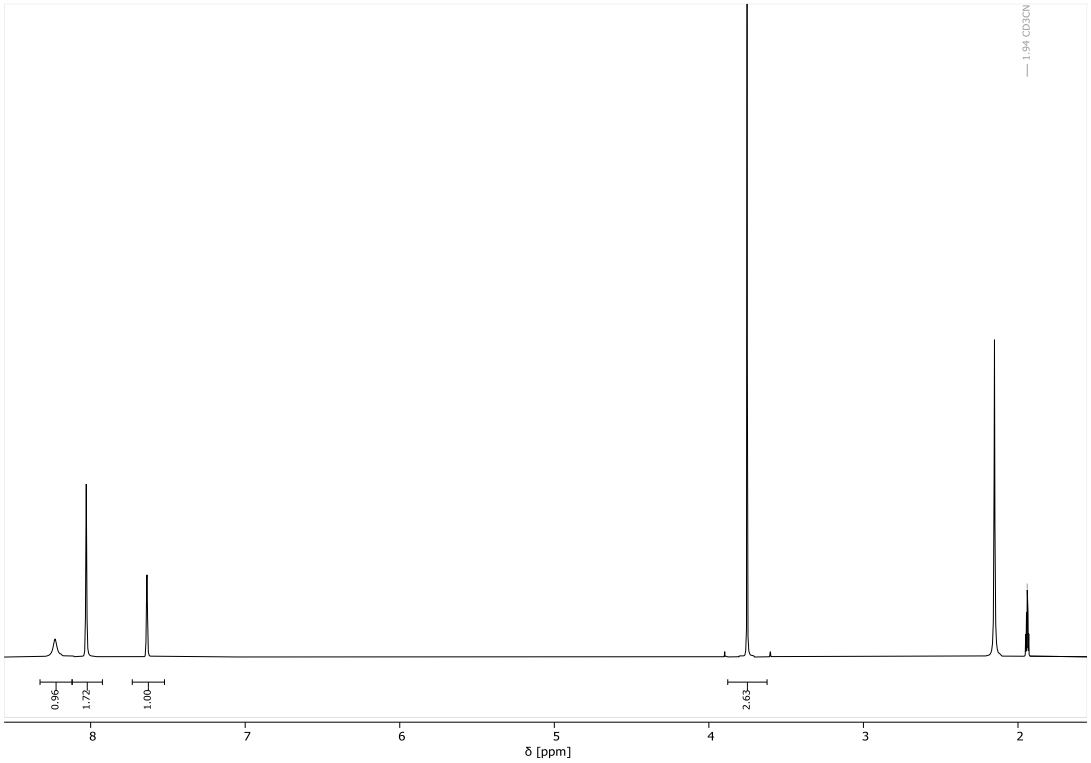

Figure S23. ^{1}H-NMR (CD_3CN, 500 MHz) of **4**.

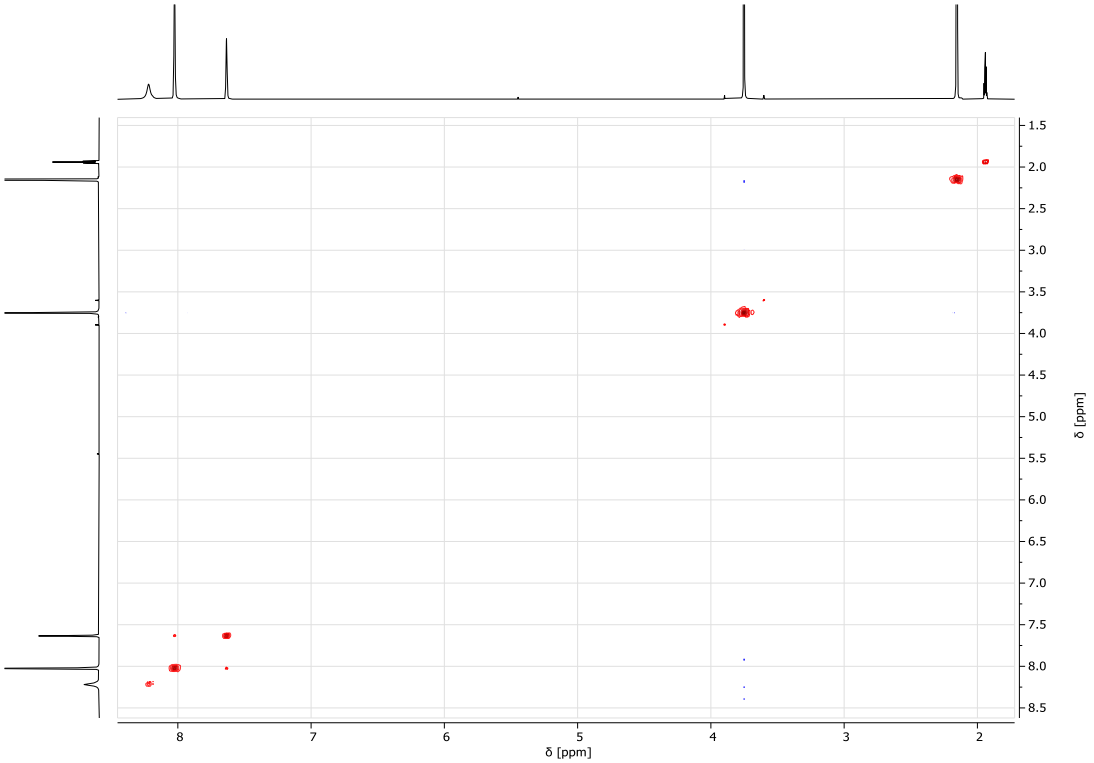

Figure S24. ^{1}H-^{1}H COSY NMR (CD_3CN, 500 MHz) of **4**.

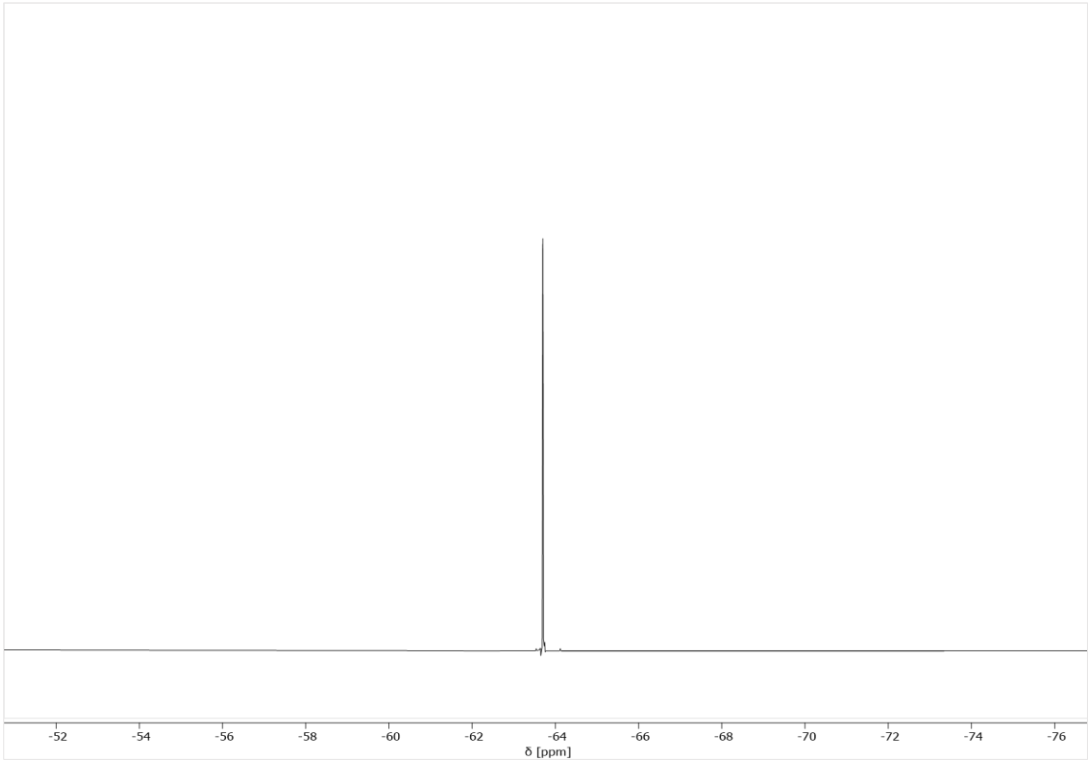

Figure S25. ^{19}F NMR (CD_3CN, 471 MHz) of **4**.

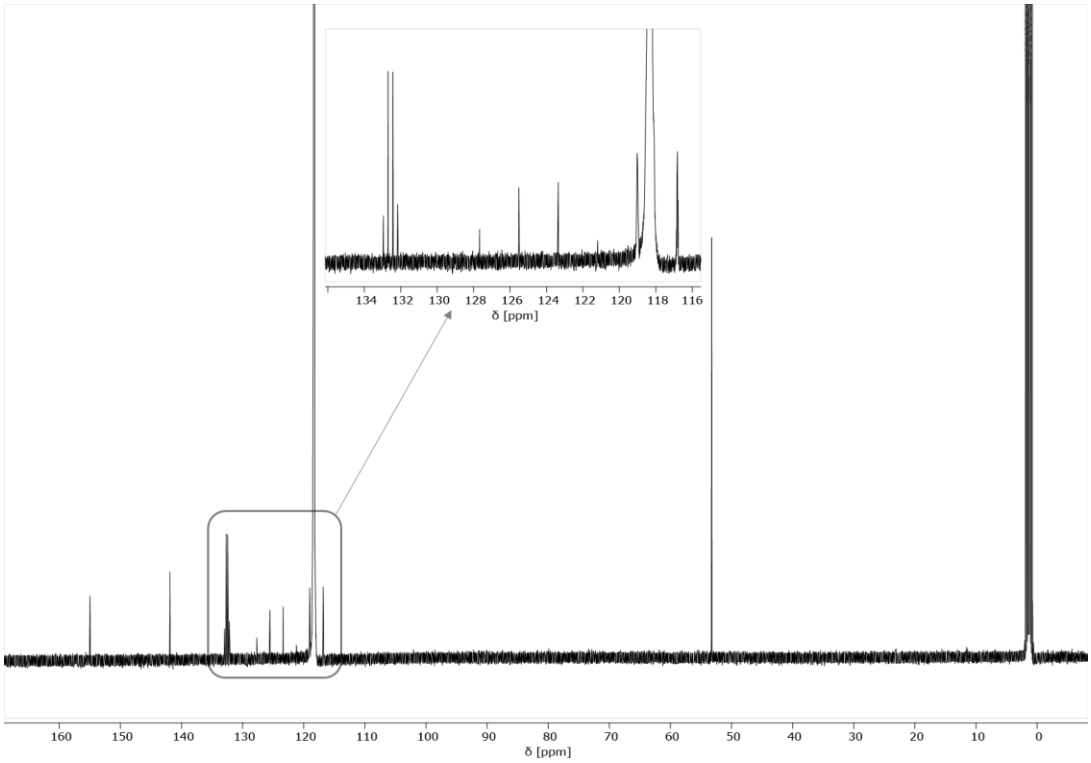

Figure S26. ^{13}C NMR (CD_3CN, 126 MHz) of **4**.

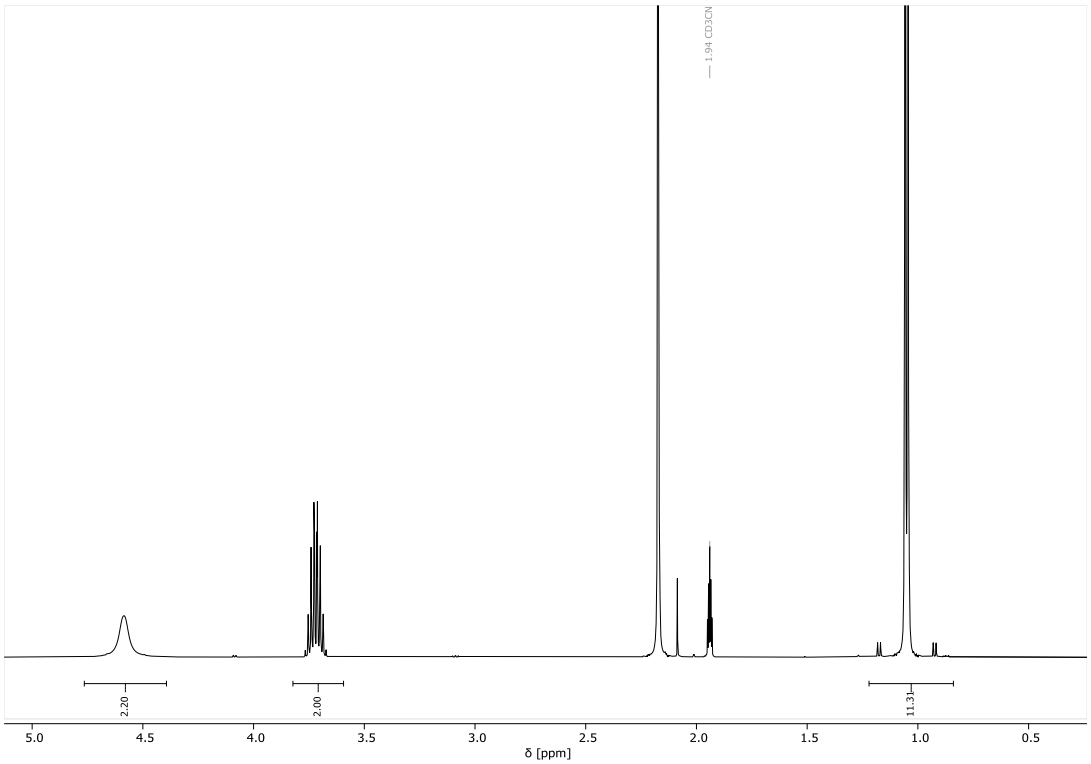

Figure S27. ^{1}H-NMR (CD_3CN, 500 MHz) of **DIU**.

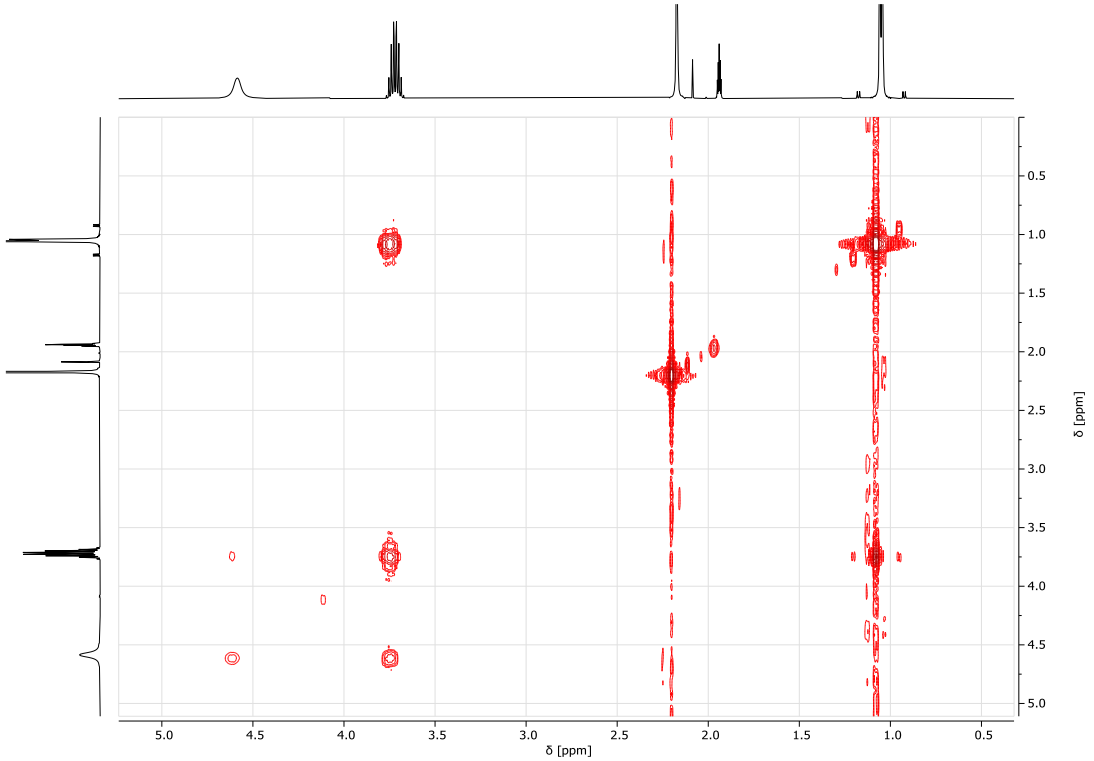

Figure S28. ^{1}H-^{1}H COSY NMR (CD_3CN, 500 MHz) of **DIU**.

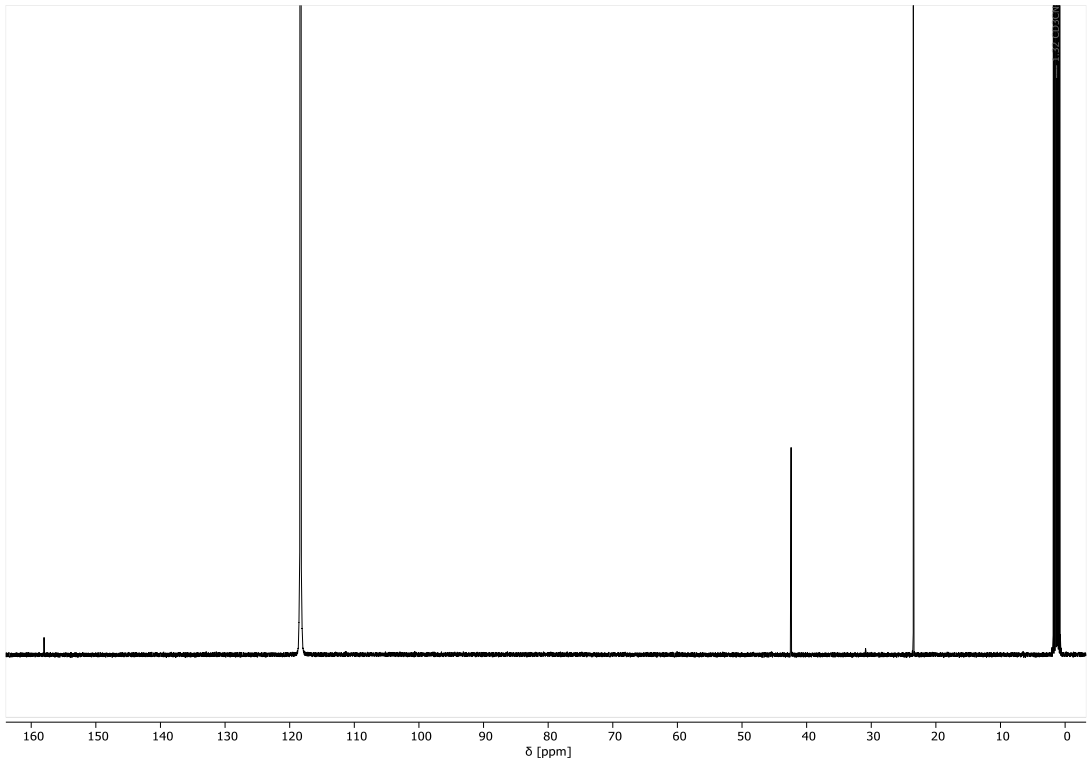

Figure S29. ^{13}C-NMR (CD_3CN, 126 MHz) of **DIU**.

4. Characterization of adducts

a. Assignment of *exo*/endo adducts

The *exo*/*endo* stereoselectivity of the studied Diels-Alder equilibria have been assigned using NMR coupling experiments (COSY) following the Karplus Equation. Complementary quantum mechanical calculations were performed on **3d'** and **3f'** as model compounds to estimate the diagnostic dihedral angles and corresponding coupling constants of their *exo*/*endo* adducts.

The calculation was done in Spartan'20 under gas phase conditions. We first screened conformers with molecular mechanics calculation (MMFF) and optimized the structures of remaining conformers with the Hartree-Fock method calculation (HF/3-21G). These geometries were further subjected to the DFT calculation (ωB97X-D/6-31G*) to compute the total energy, and only the conformers with sufficiently low energy (up to 10 kJ/mol from the lowest energy conformer) were kept. After further geometry optimization (ωB97X-D/6-31G*), the coupling constants were calculated (ωB97X-D/6-31G*). XYZ coordinates for all structures are listed in the Appendix.

The reported structures (Figure S30) are the ones of the lowest energy conformers, but the diagnostic dihedral angles (H_2-H_3, H_1-H_4) were not significantly different between conformers.

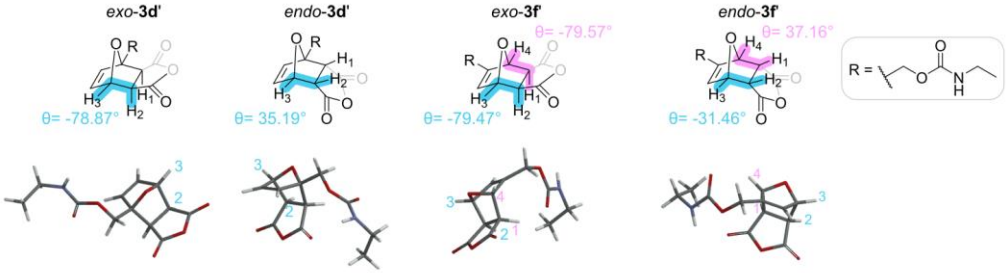

Figure S30. The calculated H_2-H_3 and/or H_1-H_4 dihedral angles of *exo* and *endo* isomers of **3d'** and **3f'** adducts (top) and their corresponding minimized energy structures (bottom). For clarity, the molecular structures of **3d'** represent the enantiomers of calculated structures. Numbers in proximity of H atoms are intended to label each atom.

Calculated coupling constants:

exo-**3d'**: $J_{H2\text{-}H3}$ = 0.5 Hz

endo-**3d'**: $J_{H2\text{-}H3}$ = 7.4-7.7 Hz (depending on the conformers)

exo-**3f'**: $J_{H1\text{-}H4}$ = $J_{H2\text{-}H3}$ = 0.5 Hz

endo-**3f'**: $J_{H1\text{-}H4}$ = 7.0-7.3 Hz, $J_{H2\text{-}H3}$ = 7.9-8.1 Hz (depending on the conformers)

Experimentally, the equilibrium reaction (**III**) between **1d** and **2'** yields both isomers with a ratio of 17:1. The major isomer has been assigned to the *exo*-**3d'** since no coupling was observed between H_3 and H_2. The minor isomer was assigned to *endo*-**3d'**, as the coupling constant between H_3 and H_2 was 5.9 Hz, close to the theoretical value of 7.4-7.7 Hz. The equilibrium reaction **III** between **1f** and **2'** yields only one isomer which was assigned to *exo*-**3f'** since no coupling was observed between H_3 and H_2, in line with the theoretical value of 0.5 Hz. The same strategy was used for the *exo* and *endo* assignment of other derivatives.

b. Characterization of adducts 3' and 3

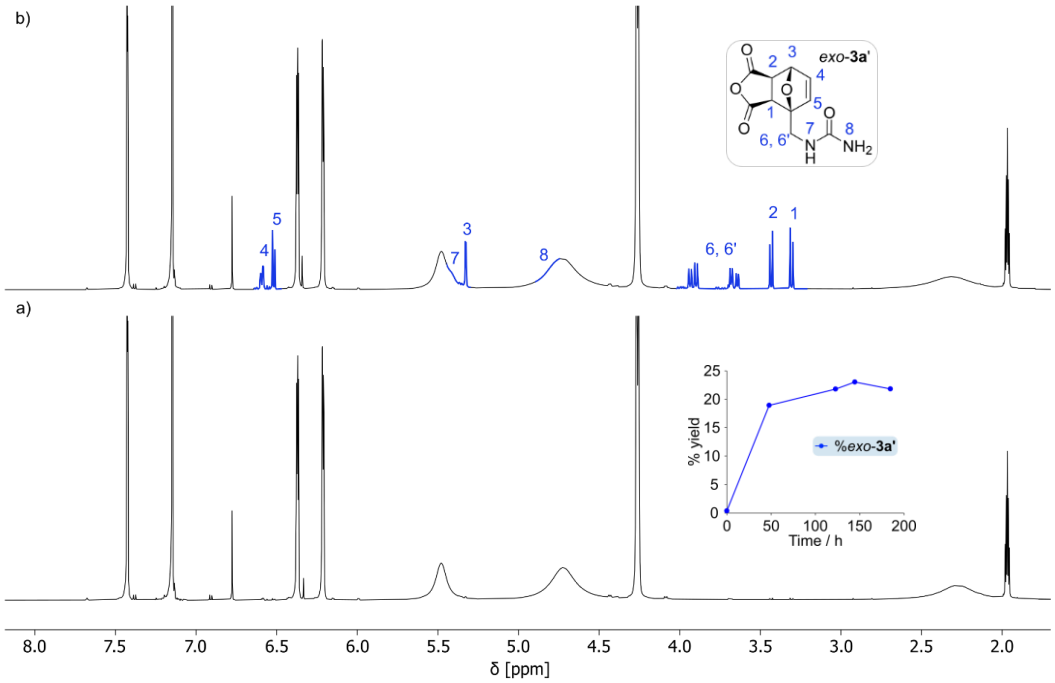

Figure S31. ^{1}H NMR spectra (CD_3CN, 400 MHz) showing the a) start and b) end points of the equilibrium **1a** + **2**' ↔ **3a**' reacted at 40°C, 100 mM of both components. *Inset*: variation of the % yield of adduct *exo*-**3a**' monitored until equilibrium is reached.

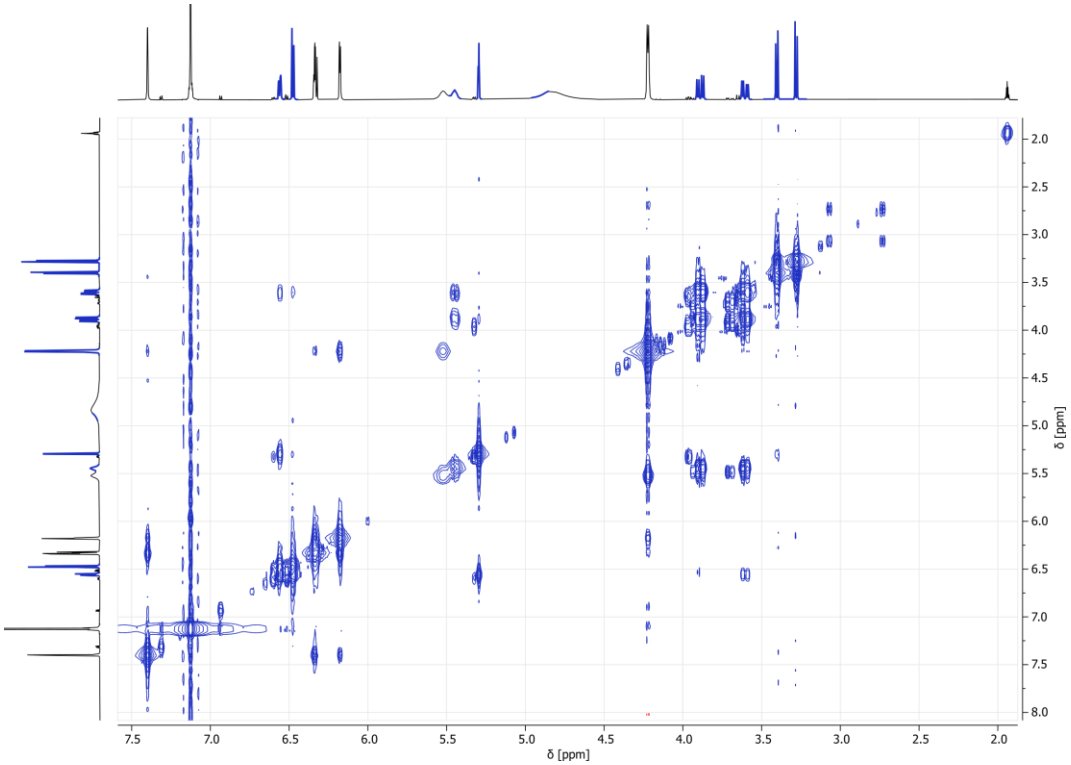

Figure S32. ^{1}H-^{1}H COSY NMR spectrum (CD_3CN, 500 MHz) of the equilibrium **1a**+ **2**' ↔ **3a**', 100 mM of **1a** and 200 mM of **2**'.

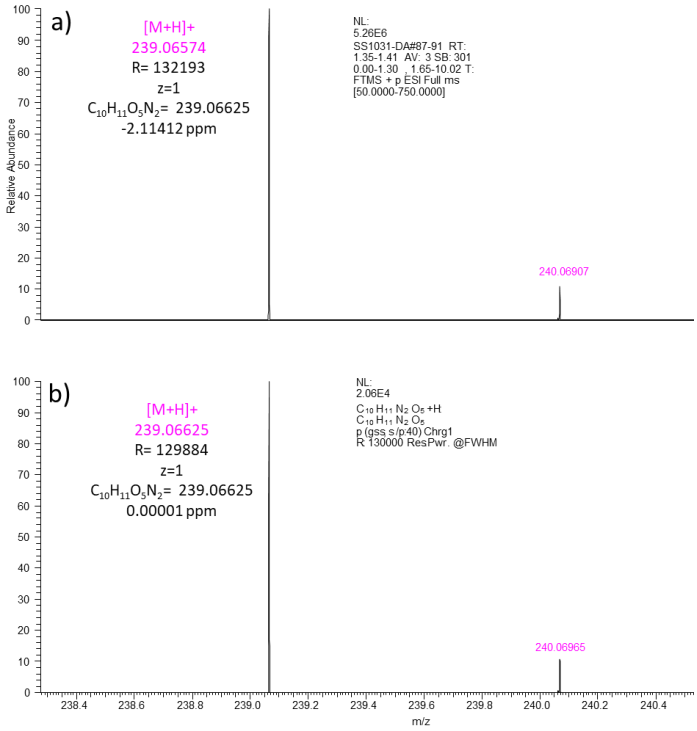

Figure S33. a) Experimental and b) calculated HRMS spectra of **3a**'. The experimental spectrum was obtained after equilibrating a mixture of **1a** and **2**' in CD_3CN.

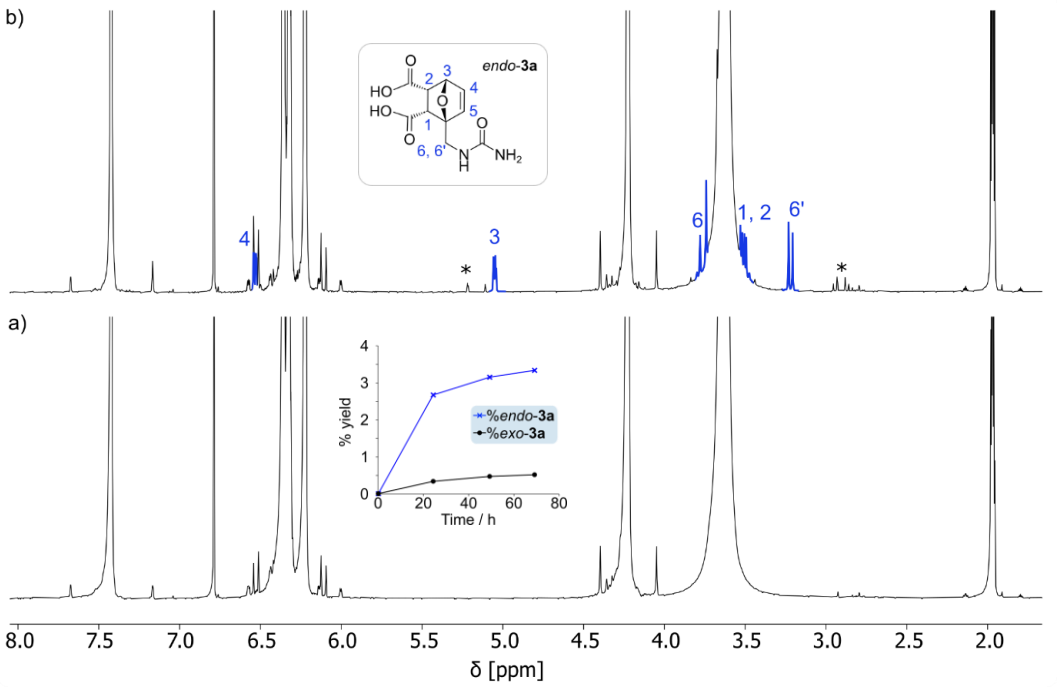

Figure S34. ^1H NMR spectra (CD_3CN:D_2O (85:15), 400 MHz) showing the a) start and b) end points of the equilibrium **1a** + **2** ↔ **3a** reacted at 40°C, 100 mM of both components. *Inset*: variation of the % yield of adducts *exo- /endo*-**3a** monitored in time.

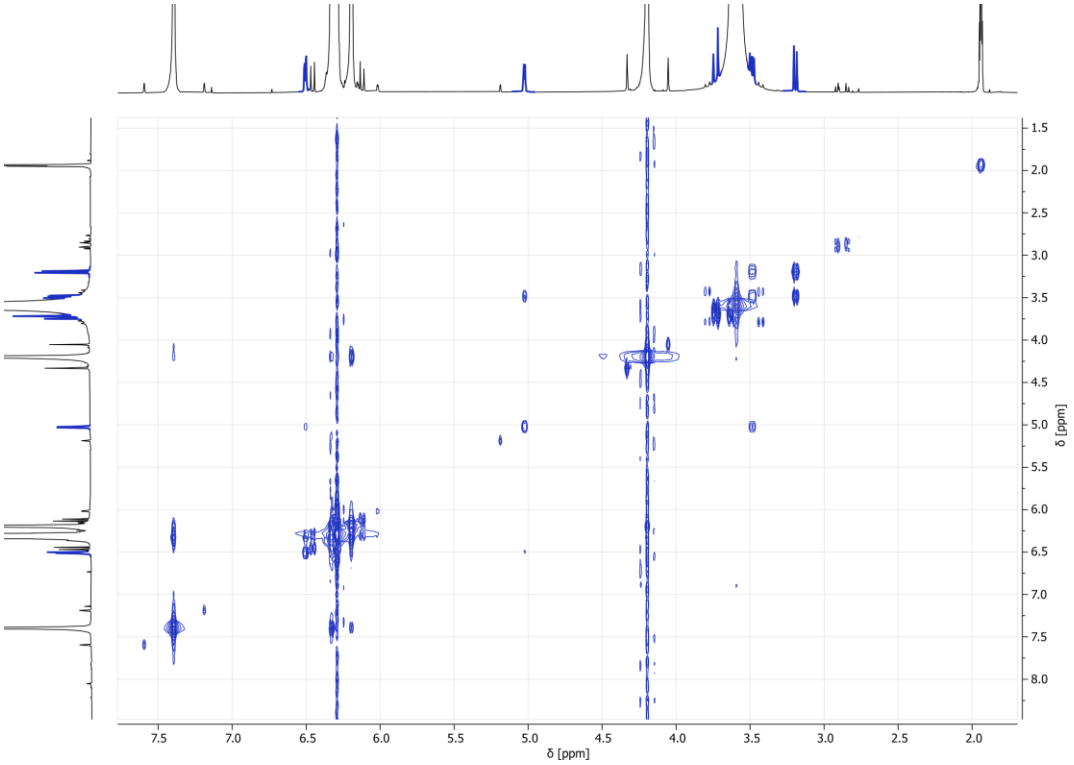

Figure S35. ^{1}H-^{1}H COSY NMR spectrum (CD_3CN: D_2O 85:15, 500 MHz) of the equilibrium **1a** + **2** ↔ **3a**, 100 mM of both components.

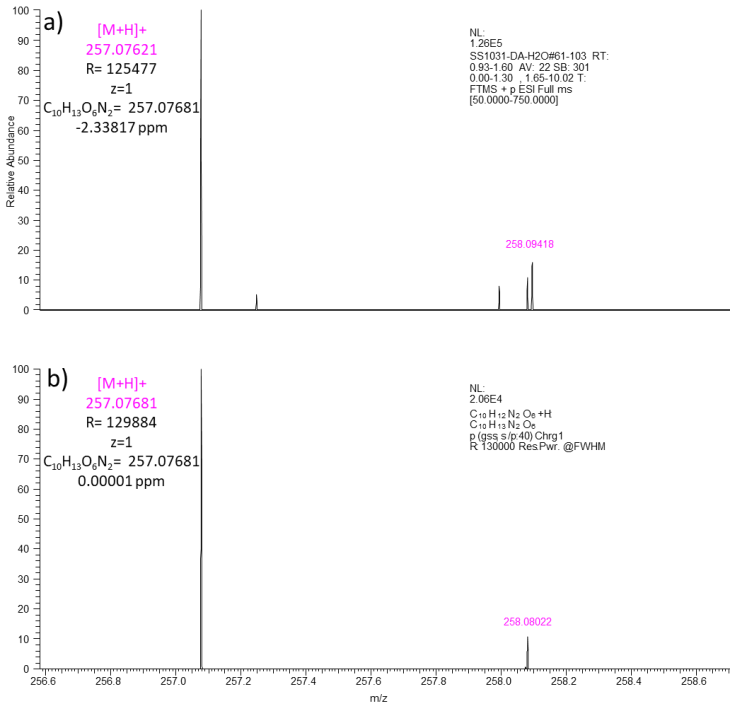

Figure S36. a) Experimental and b) calculated HRMS spectra of **3a**. The experimental spectrum was obtained after hydrolysis of **3a**' equilibrated from **1a** and **2**' in CD_3CN:D_2O (85:15).

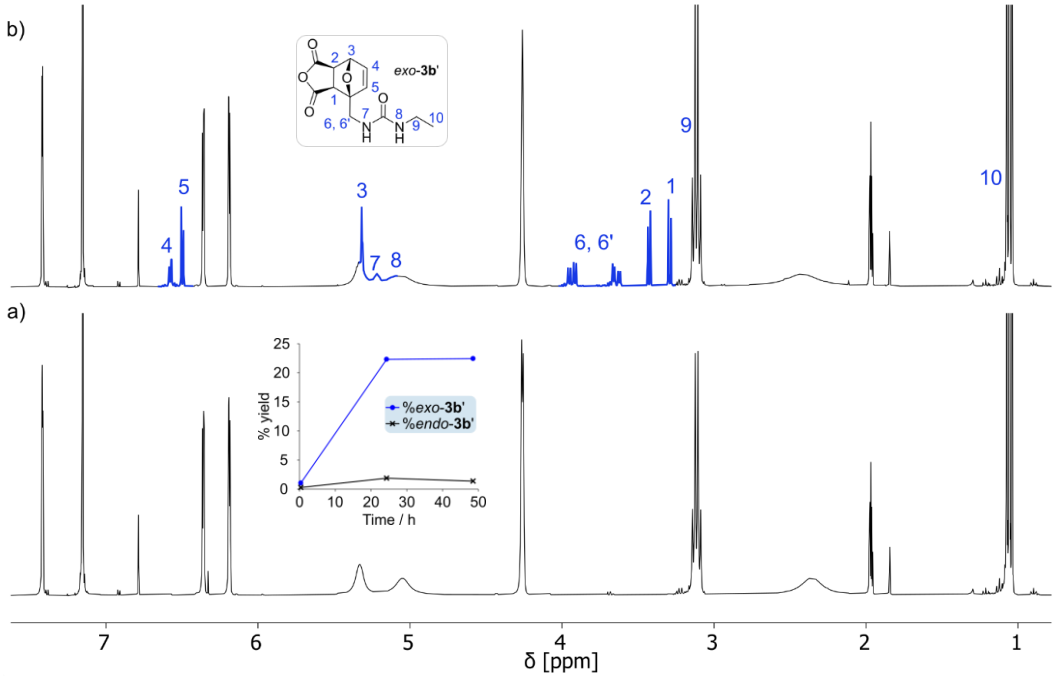

Figure S37. ^{1}H NMR spectra (CD_3CN, 400 MHz) showing the a) start and b) end points of the equilibrium **1b** + **2**' ↔ **3b**' reacted at 40°C, 100 mM of both components. *Inset*: variation of the % yield of adduct *exo- /endo*-**3b**' monitored in time.

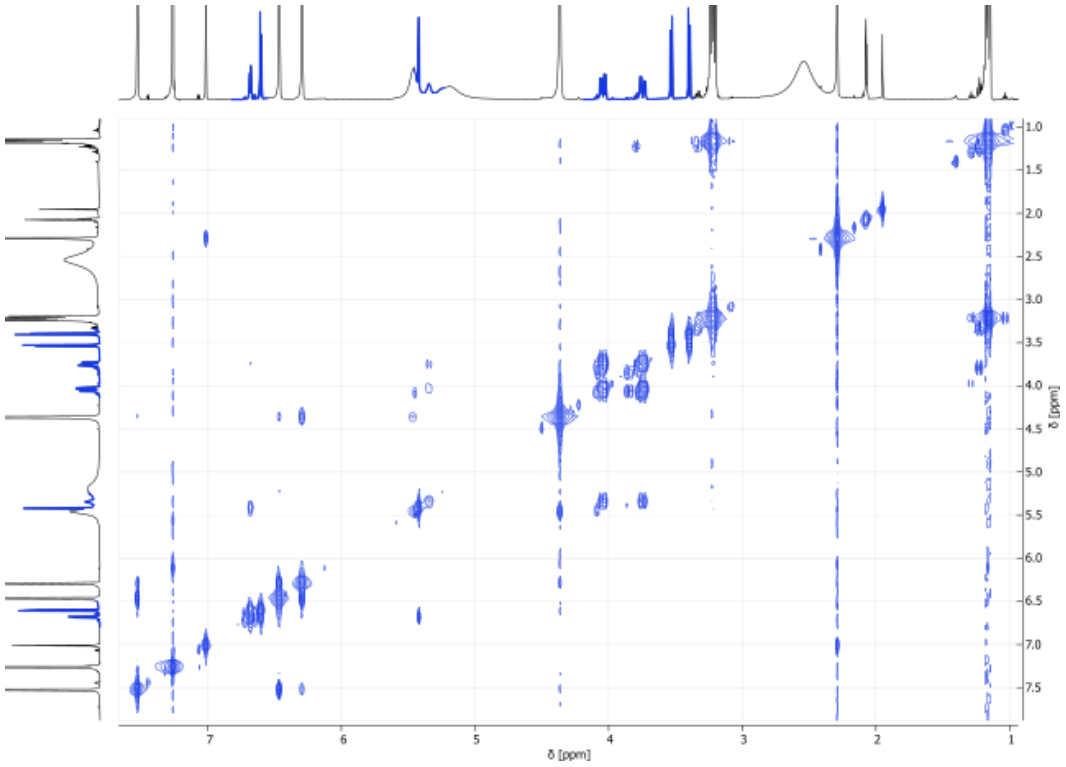

Figure S38. ^{1}H-^{1}H COSY NMR (CD_3CN, 500 MHz) of the equilibrium **1b** + **2**' ↔ **3b**', 100 mM of both components.

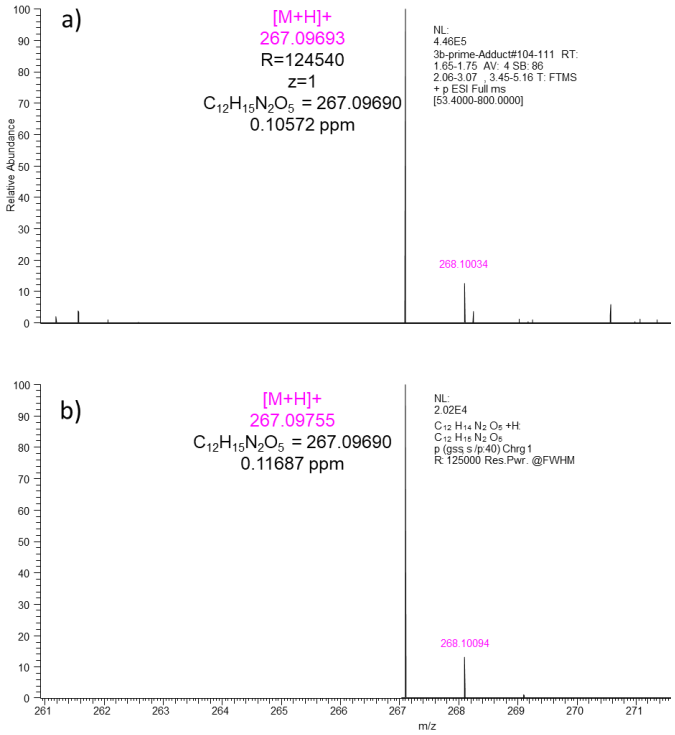

Figure S39. a) Experimental and b) calculated HRMS spectra of **3b**'. The experimental spectrum was obtained after equilibrating a mixture of **1b** and **2**' in CD_3CN.

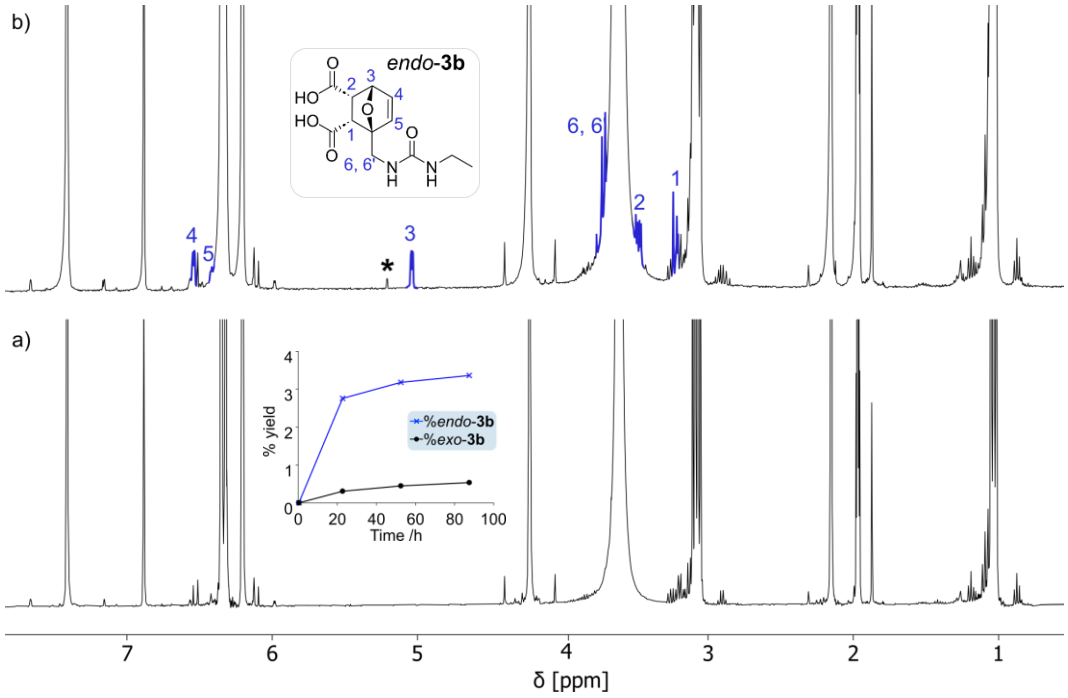

Figure S40. ^1H NMR spectra (CD_3CN:D_2O (85:15), 400 MHz) showing the a) start and b) end points of the equilibrium **1b** + **2** ↔ **3b** reacted at 40°C, 100 mM of both components. * *marks exo product. Inset*: variation of the % yield of adduct *exo- /endo*-**3b** monitored in time.

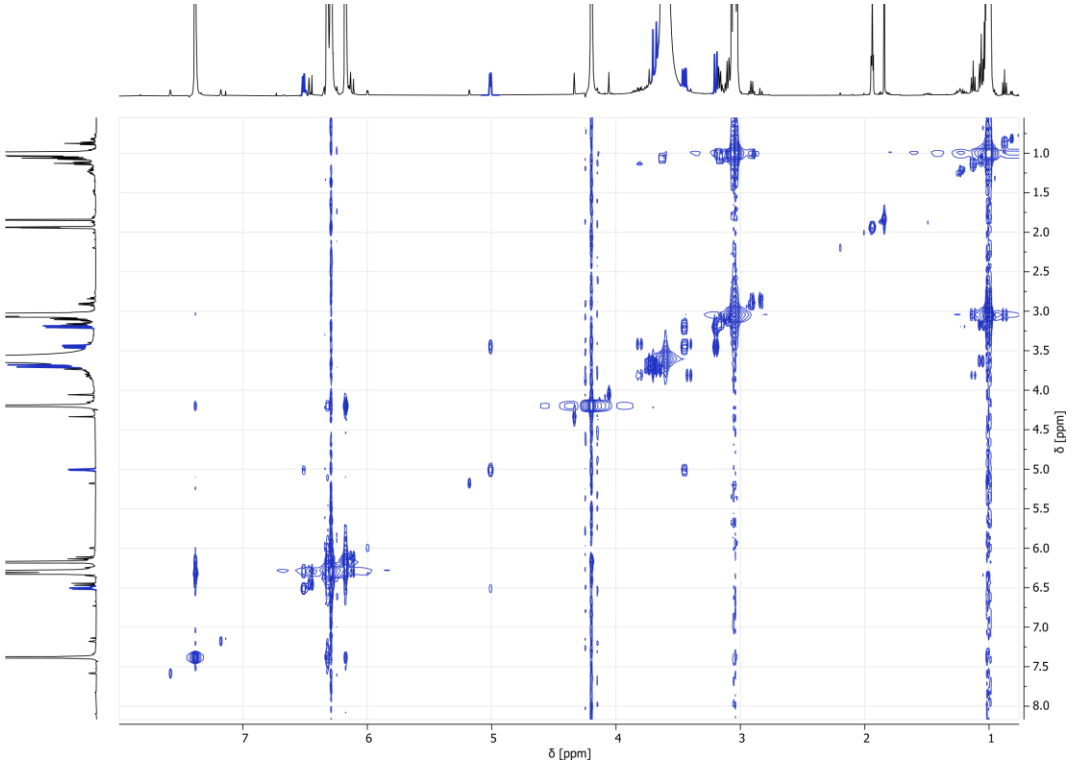

Figure S41. ^{1}H-^{1}H COSY NMR (CD_3CN:D 85:15, 500 MHz) of the equilibrium **1b** + **2** ↔ **3b**, 100 mM of both components.

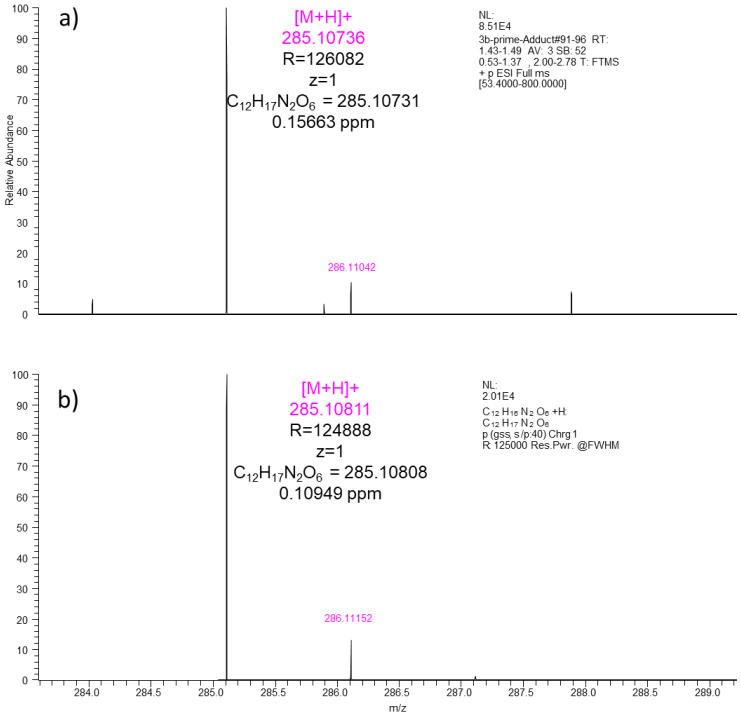

Figure S42. a) Experimental and b) calculated HRMS chromatograms of **3b** obtained after hydrolysis of **3b**' equilibrated from **1b** and **2**' in CD_3CN.

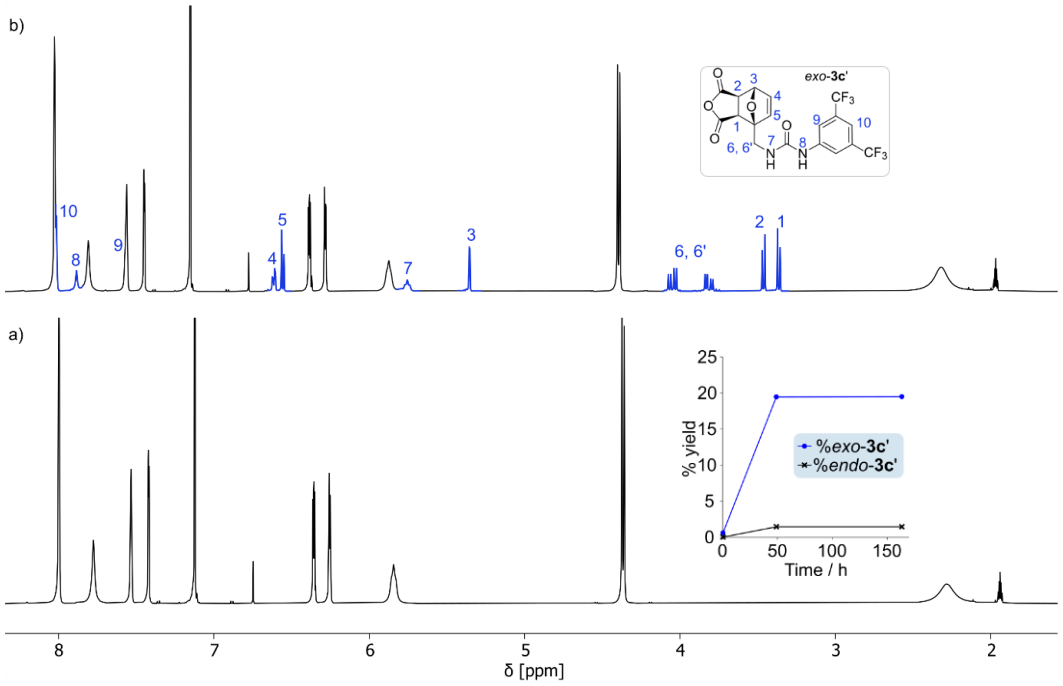

Figure S43. ^{1}H NMR spectra (CD_3CN, 400 MHz) showing the a) start and b) end points of the equilibrium **1c** + **2'** ↔ **3c'** reacted at 40°C, 100 mM of both components. *Inset*: variation of the % yield of adduct *exo- /endo*-**3c'** monitored in time.

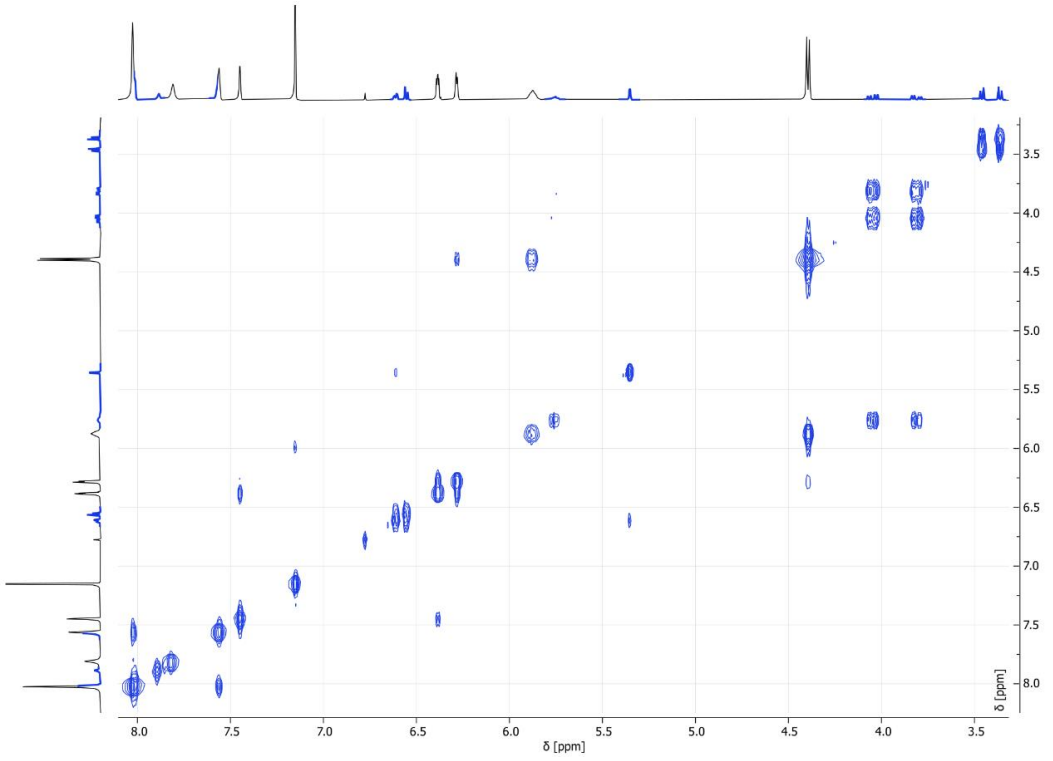

Figure S44. ^{1}H-^{1}H COSY NMR (CD_3CN, 500 MHz) of the equilibrium **1c** + **2'** ↔ **3c'**, 100 mM of both components.

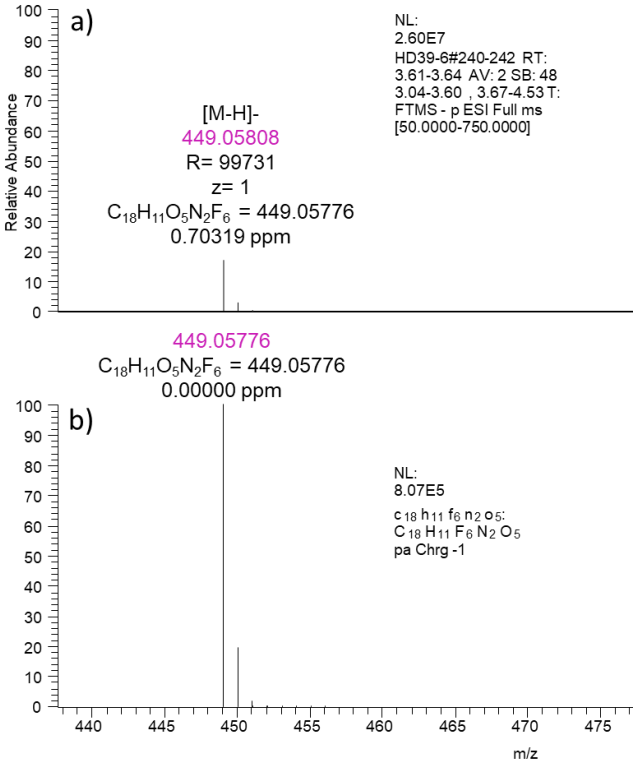

Figure S45. a) Experimental and b) calculated HRMS spectrum of **3c**'. The experimental spectrum was obtained after equilibrating a mixture of **1c** and **2**' in CD_3CN.

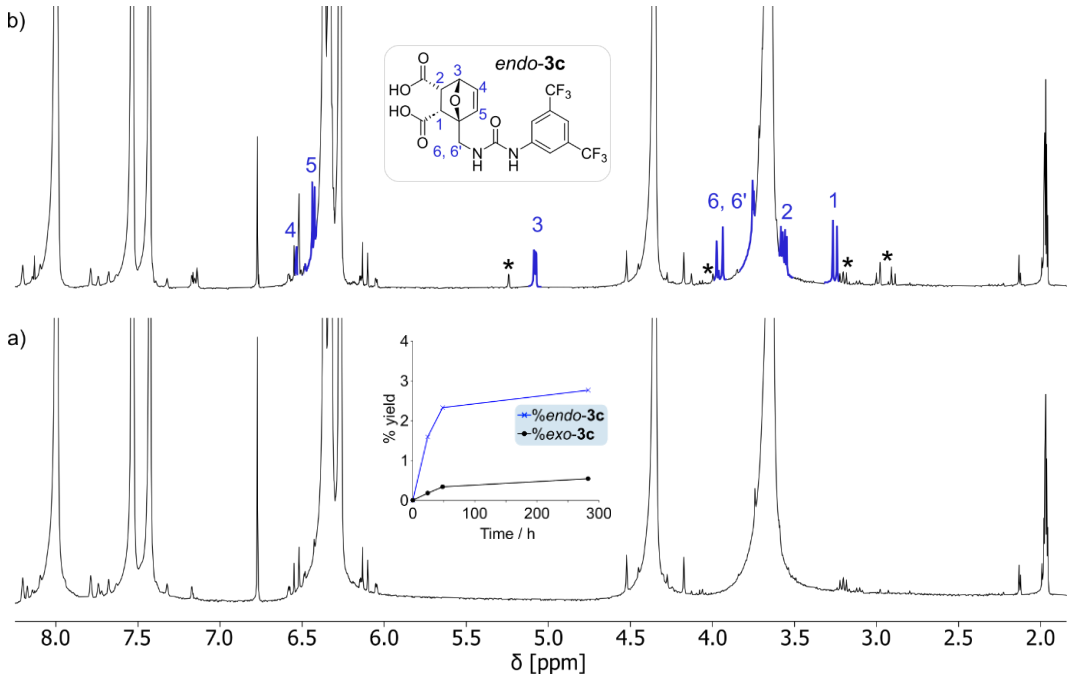

Figure S46. ^1H NMR spectra (CD_3CN:D_2O 85:15, 400 MHz) showing the a) start and b) end points of the equilibrium **1c** + **2** ↔ **3c** reacted at 40°C, 100 mM of both components. ** marks exo product. Inset*: variation of the % yield of adduct *exo- /endo*-**3c** monitored in time.

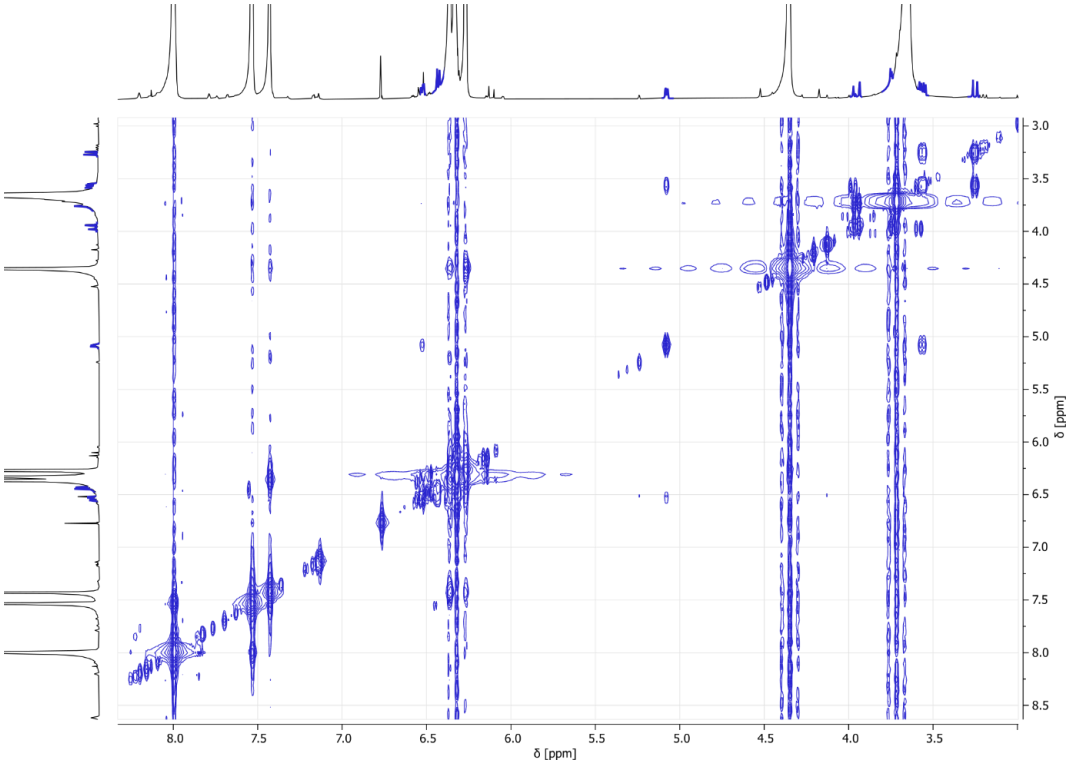

Figure S47. ^{1}H-^{1}H COSY NMR (CD_3CN:D_2O (85:15), 500 MHz) of the equilibrium **1c** + **2** ↔ **3c**, 100 mM of both components.

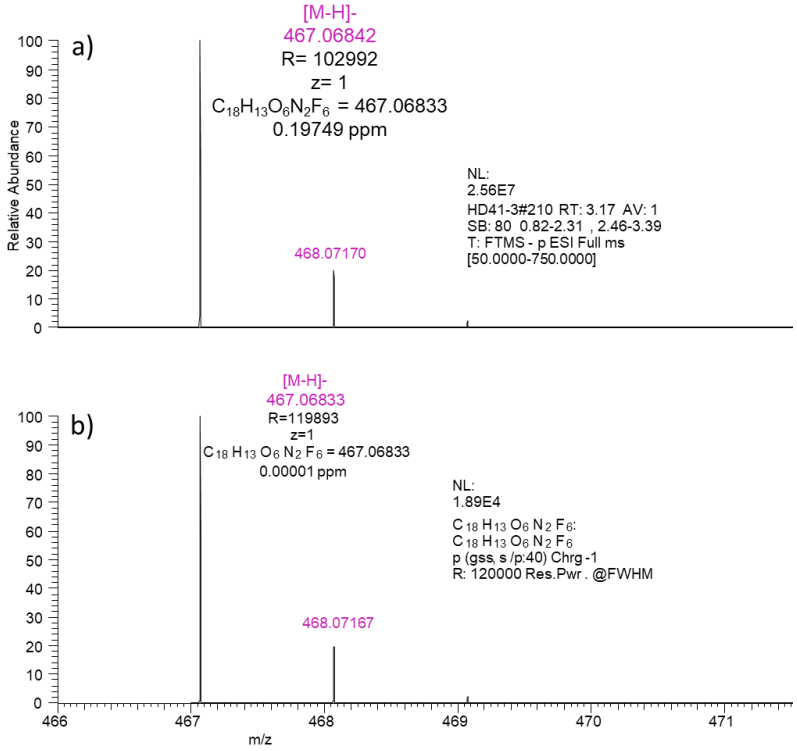

Figure S48. a) Experimental and b) calculated HRMS spectra of **3c**. The experimental spectrum was obtained from equilibrating a mixture of **1c** and **2** in CD_3CN.

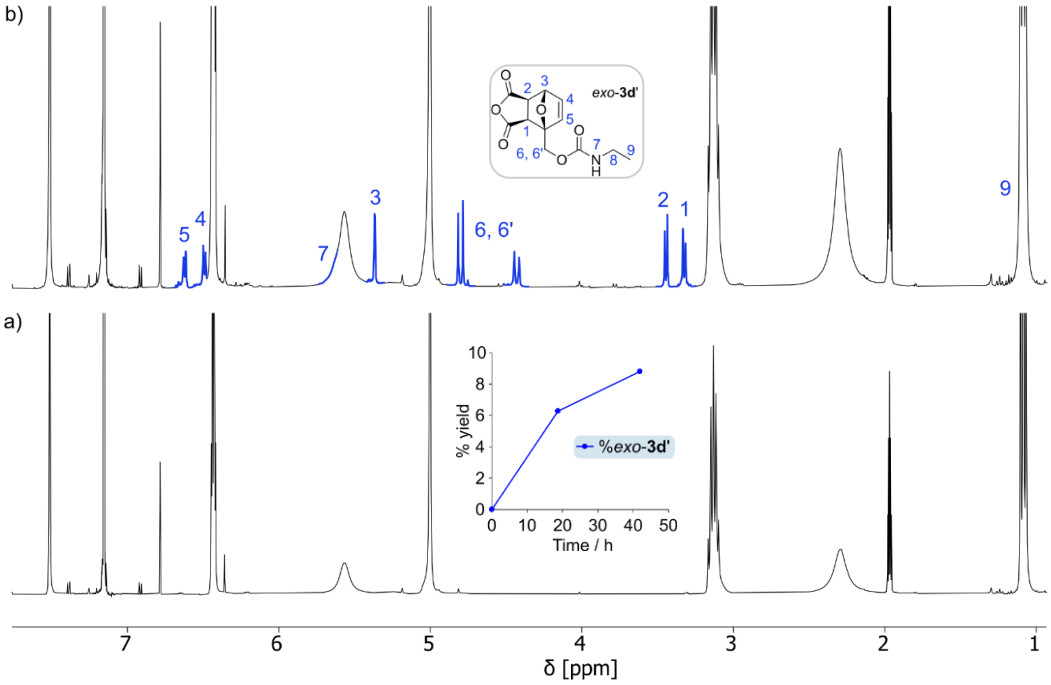

Figure S49. ^{1}H NMR spectra (CD_3CN, 400 MHz) showing the a) start and b) end points of the equilibrium **1d** + **2'** ↔ **3d'** reacted at 40°C, 100 mM of both components. *Inset*: variation of the % yield of adduct *exo*-**3d'** monitored over 42 hours.

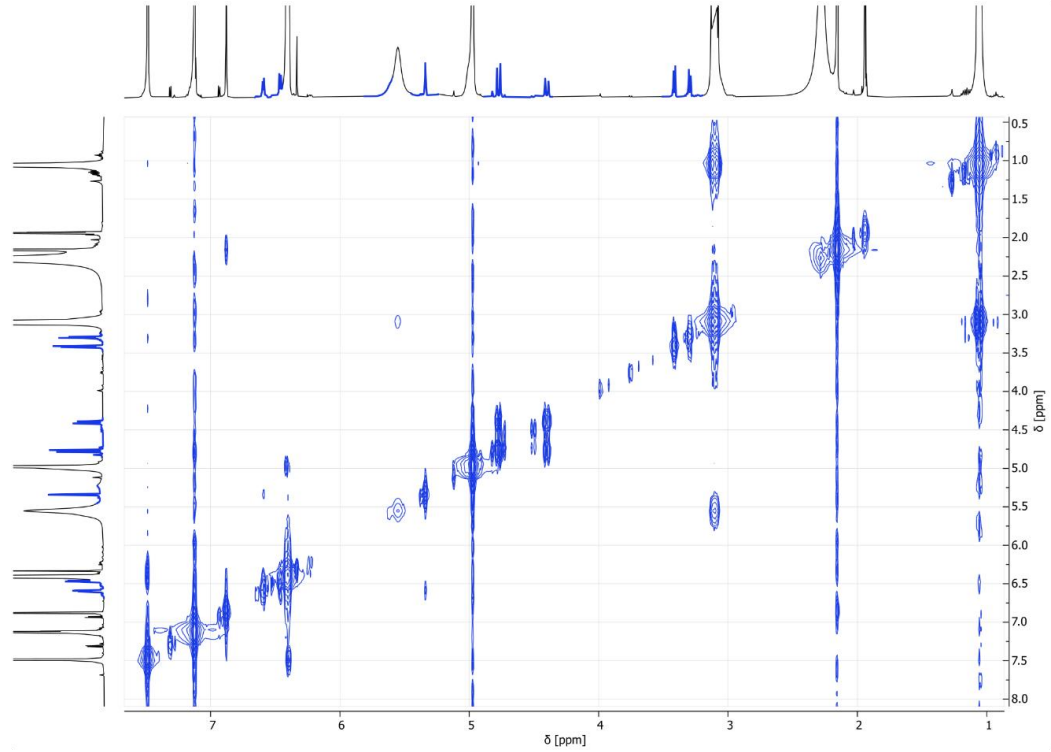

Figure S50. ^{1}H-^{1}H COSY NMR (CD_3CN, 500 MHz) of the equilibrium **1d** + **2'** ↔ **3d'**, 100 mM of both components.

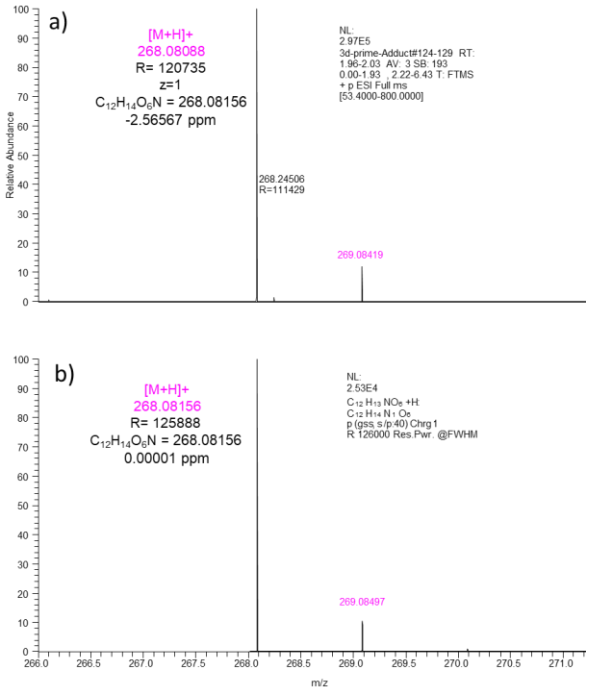

Figure S51. a) Experimental and b) calculated HRMS spectra of **3d**'. The experimental spectrum was obtained after equilibrating a mixture of **1d** and **2**' in CD_3CN.

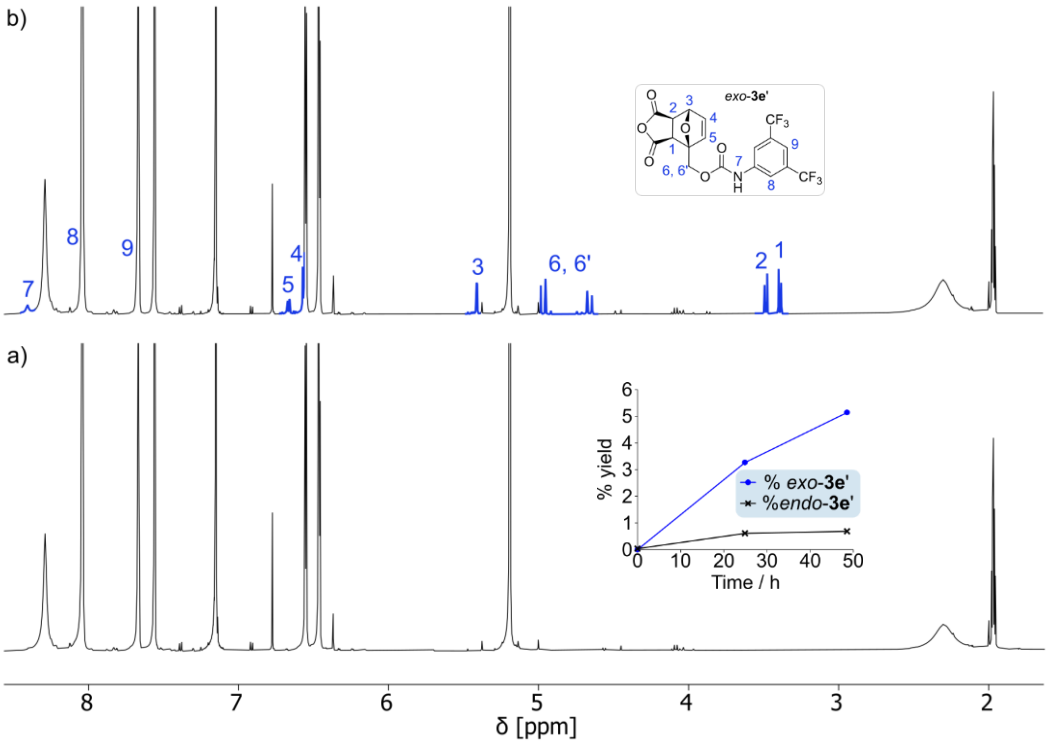

Figure S52. ^1H NMR spectra (CD_3CN, 400 MHz) showing the a) start and b) end points of the equilibrium **1e** + **2**' ↔ **3e**' reacted at 40°C, 100 mM of both components. *Inset*: variation of the % yield of adduct *exo*-**3e**' monitored over 48 hours.

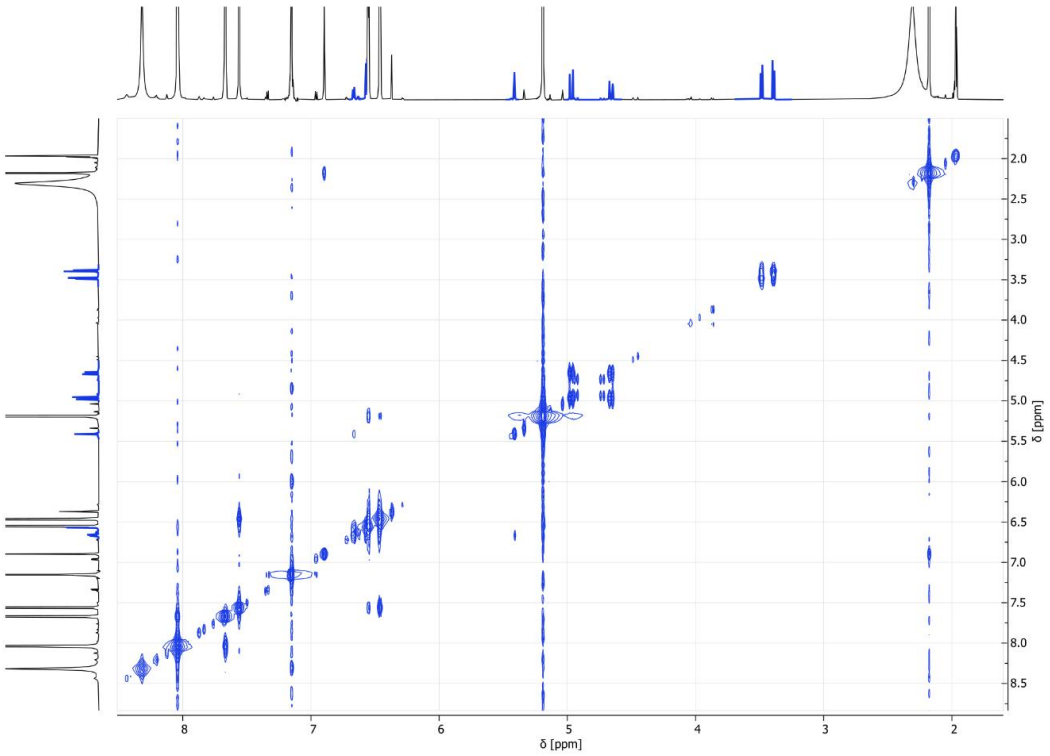

Figure S53. ^{1}H-^{1}H COSY NMR (CD_3CN, 500 MHz) of the equilibrium **1e** + **2'** ↔ **3e'**, 100 mM of both components.

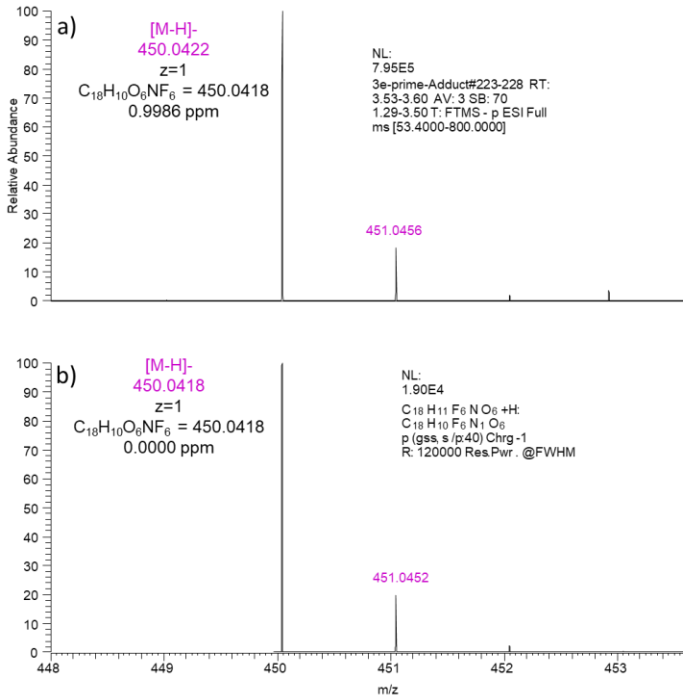

Figure S54. a) Experimental and b) calculated HRMS spectra of **3e'**. The experimental spectrum was obtained after equilibrating a mixture of **1e** and **2'** in CD_3CN.

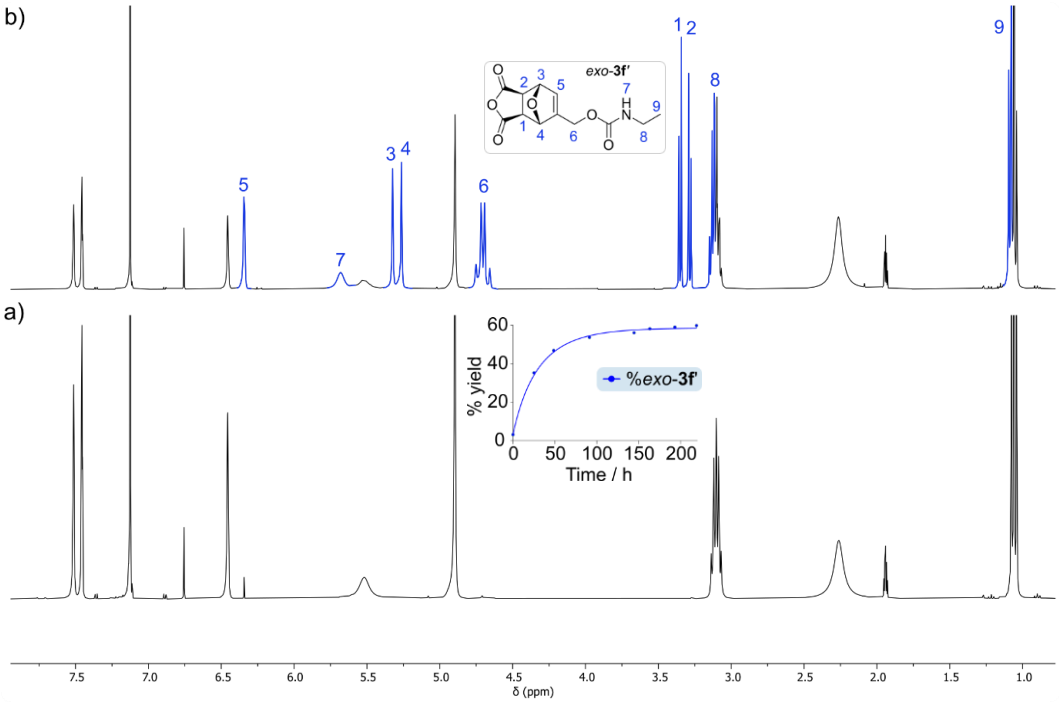

Figure S55. Superimposed ^{1}H NMR spectra (CD_3CN, 400 MHz) showing the a) start and b) end points of the equilibrium **1f** + **2**' ↔ **3f**' reacted at 40°C, 100 mM of both components. *Inset*: variation of the % yield of adduct *exo*-**3f**' in time (blue dots). The kinetic trace was fitted according to a second-order kinetic model (full line), obtaining a forward (assembly) rate constant of 5.6×10^{-5} M^{-1} s^{-1} and a backward rate constant of 1.9×10^{-6} s^{-1}; under these experimental conditions, the half-life of the forward process is 19 h.

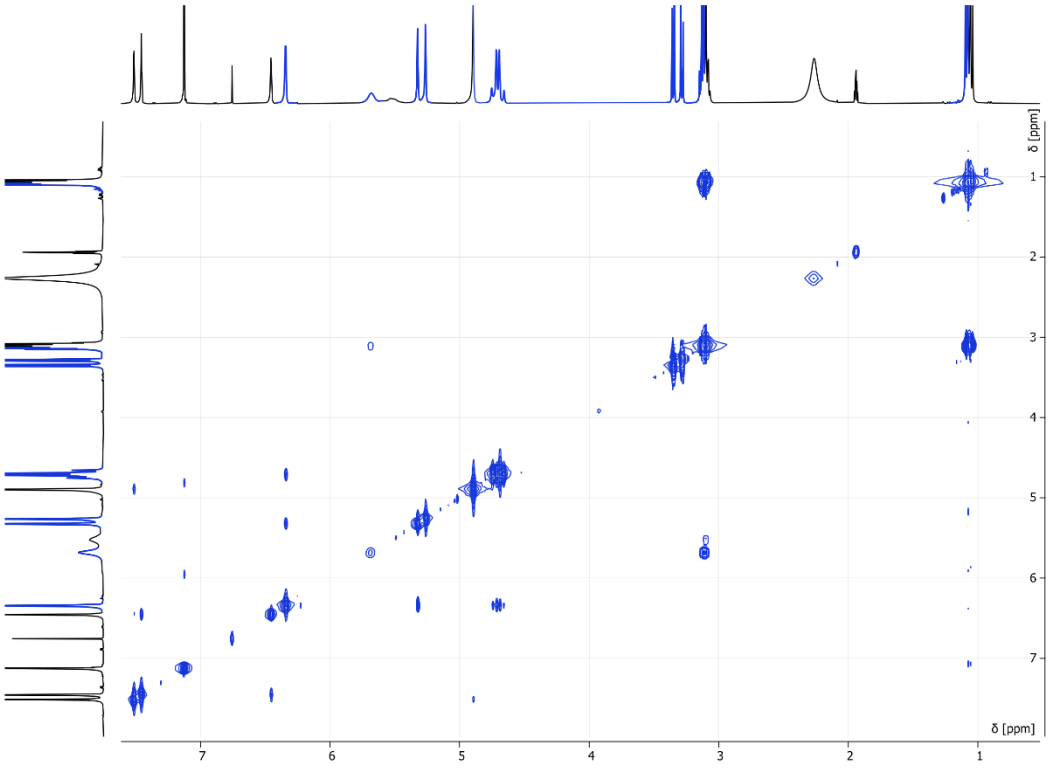

Figure S56. ^{1}H-^{1}H COSY NMR (CD_3CN, 500 MHz) of the equilibrium **1f** + **2**' ↔ **3f**',100 mM of both components.

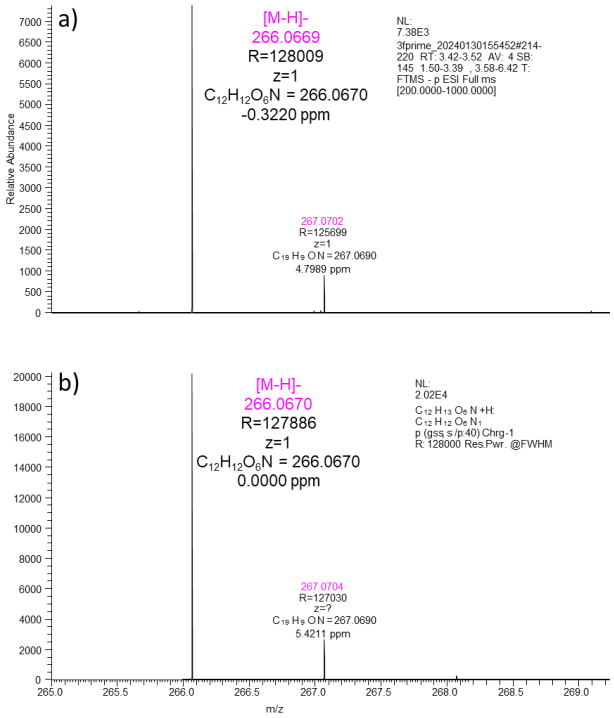

Figure S57. a) Experimental and b) calculated HRMS spectra of **3f**'. The experimental spectrum was obtained after equilibrating a mixture of **1f** and **2**' in CD_3CN.

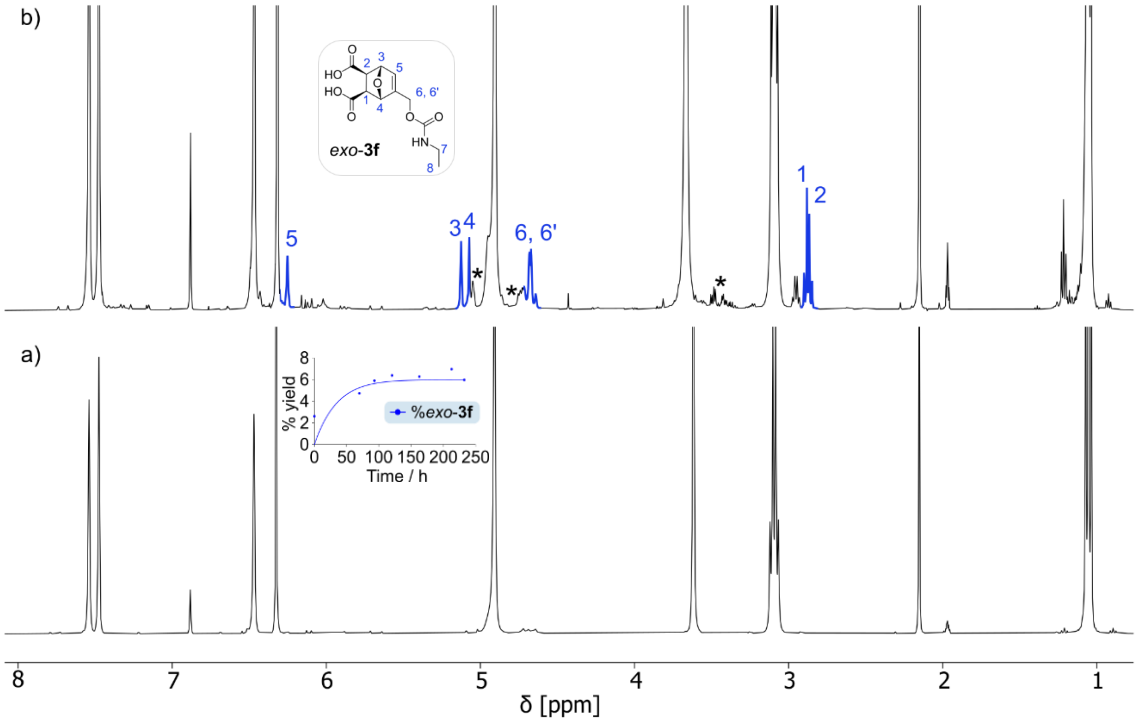

Figure S58. ^1H NMR spectra (CD_3CN:D_2O (85:15), 400 MHz) showing the a) start and b) end points of the equilibrium **1f** + **2** ↔ **3f** reacted at 40°C,100 mM of both components. * *marks endo product Inset*: variation of the % yield of adduct *exo*-**3f** in time (blue dots). The kinetic trace was fitted according to a second-order kinetic model (full line), obtaining a forward (assembly) rate constant of 6.1×10^{-6} M^{-1} s^{-1} and a backward rate constant of 1.51×10^{-6} s^{-1}, corresponding to a half-life of 29 h for the retro Diels-Alder reaction.

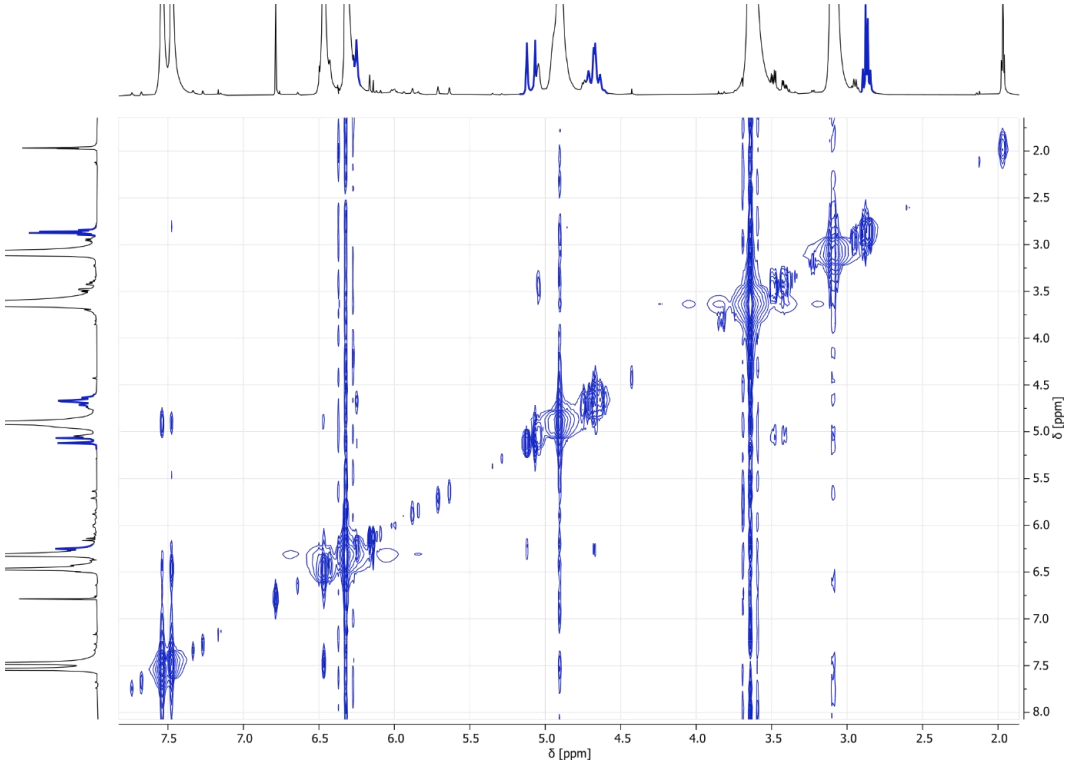

Figure S59. ^{1}H-^{1}H COSY NMR (CD_3CN:D_2O (85:15), 500 MHz) of the equilibrium **1f** + **2** ↔ **3f**,100 mM of both components.

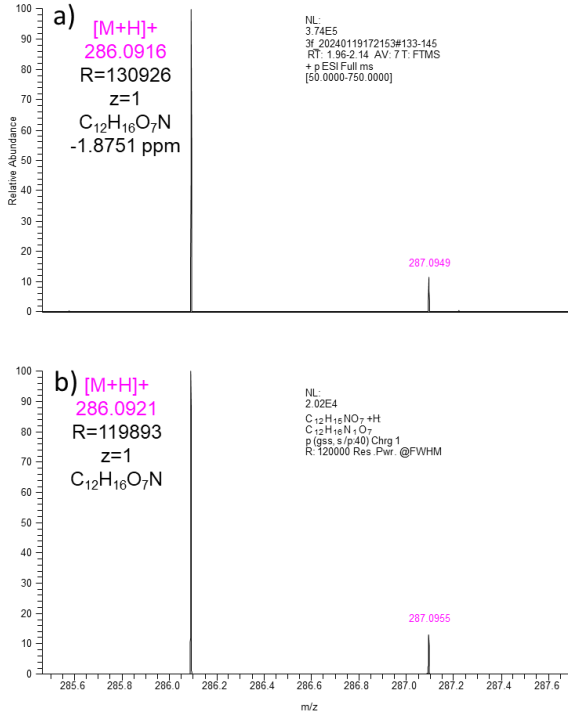

Figure S60. a) Experimental and b) calculated HRMS spectra of **3f**. The experimental spectrum was obtained from equilibrating a mixture of **1f** and **2** in CD_3CN:D_2O (85:15).

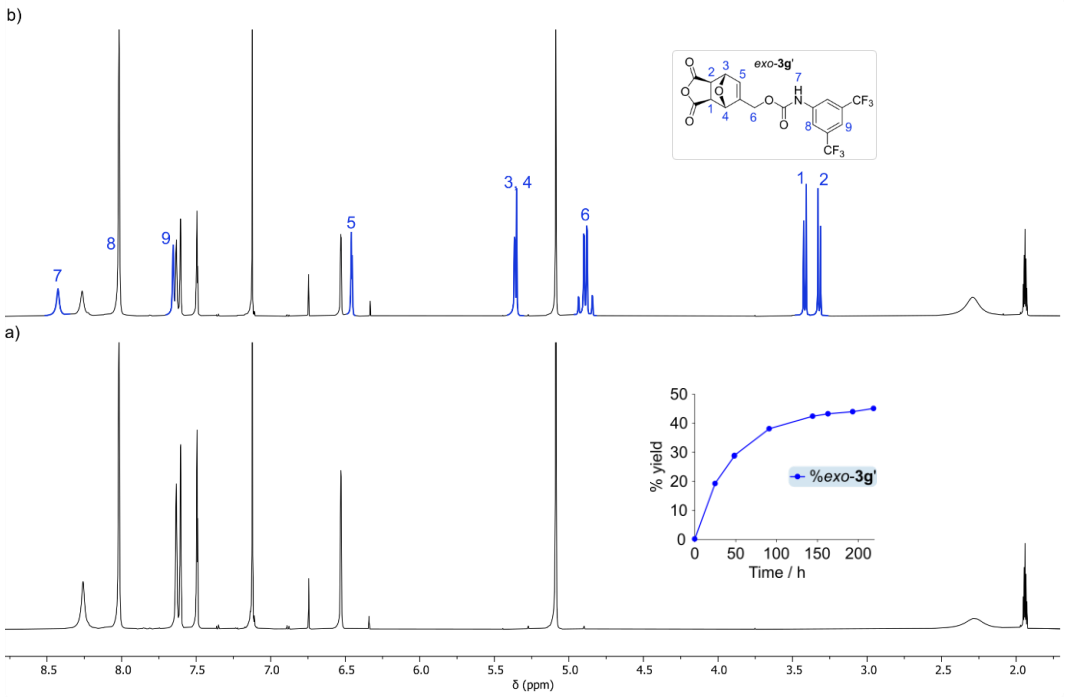

Figure S61. ^{1}H NMR spectra (CD_3CN, 400 MHz) showing the a) start and b) end points of the equilibrium **1g** + **2'** ↔ **3g'** reacted at 40°C,100 mM of both components. *Inset*: variation of the % yield of adduct *exo*-**3g'** monitored in time.

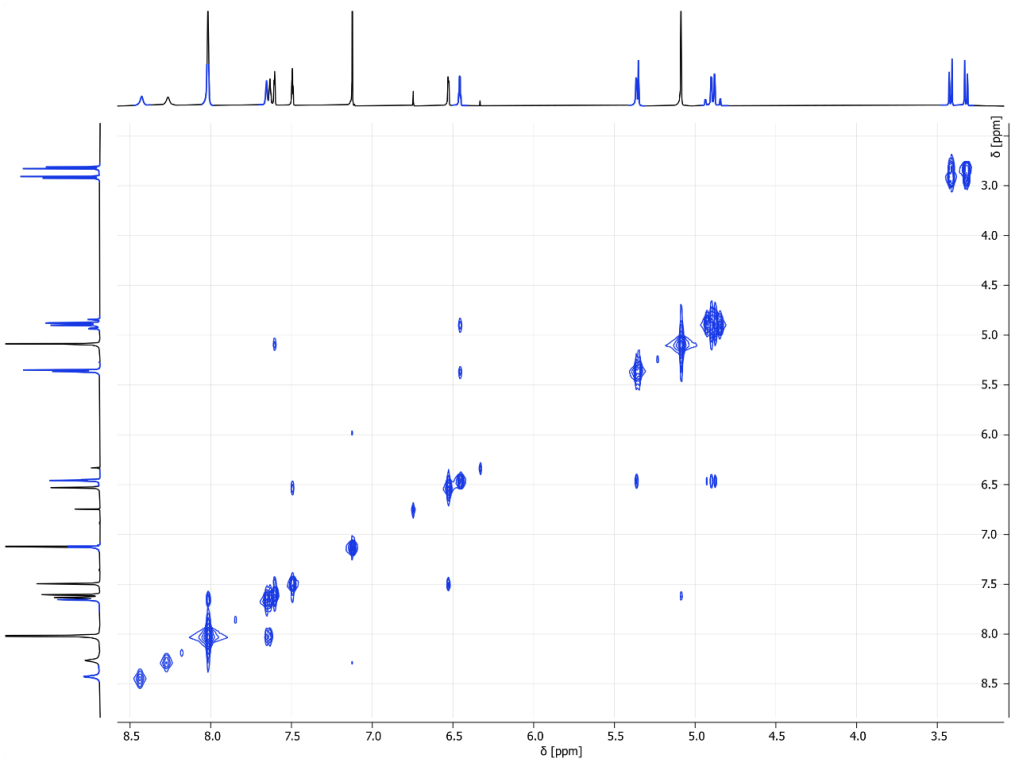

Figure S62. ^{1}H-^{1}H COSY NMR (CD_3CN, 500 MHz) of the equilibrium **1g** + **2'** ↔ **3g'**,100 mM of both components.

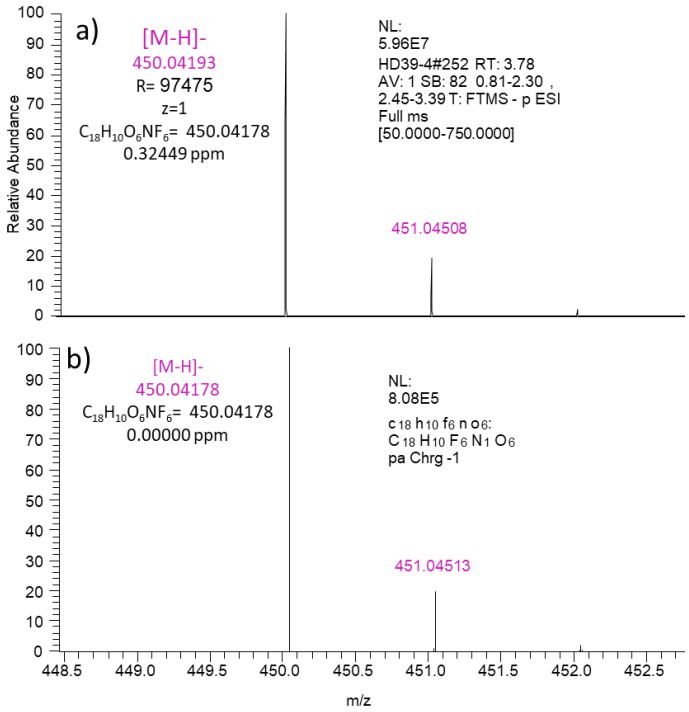

Figure S63. a) Experimental and b) calculated HRMS spectra of **3g'**. The experimental spectrum was obtained after equilibrating a mixture of **1g** and **2'** in CD_3CN.

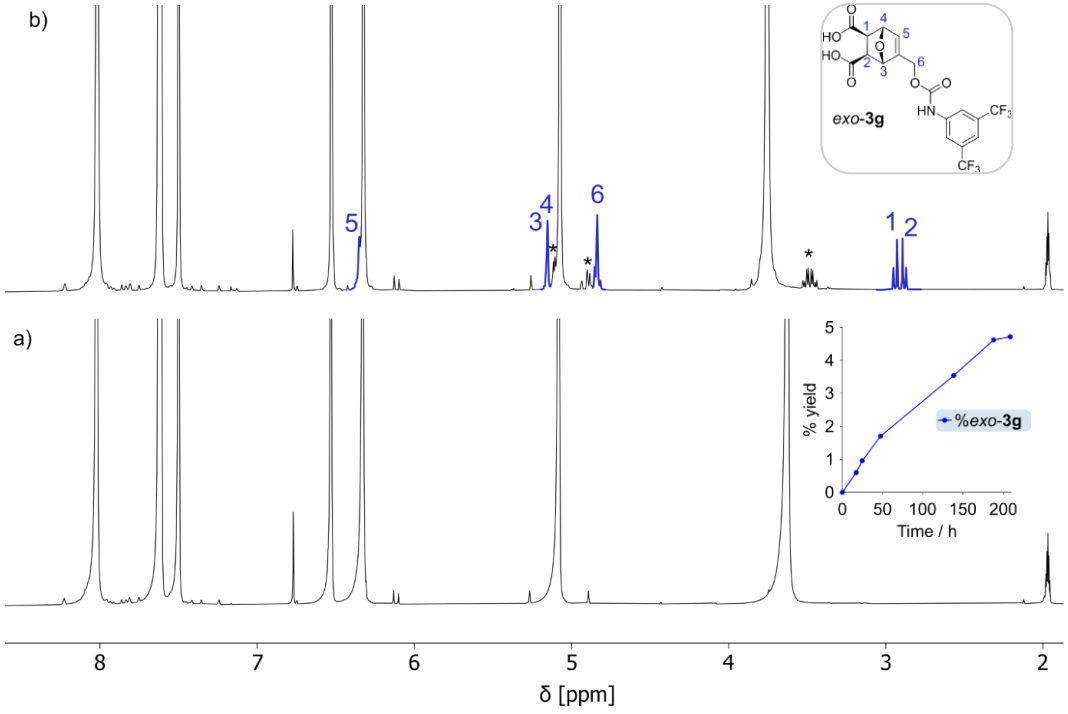

Figure S64. Superimposed ^1H NMR spectra showing the a) start and b) end points of the equilibrium **1g** + **2** ↔ **3g** reacted at 40°C,100 mM of both components. CD_3CN:D_2O (85:15), 400 MHz). * marks *endo* product *Inset*: variation of the % yield of adduct *exo*-**3g** monitored in time.

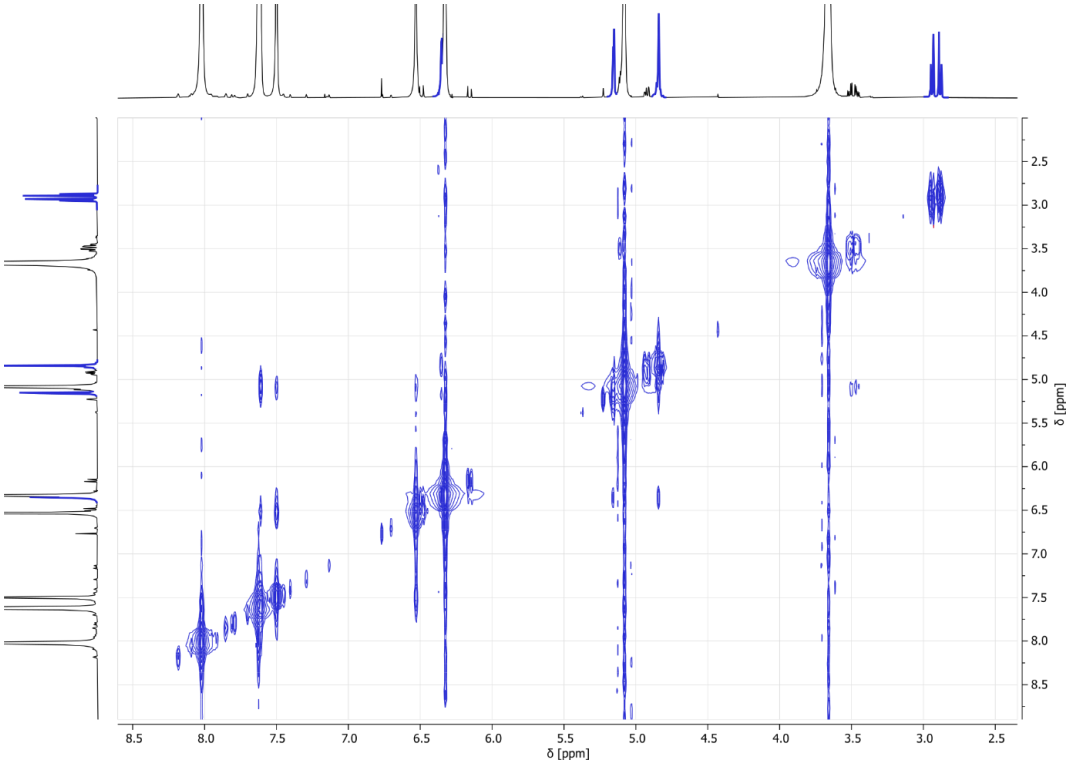

Figure S65. ^{1}H-^{1}H COSY NMR (CD_3CN:D_2O (85:15), 500 MHz) of the equilibrium **1g** + **2** ↔ **3g**,100 mM of both components.

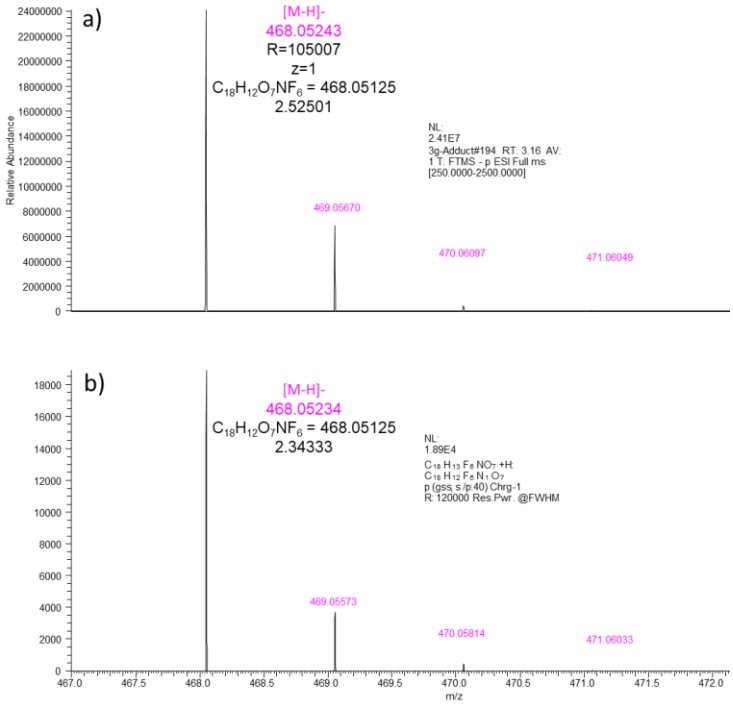

Figure S66. a) Experimental and b) calculated HRMS spectra of **3g**. The experimental spectrum was obtained from equilibrating a mixture of **1g** and **2** in CD_3CN.

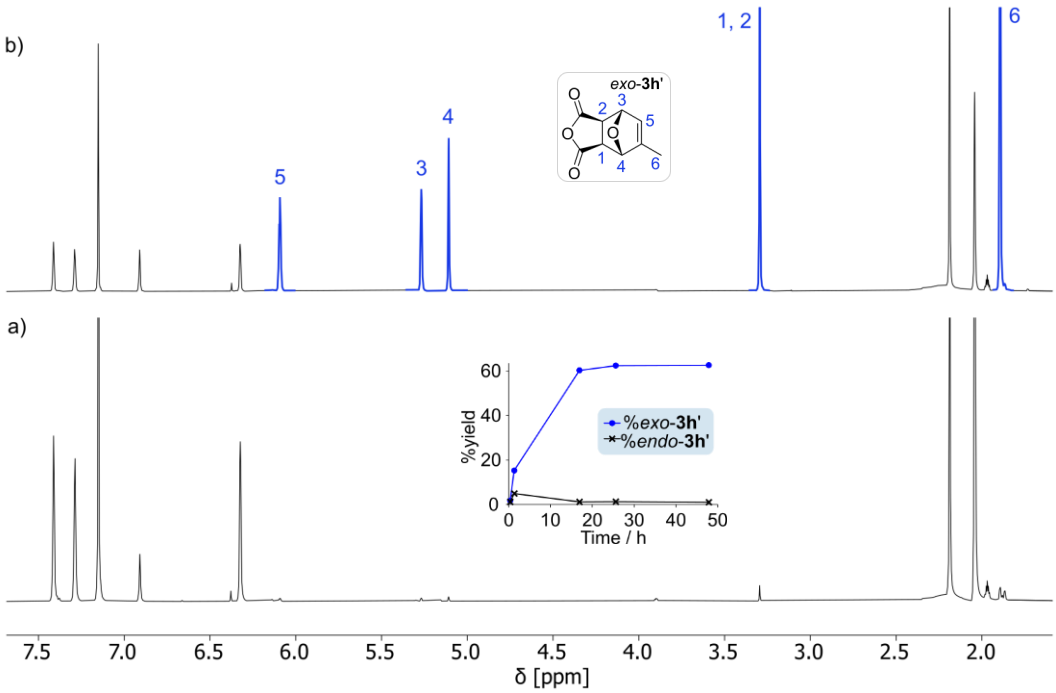

Figure S67. ^{1}H NMR spectra (CD_3CN, 400 MHz) showing the a) start and b) end points of the equilibrium **1h** + **2'** ↔ **3h'** reacted at 40°C,100 mM of both components. *Inset*: variation of the % yield of adduct *exo- /endo*-**3h'** monitored in time.

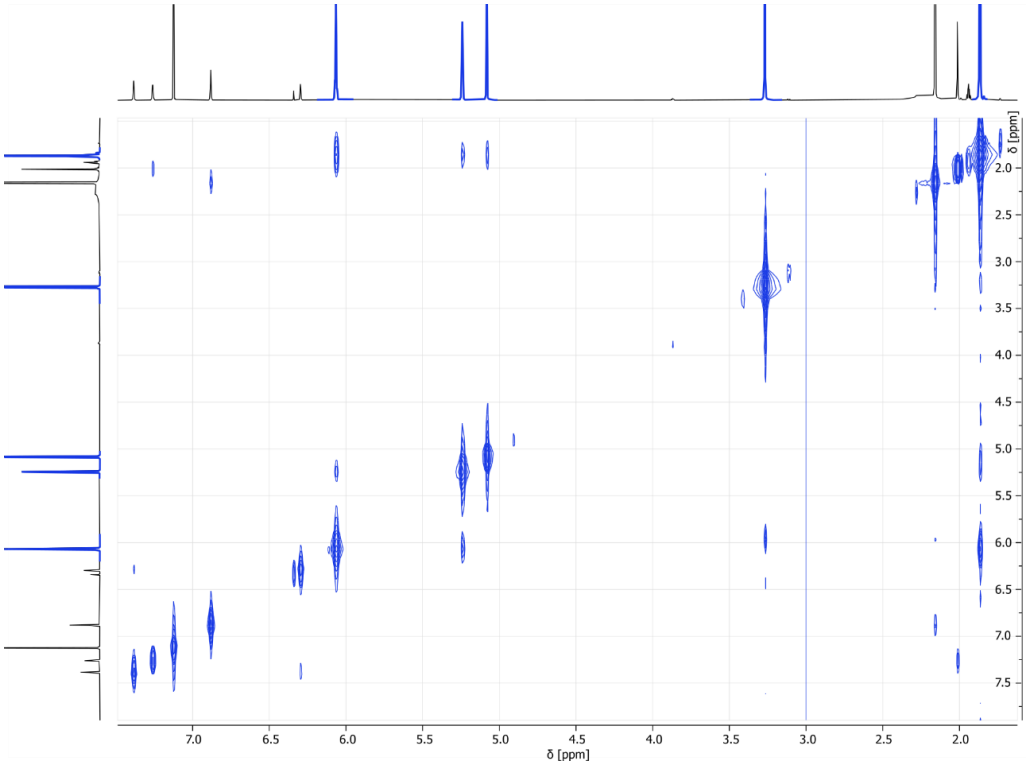

Figure S68. ^{1}H-^{1}H COSY NMR (CD_3CN, 500 MHz) of the equilibrium **1h** + **2'** ↔ **3h'**,100 mM of both components.

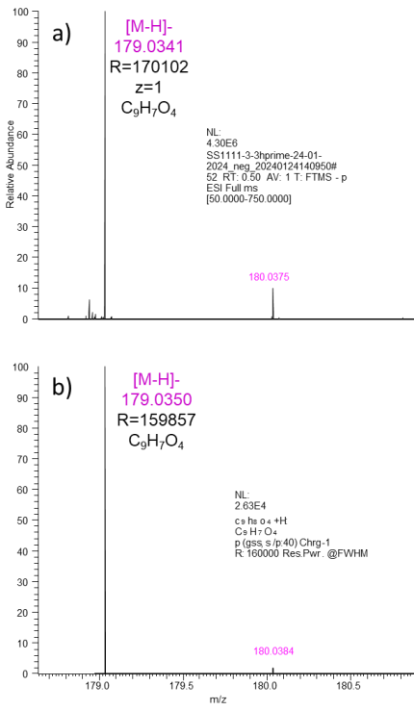

Figure S69. a) Experimental and b) calculated HRMS spectra of **3h'**. The experimental spectrum was obtained after equilibrating a mixture of **1h** and **2'** in CD_3CN.

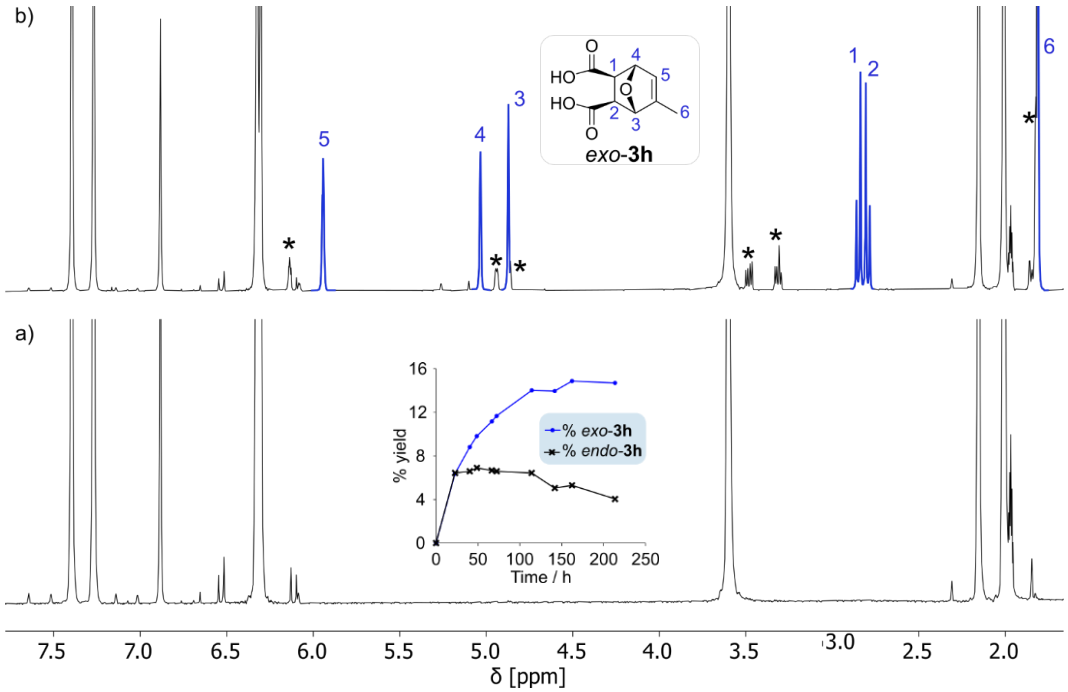

Figure S70. ^1H NMR spectra (CD_3CN:D_2O (85:15), 400 MHz) showing the a) start and b) end points of the equilibrium **1h** + **2** ↔ **3h** reacted at 40°C,100 mM of both components. * marks *endo* product. *Inset*: variation of the % yield of adduct *exo- /endo*-**3h** monitored in time.

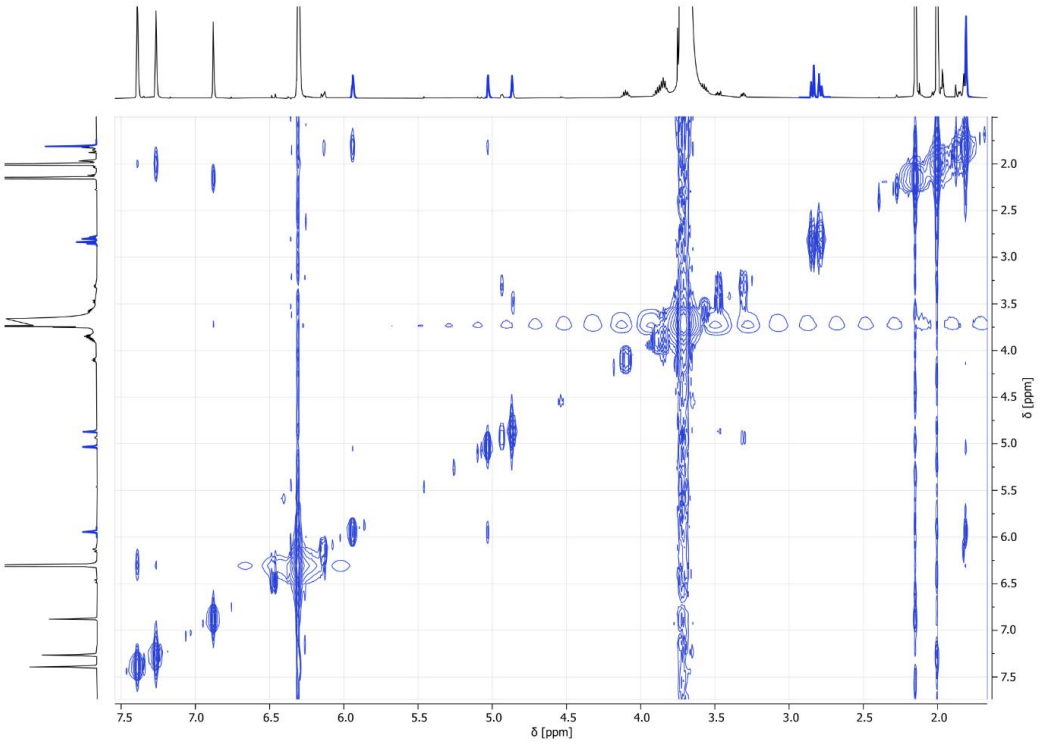

Figure S71. ^{1}H-^{1}H COSY NMR (CD_3CN:D_2O (85:15), 500 MHz) of the equilibrium **1h** + **2** ↔ **3h**,100 mM of both components.

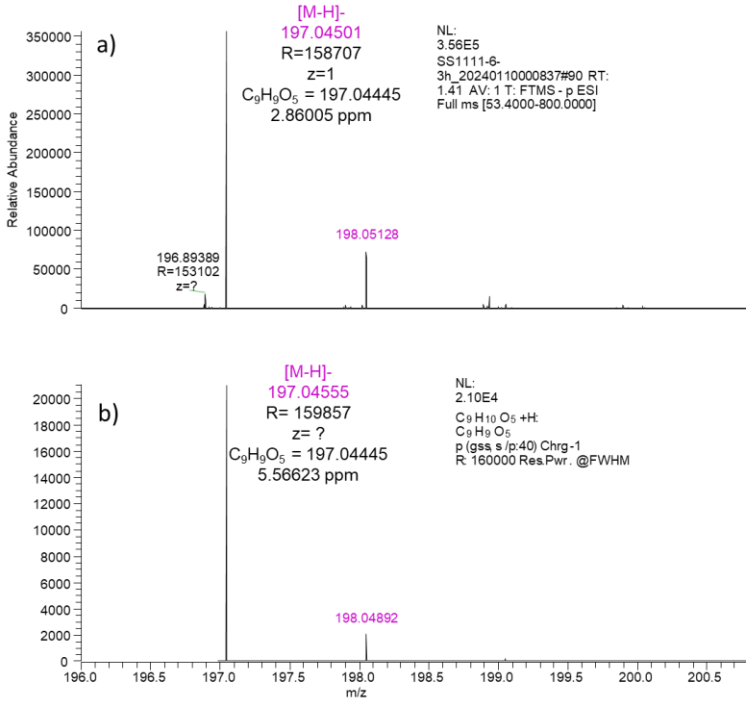

Figure S72. a) Experimental and b) calculated HRMS spectra of **3h**. The experimental spectrum was obtained from equilibrating a mixture of **1h** and **2** in CD_3CN:D_2O (85:15).

c. Confirmation of species 3 characterization

On top of the data presented so far, the characterization of acid adducts **3a** and **3f**, chosen as representative examples, was corroborated by comparing the NMR spectra obtained from the equilibrium **1** + **2** ↔ **3** (reaction **I** in Figure S1; spectrum (f) in Figure S73 or spectrum (e) in Figure S74, left) in aqueous acetonitrile to that of **1** + **2'** ↔ **3'** under the same conditions, that lead to the hydrolysis of **3'** over time (reactions **III** and **IV** in Figure S1; spectra (a-e) in Figure S73 or (a-d) in Figure S74, left). The alignment of the peaks observed upon the hydrolysis of **3'** in the latter reaction and those obtained in the former demonstrates that the species observed in both cases as well as in the fueling experiments correspond to **3** upon the hydrolysis of **3'**. Complementary ^{1}H-^{1}H COSY NMR and HRMS further supported the assignment in these experiments.

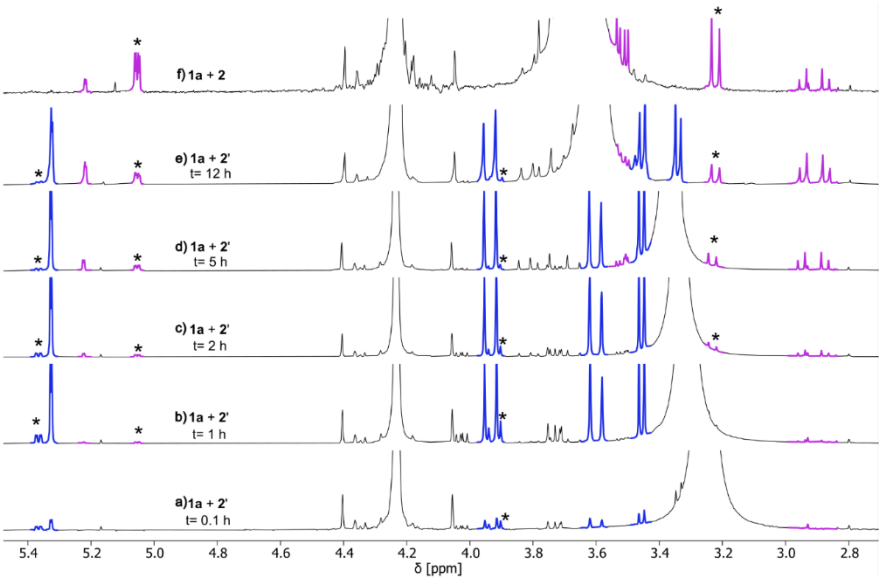

Figure S73. a-d) Diels-Alder equilibrium between **1a** and **2'** in aqueous acetonitrile (CD_3CN:D_2O 85:15) showing the consecutive formation and hydrolysis of **3a'** (blue peaks) into **3a** (purple peaks) which match the peaks obtained upon mixing f) **1a** and **2** under the same conditions (100 mM of both components, CD_3CN:D_2O 85:15, 40° C, 400 MHz). * marks the *endo* adduct

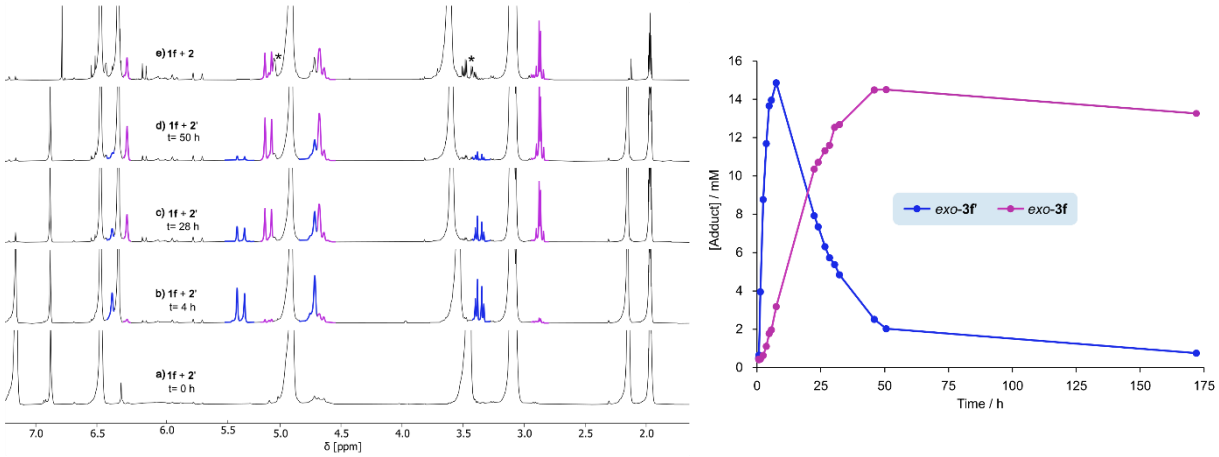

Figure S74. *Left*: a-d) NMR spectra of the Diels-Alder equilibrium between **1f** and **2'** in aqueous acetonitrile (CD_3CN:D_2O 85:15) showing the consecutive formation and hydrolysis of **3f'** (blue peaks) into **3f** (purple peaks) which match the peaks obtained upon mixing e) **1f** and **2** under the same conditions (100 mM of both components, CD_3CN:D_2O 85:15, 40° C, 400 MHz). * marks the *endo* adduct. *Right*: The corresponding plot showing the evolution of the adducts' concentrations with time, *exo*-**3f'** (in blue) and *exo*-**3f** (in purple), upon mixing **1f** and **2'** in aqueous acetonitrile (100 mM of both components, CD_3CN:D_2O 85:15).

5. Fueling experiments

a. Relation to theoretical frameworks

The reference kinetic models employed by the community of chemists that develop molecular ratchets tend to describe the two complementary cases of energy or information ratchet. When presenting information ratchet-based descriptions, the species identified as fuel and waste are chemostatted. Prins *et al.* used this condition when defining Class 1-4 systems.[2] Here, as the concentration of fuel and waste is not chemostatted, we cannot apply in a strict sense the framework proposed by Prins to categorize the following experiments. An alternative framework is that of energy ratchet mechanisms. Descriptions of systems based on energy ratchet mechanisms tend to assume either a periodic switching, leading to a periodic steady-state, or a complete equilibration before switching. Neither of these cases applies to our system, as the switching is not periodic, there is no complete equilibration, and kinetic effects associated with the switching processes (anhydride formation and hydrolysis) are clearly relevant for the overall mechanism, as control experiments indicate. A pure energy ratchet effect – featuring equilibration before switching – would not afford the multi-step adaptation effects discussed herein. To the best of our current understanding, we would describe the presented systems as operated according to a mixed energy and information ratchet mechanism.

b. Experimental error

Even when the same experiment was repeated three times (e.g. as for **3g**, Figure S78), the exact time at which each NMR spectrum is recorded may differ, as it depends from the instrument availability. Therefore, it was not possible for us to add error bars to each point using the standard deviations of three different experiments. The error on the end point is much more reliable, being ±1.3% yield in the case of the experiment of Figure S78.

To evaluate the error bars associated with the experiments reported in figure 4, a possibility is to consider the error on NMR peak integration (the approach used by Leigh et. al in the related manuscript "Endergonic synthesis driven by chemical fueling." *Nat. Synth*. (2024). https://doi.org/10.1038/s44160-024-00493-w). We performed a statistic on the integration error on starting material (involving two different users), and found an error of ±1.7% relative to peak integration. The fueling experiment reported in Figure 4 reach about 25 mM product, corresponding to an error of about ±0.4% yield. This error is significantly lower than the error on the endpoint ±1.3% yield, therefore, we find the latter more informative, and used this reference value.

Since the experiments are performed in a mixed solvent system, we have experienced shimming difficulties from time to time. It was not always possible to improve the shimming in the NMR time slot allocated to the measurement, so some data points that appear "off" may reflect an unsatisfactory shimming, rather than other factors. The end-points, used for energy calculations, were always recorded after a satisfactory shimming was obtained.

c. Equilibration of reaction I

Mother solutions of the different reagents were prepared in CD_3CN: 500 mM of **1** (S_1), 250 mM of **2** (S_2) and 250 mM of 1,2,4,5-tetramethylbenzene (**TMB**) as an inert internal standard (S_{TMB}). The final solutions were prepared by mixing **1** (100 µL of S_1, final concentration 100 mM, 0.05 mmol), **2** (200 µL of S_2, final concentration 100 mM, 0.05 mmol), and **TMB** (20 µL S_{TMB}, final concentration 10 mM, 0.005 mmol) in an NMR tube

containing 75 µL of D_2O and 105 µL of CD_3CN (final volume 500 µL; 85:15 CD_3CN:D_2O). An NMR spectrum was acquired just after mixing: usually 5-10 minutes passed from solution preparation to the acquisition of the first scan. The NMR tube was placed in a sand bath preheated at 40°C. NMR spectra were then acquired over the course of several days until no appreciable changes were observed (usually after 3 – 10 days, considered the equilibrium distribution).

d. Fueling with 3 equivalents of DIC over 1 cycle

To a pre-equilibrated NMR tube of **1** and **2** (as described in Section 5**c**), 23.4 µL of **DIC** (0.15 mmol, 3 equiv.) were added. The NMR tube was kept in the sand bath at 40°C and removed periodically (every 1-2 h) to monitor species evolution via NMR. Once **DIC** was fully consumed and the concentration of **3'** reached a plateau, NMR spectra were then recorded over longer time spans.

The concentrations of the species at each point were obtained relative to the integration of the internal standard peak, thus taking into consideration the dilution coming from the addition of **DIC**. The % yield of each adduct is then plotted versus time (Figure S75).

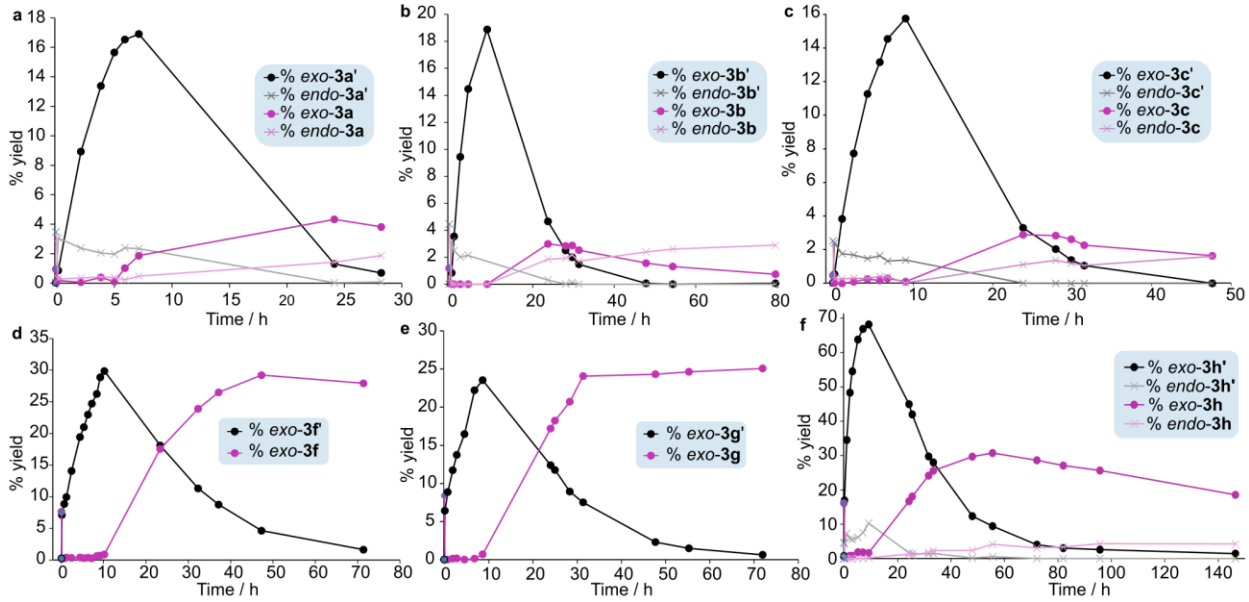

Figure S75. Evolution in time of %*exo*-**3** (purple), %*endo*-**3** (pink), %*exo*-**3'** (black) and *endo*-**3**' (grey) upon addition of 3.0 equivalents of carbodiimide **DIC** to a solution of a) **1a**, b) **1b**, c) **1c**, d) **1f**, e) **1g** or f) **1h** and **2**. The experiment starts from the equilibrium distribution of **1**, **2**, and **3** (blue circle/cross at t=0), with concentrations monitored by ^{1}H NMR. Conditions: CD_3CN:D_2O (85:15) at 40 °C. Note that amount of *exo*-**3f** formed in this experiment (d) is higher than the amount formed when mixing **1f** with **2'** (Figure S74) in aqueous acetonitrile because in the present case the experiment starts from an equilibrated mixture of **1f** and **2**, where **3f** is already present, and the adding of 3 equivalents of **DIC** extends the lifetime of **2'**.

e. Fueling with 3 equivalents of DIC over 2 cycles

To pre-equilibrated NMR tubes of **1f** or **1g** and **2** (as described in Section **5c**), 12.5 µL (0.08 mmol, 1.6 equiv.) or 11.7 µL (0.075 mmol, 1.5 equiv.) of **DIC** were added, respectively. The NMR tubes were kept in the sand

bath at 40°C and removed periodically (every 1-2 h) to acquire an NMR spectrum and monitor the systems. Once **DIC** was fully consumed and the concentration of **3f'** or **3g'** reached a plateau, NMR spectra were then recorded over longer time spans until **3f'** or **3g'** was fully hydrolyzed to **3f** or **3g** ([**3**'] ≤ 1 mM). At this point a second batch of **DIC** (12.5 µL or 11.7 µL, respectively) was added to start the second cycle.

The concentrations of the species at each point were obtained relative to the integration of the internal standard peak while taking into consideration the dilution coming from the addition of **DIC** in each cycle. The % yield of each adduct is then plotted versus time as illustrated in Figure 4a,b of the main text. Figure S76 reports the same data of Figure 4a, including a longer time window to monitor the relaxation towards equilibrium.

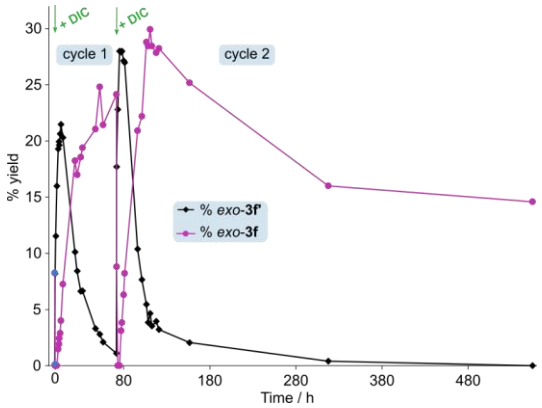

Figure S76. Evolution in time of % yield of exo-**3f** (purple) and %exo-**3f'** (black), upon repeated additions of 1.6 equivalents of **DIC**, performed in correspondence of the arrows. The experiment starts from the equilibrium distribution of **1f**, **2**, and **3f** (blue circle/diamond at t = 0), with concentrations monitored by ^{1}H NMR. Conditions: CD_3CN:D_2O 85:15 at 40 °C.

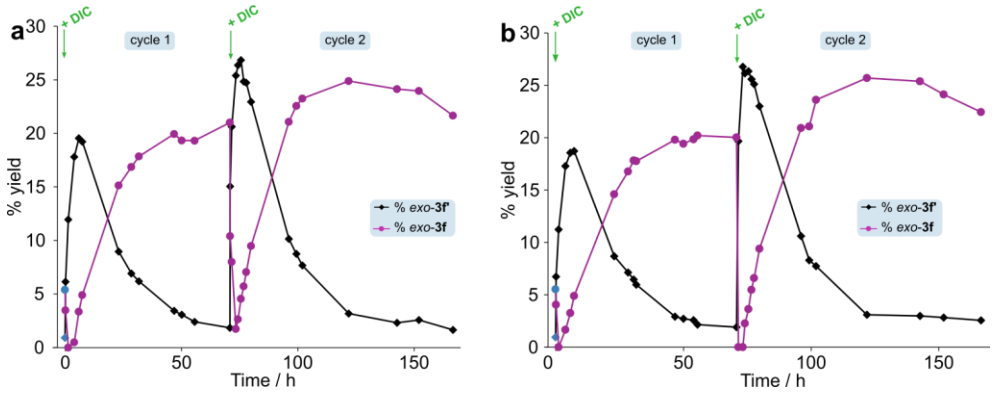

Figure S77. a-b) Evolution in time of % yield of *exo*-**3f** (purple) and *exo*-**3f'** (black), upon repeated additions of 1.5 equivalents of **DIC**, performed in correspondence of the arrows. The experiment starts from the equilibrium distribution of **1f**, **2**, and **3f** (blue circle/diamond at t = 0), with concentrations monitored by ^{1}H NMR. Conditions: CD_3CN:D_2O 85:15 at 40 °C. The two experiments (a and b) are reported to illustrate the reproducibility.

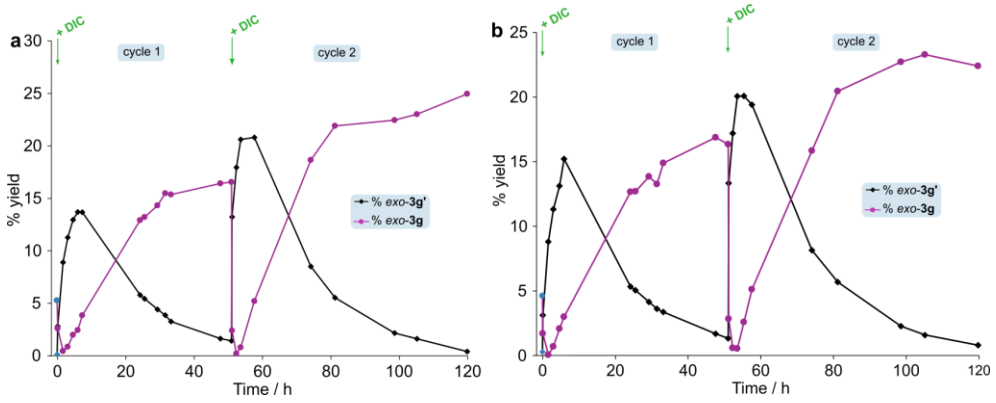

Figure S78. a-b) Evolution in time of % yield of *exo*-**3g** (purple) and *exo*-**3g**' (black), upon repeated additions of 1.5 equivalents of **DIC**, performed in correspondence of the arrows. The experiment starts from the equilibrium distribution of **1g**, **2**, and **3g** (blue circle/diamond at t = 0), with concentrations monitored by ^{1}H NMR. Conditions: CD_3CN:D_2O 85:15 at 40 °C. The two experiments (a and b) are reported to illustrate the reproducibility. This experiment was reproduced three times, and comparison of the endpoint afforded an error on the endpoint value of ±1.3%.

f. Fueling with 3 equivalents of DIC over 3 cycles

To pre-equilibrated NMR tubes of **1f-h** and **2** (as described in Section **5c**), 7.8 µL (0.05 mmol, 1.0 equiv.) of **DIC** were added. The NMR tube was kept in a sand bath at 40°C and removed periodically to monitor the system via NMR. Once **DIC** was fully consumed and the concentration of **3f-h**' reached a plateau, NMR spectra were then recorded over longer time spans until **3f-h**' were fully hydrolyzed to **3f**-**h** ([**3**'] ≤ 1mM). At this point, a second batch of **DIC** (7.8 µL) was added to start the second cycle. At the end of the second cycle ([**3**'] ≤ 1mM), a third batch of **DIC** (7.8 µL) was added to start the third cycle.

The concentrations of the species at each point were obtained relative to the integration of the internal standard peak while taking into consideration the dilution coming from the addition of **DIC** in each cycle. The % yield of each adduct is then plotted versus time (Figure S79). The data in Figure 4c of the Main Text corresponds to the concentrations recorded at equilibrium and at the end of each cycle.

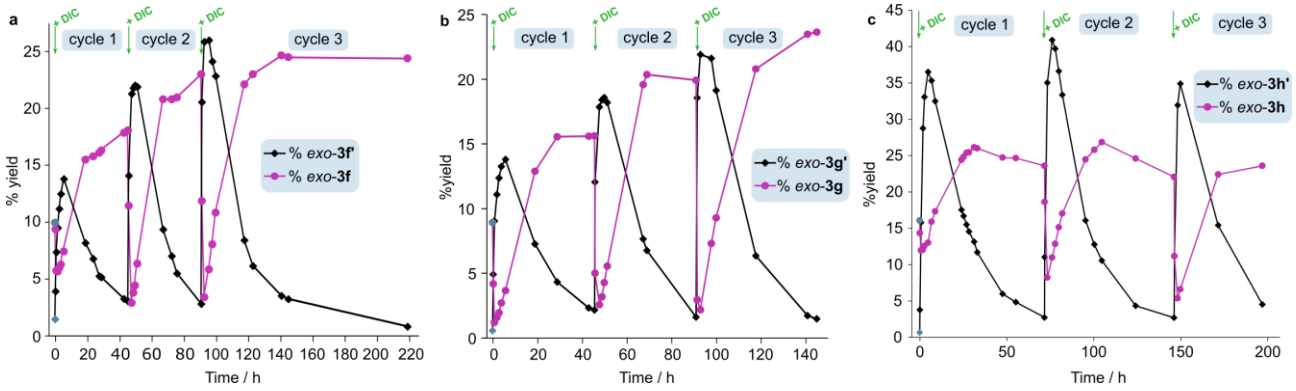

Figure S79. Evolution in time of the % yield of (a) *exo*-**3f** (purple) and *exo*-**3f**' (black), (b) *exo*-**3g** (purple) and *exo*-**3g**' (black) or (c) *exo*-**3h** (purple) and *exo*-**3h**' (black), upon repeated additions of 1.0 equivalent of **DIC**, performed in correspondence of the arrows. The experiment starts from the equilibrium distribution of **1f-h**, **2**, and **3f**-**h** (blue circle/diamond at t=0), with concentrations monitored by ^{1}H NMR. Conditions: $[\mathbf{1}]_0 = [\mathbf{2}]_0$ = 100 Mm, CD_3CN:D_2O 85:15 at 40 °C.

g. Fueling with 3 equivalents of DIC at 25 mM

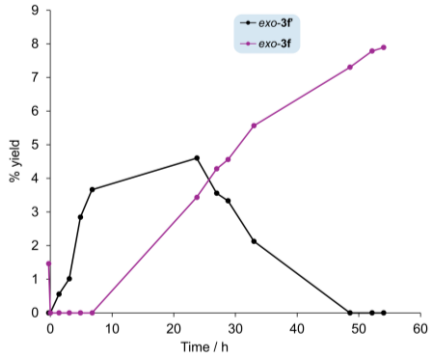

Figure S80. Evolution in time of the % yield of *exo*-**3f** (purple) and *exo*-**3f'** (black), upon addition of 3.0 equivalents of **DIC** in a single batch at a lower concentration. The experiment starts from the equilibrium distribution of **1f**, **2**, and **3f** with concentrations monitored by ^{1}H NMR. Conditions: [**1f**]$_0$ = [**2**]$_0$ = 25 mM, CD_3CN:D_2O 85:15 at 40 °C.

h. Limit of multiple fueling experiments

In order to check how the limit of stepwise fueling we fueled multiple times a pre-equilibrated NMR tube of **1f**, **2** and **3f** (as described in Section **5c**). The tube was fueled with 11.7 µL of **DIC** (0.075 mmol, 1.5 equiv.) every 48 hours and concentrations were monitored by ^{1}H NMR. until adducts *exo*-**3f'** and *exo*-**3f** stopped.

The concentrations of the species at each point were obtained relative to the integration of the internal standard peak, thus taking into consideration the dilution coming from the addition of **DIC**. The % yield of each adduct is then plotted versus time (Figure S81).

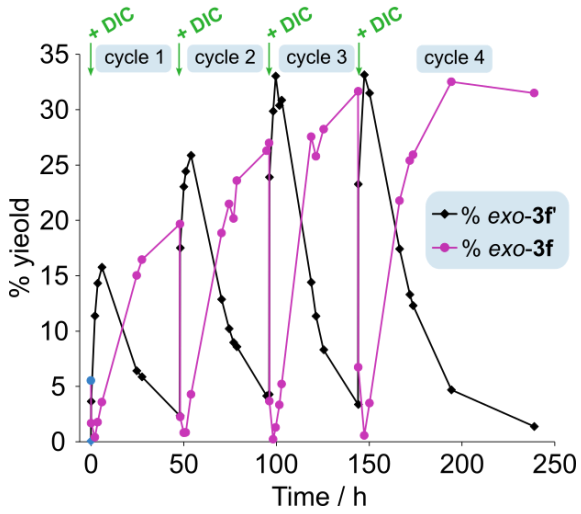

Figure S81. Evolution in time of the % yield of *exo*-**3f** (purple) and *exo*-**3f'** (black), upon addition of 1.5 equivalents of **DIC** every 48 hours; the additions were performed in correspondence of the arrows. The experiment starts from the equilibrium distribution of **1f**, **2**, and **3f** with concentrations monitored by ^{1}H NMR. Conditions: [**1f**]$_0$ = [**2**]$_0$ = 100 mM, CD_3CN:D_2O 85:15 at 40 °C.

6. Effect of waste

a. Effect of waste accumulation on equilibrium 1 + 2 ↔ 3

The effect on reaction I of the accumulated **DIU** after each fueling cycle was investigated by preparing fresh mixtures of **1** and **2** in presence of 3 equivalents of **DIU**. The mixtures were monitored by NMR until equilibrium was reached. The data obtained are collected in Table S1. The equilibrium distribution in presence of **DIU** is similar to that in its absence, while in most cases the equilibrium is shifted towards the separated components. We observed that in the presence of **DIU** more time is usually required to reach equilibrium.

Table S1. Concentrations in mM of the *exo* and *endo* isomers of **3a-c,f-h** obtained upon equilibrating **1a-c,f-h** and **2** in aqueous acetonitrile in presence and absence of **DIU**. Conditions: [**1**] = [**2**] = 100 mM; [**5**] < 300 mM (see note [a]; T= 40° C; CD_3CN:D_2O (85:15))

Diene	**in presence of DIU**[a]		**in absence of DIU**	
	[*endo*] (mM)	[*exo*] (mM)	[*endo*] (mM)	[*exo*] (mM)
3a	2.7	0.4	3.2	0.5
3b	1.9	0.5	2.4	0.5
3c	3.2	0.6	3.0	0.6
3f	n.d.	6.0	3.2	6.1
3g	n.d.	5.5	2.0	7.1
3h	3.7	12.3	4.2	15

[a]: **DIU** is not fully soluble at this concentration. n.d.: not determined due to overlapping NMR peaks.

b. Effect of waste accumulation on fueling

The effect of **DIU** accumulation on the yields of the endergonic formation of the Diels-Alder adduct was assessed using **1f** as an example. To a previously equilibrated mixture of **1f**, **2** and **3f** following the procedure described in **5c**, **DIU** was added (21.6 mg, 0.015 mmol, 3 equiv.). The mixture was then fueled with **DIC** (11.7 µL, 1.5 equiv.) and the NMR was recorded over 48h. A similar experiment was conducted in the absence of **DIU**.

The concentrations of the species at each point were obtained relative to the integration of the internal standard peak, thus taking into consideration the dilution coming from the addition of **DIC**. The % yield of each adduct is then plotted versus time (Figure S82).

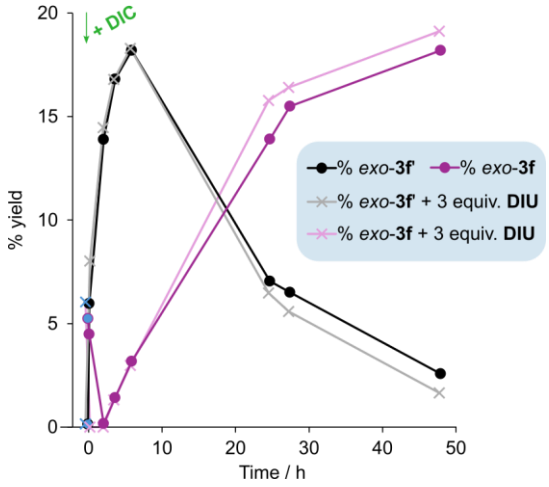

Figure S82. Evolution in time of the % yield of exo-**3f'** in absence (black circles) or presence (gray crosses) of 3 equivalents of **DIU**, and of exo-**3f** in absence (purple circles) or presence (pink crosses) of 3 equivalents of **DIU** upon addition of 1.*5* equivalent*s* of **DIC**, performed in correspondence of the arrow. The experiment starts from the equilibrium distribution of **1f**, **2**, and **3f** (blue circles/crosses at t=0), with concentrations monitored by ^{1}H NMR. Conditions: CD_3CN:D_2O (85:15) at 40 °C.

7. Effect of carbamate group on hydrolysis of 3’

To assess the effect of the carbamate group on the hydrolysis of adduct **3**' to **3**, the kinetics of the hydrolysis of carbamate-substituted *exo*-**3g**' and methyl-substituted *exo*-**3h**' into *exo*-**3g** and *exo*-**3h**, respectively, are compared. The data (Figure S83a) is extracted from the corresponding fueling experiments with 3 equiv. of **DIC** reported in Section**5d** (Figure S75e-f).

The rate of hydrolysis of *exo*-**3h**' was then checked in presence and absence of an external carbamate **4**. Two NMR tubes of **1h** (100 µL of 0.5 M mother solution in CD_3CN, 0.05 mmol) and **2**' (62.5 µL of 0.8 M mother solution in CD_3CN, 0.05 mmol) were prepared and carbamate **4** (100 µL of 0.5 M mother solution in CD_3CN, 0.05 mmol) was only added to one of the tubes. **TMB** (20 µL of 0.25 M mother solution in CD_3CN, 0.005 mmol) was added an internal standard. The solutions were diluted to 425 µL using CD_3CN, then monitored by ^1H NMR until equilibrium was reached. D_2O (75µL) was then added to both tubes to afford a mixture of CD_3CN:D_2O with 85:15 ratio (500 µL). The data are reported in Figure S83b.

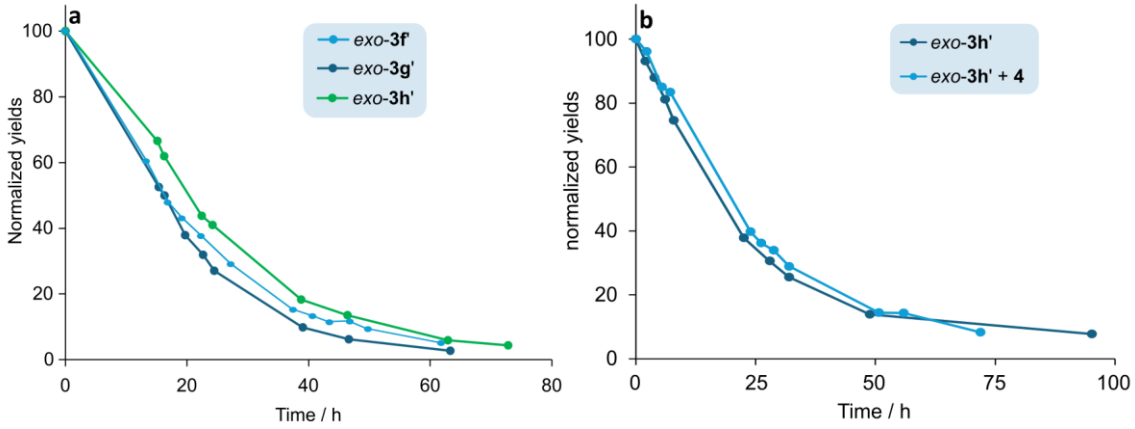

Figure S83. (a) kinetics of the hydrolysis of *exo*-**3f**' (light blue circles), *exo*-**3g**' (dark blue circles), and *exo*-**3h**' (green circles) upon the fueling of equilibrated reaction (I) between **1**(**f**,**g**,**h**) and **2**, with 3 equiv. of **DIC**. Normalized yields of **3**' are reported starting from the plateau of the anhydride adduct when hydrolysis started. Conditions: CD_3CN:D_2O 85:15 at 40 °C. (b) kinetics of hydrolysis of *exo*-**3h**' in absence (dark blue) and presence (light blue) of carbamate **4** in solution. Normalized yields of *exo*-**3h**' are reported starting from the point of addition of D_2O to an equilibrated mixture of **1h** and **2**'.

8. Calculation of stored energy and thermodynamic efficiency

In this paper, the energy stored in the system is defined as the difference between the Gibbs free energy density of a certain nonequilibrium state after the fueling, and the Gibbs free energy density of the corresponding local equilibrium state that can be obtained by relaxing the Diels-Alder reactions (driven reactions, steps **I** and **III**) to equilibrium. Note that this state is local equilibrium, because the driving reactions (steps **II** and **IV**) may still be out of equilibrium. We adopted this definition because we are specifically interested in the energy stored in the driven reactions. This definition is also consistent with the ones employed in previous studies.[3–5]

The energy stored in the system (ΔG_{DA}) was calculated using the following equation:[6]

$$\Delta G_{DA} = RT\left\{\sum_i [i]\, ln\frac{[i]}{[i]_{eq}} - [i] + [i]_{eq},\right\} \qquad \text{(S1)}$$

where R and T are the gas constant and the temperature in Kelvin, respectively, $[i]$ the concentration of chemical species in the nonequilibrium state, $[i]_{eq}$ the concentration of chemical species in the local equilibrium state.

In the main text we focus only on the energy stored as a result of the non-equilibrium distribution of species in step **I** (i = **1**, **2**, *endo*-**3**, *exo*-**3**), which is a lower bound for the total energy stored in the system. This is because the energy stored in the distribution of species related to step **III** (i = **2**', *endo*-**3**', *exo*-**3**') is strongly dependent on the equilibrium constants of step **III**, which were available from the experiments in pure acetonitrile reported in Table 1 of the main text (upon letting the mixtures reach equilibrium, if more than 48 h were required for that). These values will be different from the equilibrium constants in the aqueous acetonitrile mixture (CD_3CN:D_2O 85:15) used for the fueling experiments, which makes the estimation of the stored energy inaccurate. Moreover, the low concentration of **2**', *endo*-**3**', *exo*-**3**' at the end of each cycle would lead to further inevitable inaccuracy in the calculation of the energy stored in step **III**. Still, the calculated energy stored in the distribution of step III (i = **2**', *endo*-**3**', *exo*-**3**') only accounts for 11% of the total stored energy at maximum (see Table S6). Therefore, even if this energy is taken into consideration, the total energy stored will not be considerably larger than the reported lower bounds.

The thermodynamic efficiency of the energy storage process was calculated by dividing the stored energy by the total free energy released from the hydration of **DIC**. The latter is defined as the difference between the Gibbs free energy density of the state immediately after the fuel addition and the Gibbs free energy density of the corresponding equilibrium state. Therefore, the energy released from the driving reaction can also be calculated using Equation (S1). Note that our definition of the thermodynamic efficiency is slightly different from some of the previous studies,[3,7] as they consider a non-equilibrium steady state, and thus defined the thermodynamic efficiency as the efficiency of energy transduction from a driving process to a driven process at the steady state.

The values of stored energy reported for a pseudorotaxane system assembled at non-equilibrium concentrations[8] (4.4 J/L) and polymer chain entanglement driven by a light-driven molecular rotor[9] (72 J/L) were obtained using an analogous procedure. In particular, for the latter calculation the following data were employed. The total concentration was set to be 0.01 M based on the NMR experiment in Figure 4 of that work. The photostationary state (PSS) distribution was obtained from the UPLC measurement in Figure 3c (SI page S15) of that work. The PSS in the NMR experiment was assumed to be the same with the one shown in Figure 3c.

For consistency, we calculated the energy stored in the endergonic formation of a Diels-Alder adduct[10] using the same procedure used in our case, and found a value of 14 J/L. This value is almost identical to the 13 J/L that one would obtain using the energy values provided in that work.

a. Fueling with 3 equiv. of DIC over 1 cycle

The nonequilibrium distributions were obtained from the fueling experiments reported in Figure S75 and are reported in Table S2. By the timepoints of distributions shown in Table S2, all **DIC** fuel had been consumed and [**3**] was not increasing any longer.

Table S2. Nonequilibrium distributions obtained from the fueling experiments with 3 equiv. of **DIC** over 1 cycle (Section **5d**).

Diene	[**1**] (mM)	[**2**] (mM)	[*endo*-**3**] (mM)	[*exo*-**3**] (mM)	[**2'**] (mM)	[*endo*-**3'**] (mM)	[*exo*-**3'**] (mM)
1a	85	83	2	3	1	0	1
1b	94	94	2	3	1	0	1
1c	82	93	1	2.6	1	0	1
1f	67	72	0	23	0	0	1
1f at 25 mM	22	24	0	1.6	0.1	0	0.3
1g	62	68	0	21	0	0	0.7
1h	53	110	2	26	0	0	1

For the calculation of corresponding local equilibrium distributions, we first need equilibrium constants for step **I** and **III**, which are:

$$K_{I,endo} = \frac{[endo-\mathbf{3}]_{eq}}{[\mathbf{1}]_{eq}[\mathbf{2}]_{eq}}, \quad K_{I,exo} = \frac{[exo-\mathbf{3}]_{eq}}{[\mathbf{1}]_{eq}[\mathbf{2}]_{eq}},$$

$$K_{III,endo} = \frac{[endo-\mathbf{3'}]_{eq}}{[\mathbf{1}]_{eq}[\mathbf{2'}]_{eq}}, K_{III,exo} = \frac{[exo-\mathbf{3'}]_{eq}}{[\mathbf{1}]_{eq}[\mathbf{2'}]_{eq}},$$

(S2–5)

respectively. $K_{I,endo}$ and $K_{I,exo}$ were calculated from the concentration distributions before the fuel addition in the fueling experiments (Table S3).

Table S3. $K_{I,endo}$ and $K_{I,exo}$ calculated from the concentration distributions before the fuel addition in the fueling experiments (Section **5a**).

Diene	[**1**] (mM)	[**2**] (mM)	[*endo*-**3**] (mM)	[*exo*-**3**] (mM)	$K_{I,endo}$ (mM^{-1})	$K_{I,exo}$ (mM^{-1})
1a	92	95	3	0.5	3.4×10^{-4}	5.7×10^{-5}
1b	94	106	3	0.5	3.0×10^{-4}	5.0×10^{-5}
1c	88	94	2	0.5	2.4×10^{-4}	6.0×10^{-5}
1f	79	83	3	6	4.6×10^{-4}	9.2×10^{-4}
1f at 25 mM	24	25	0	0.25	4.6×10^{-4}	9.2×10^{-4}
1g	82	87	2	7	2.8×10^{-4}	9.8×10^{-4}
1h	62	106	4	15	6.1×10^{-4}	2.3×10^{-3}

$K_{III,endo}$ and $K_{III,exo}$ were calculated from the concentration distributions in the equilibration experiments in pure acetonitrile (Table S4). They could not be obtained from experiments in the aqueous acetonitrile mixture

(CD_3CN:D_2O 85:15) used in the fueling experiments, because water causes the hydrolysis of anhydrides (**2**' and **3**').

Table S4. $K_{III,endo}$ and $K_{III,exo}$ calculated from the concentration distributions in the equilibration experiments in pure acetonitrile.

Diene	[**1**] (mM)	[**2**'] (mM)	[*endo*-**3**'] (mM)	[*exo*-**3**'] (mM)	$K_{III,endo}$ (mM^{-1})	$K_{III,exo}$ (mM^{-1})
1a	83	75	0.8	20	1.3×10^{-4}	3.2×10^{-3}
1b	78	80	0.9	20	1.4×10^{-4}	3.2×10^{-3}
1c	75	76	0.9	22	1.6×10^{-4}	3.9×10^{-3}
1f	47	46	0.3	65	1.4×10^{-4}	3.0×10^{-2}
1g	54	42	0	50	$<1.0 \times 10^{-5}$	2.2×10^{-2}
1h	32	34	0	72	$<1.0 \times 10^{-5}$	6.6×10^{-2}

The local equilibrium distributions were calculated by starting from the nonequilibrium distributions (Table S2), and relaxing step **I** and **III** to equilibrium. Step **I** and **III** were deemed to be equilibrated when the equilibrium constants calculated from the derived distributions agreed to the ones obtained experimentally (Table S3 and Table S4). During this calculation, the following mass balances were respected:

$$[\mathbf{1}] + [endo-\mathbf{3}] + [exo-\mathbf{3}] + [endo-\mathbf{3}'] + [exo-\mathbf{3}'] = [\mathbf{1}]_{eq} + [endo-\mathbf{3}]_{eq} + [exo-\mathbf{3}]_{eq} + [endo-\mathbf{3}']_{eq} + [exo-\mathbf{3}']_{eq}$$

$$[\mathbf{2}] + [endo-\mathbf{3}] + [exo-\mathbf{3}] = [\mathbf{2}]_{eq} + [endo-\mathbf{3}]_{eq} + [exo-\mathbf{3}]_{eq}$$

$$[\mathbf{2}'] + [endo-\mathbf{3}'] + [exo-\mathbf{3}'] = [\mathbf{2}']_{eq} + [endo-\mathbf{3}']_{eq} + [exo-\mathbf{3}']_{eq}.$$

(S6–8)

Because of the constraints of the equilibrium constants and the mass balances, the local equilibrium distributions corresponding to the initial nonequilibrium distributions could be unambiguously determined (Table S5).

Table S5. Local equilibrium distributions corresponding to the initial nonequilibrium distributions.

Diene	[**1**] (mM)	[**2**] (mM)	[*endo*-**3**] (mM)	[*exo*-**3**] (mM)	[**2**'] (mM)	[*endo*-**3**'] (mM)	[*exo*-**3**'] (mM)
1a	88	85	2.6	0.43	1.5	1.7×10^{-2}	0.44
1b	96	96	2.8	0.46	1.5	2.2×10^{-2}	0.47
1c	84	94	1.9	0.48	1.5	1.9×10^{-2}	0.48
1f	81	86	3.2	6.3	0.29	3.4×10^{-3}	0.71
1f at 25 mM	24	25	$<1.0 \times 10^{-3}$	0.25	0.26	$<1.0 \times 10^{-3}$	0.18
1g	75	81	1.8	6.1	0.26	$<1.0 \times 10^{-3}$	0.44
1h	61	117	4.3	16	0.20	$<1.0 \times 10^{-3}$	0.80

By plugging the initial nonequilibrium distributions and the corresponding local equilibrium distributions into Equation (S1), the energy stored in the distribution of species mainly related to step **I** (i = **1**, **2**, *endo*-**3**, *exo*-**3**) and the energy stored in the distribution of species related to step **III** (i = **2**', *endo*-**3**', *exo*-**3**') were calculated individually (Table S6). As was discussed at the beginning of this section, the latter only accounts for 11% of the total stored energy at maximum, and the former energy was reported as the lower bound of the total stored energy in the main text.

Table S6. Energy stored in the distribution of species **1**, **2**, *endo*-**3**, *exo*-**3** and in the distribution of species **2'**, *endo*-**3'**, *exo*-**3'**, and corresponding thermodynamic efficiency. R = 8.314 J/mol·K and T = 40° C.

Diene	**1**, **2**, *endo*-**3**, *exo*-**3**		**2'**, *endo*-**3'**, *exo*-**3'**	
	Stored energy (J/L)	Efficiency (%)	Stored energy (J/L)	Efficiency (%)
1a	8.8	3.8×10^{-2}	1.0	4.4×10^{-3}
1b	8.4	3.6×10^{-2}	0.91	3.9×10^{-3}
1c	6.7	2.9×10^{-2}	0.84	3.6×10^{-3}
1f	49	0.21	0.91	3.9×10^{-3}
1f at 25 mM	4.6	7.4×10^{-2}	0.15	2.4×10^{-3}
1g	40	0.17	0.86	3.7×10^{-3}
1h	10	4.4×10^{-2}	0.58	2.5×10^{-3}

For calculating the energy released from hydration of the DIC fuel, we first obtained the distribution of **DIC**, D_2O and **DIU** immediately after the fuel addition in the fueling experiments (Table S7).

Table S7. Distribution of **DIC**, D_2O and **DIU** immediately after the fuel addition, estimated equilibrium constant for the fuel hydration reaction, estimated equilibrium distribution, and the calculated energy released from the fuel hydration reaction. R = 8.314 J/mol·K and T = 40° C.

Nonequilibrium distribution			K_h (mM^{-1})	Estimated equilibrium distribution			Released energy (J/L)
[**DIC**] (mM)	[D_2O] (mM)	[**DIU**] (mM)		[**DIC**] (mM)	[D_2O] (mM)	[**DIU**] (mM)	
280	7600	0	2.2×10^{10}	1.7×10^{-12}	7320	280	2.3×10^{4}
73	7600	0	2.2×10^{10}	4.4×10^{-13}	7527	73	6.2×10^{3}

The equilibrium constant for the fuel hydration reaction,

$$K_h = \frac{[\mathbf{DIU}]_{eq}}{[\mathbf{DIC}]_{eq}[D_2O]_{eq}} = \exp\left(-\frac{\Delta G^\circ{}_h}{RT}\right), \qquad \text{(S9)}$$

was calculated from the standard Gibbs free energy of reaction obtained from theoretical calculation ($\Delta G^\circ{}_h$ = −80 kJ/mol).[11] The equilibrium distribution was calculated by starting from the nonequilibrium distribution, and relaxing the hydration reaction to equilibrium. The reaction was deemed to be equilibrated when the equilibrium constant calculated from the derived distribution agreed to the one obtained from theoretical calculation. During this calculation, the following mass balances were respected:

$$[\mathbf{DIC}] + [\mathbf{DIU}] = [\mathbf{DIC}]_{eq} + [\mathbf{DIU}]_{eq}, \qquad [D_2O] + [\mathbf{DIU}] = [D_2O]_{eq} + [\mathbf{DIU}]_{eq}. \qquad \text{(S10, 11)}$$

By plugging the initial nonequilibrium distribution and the corresponding equilibrium distribution into Equation (S1), the total energy released from the hydration reaction of the fuel was calculated (Table S7). The thermodynamic efficiencies shown in Table S6 were calculated by dividing the stored energies by the total free energy released from the hydration reaction.

b. Fueling with 3 equivalents of DIC over 2 cycles

The stored energy and corresponding thermodynamic efficiency after the first fuel addition in the multiple fuel addition experiments (1.6 eq. × 2) were calculated in the same way as the single fuel addition experiments (Tables S8).

Tables S8. Nonequilibrium distributions after the first fueling obtained from the fueling experiments (5e), corresponding local equilibrium distributions, energy released from the fuel hydration reaction, and stored energy and thermodynamic efficiency. R = 8.314 J/mol·K and T = 40° C.

Nonequilibrium Distributions

Diene	[**1**] (mM)	[**2**] (mM)	[*endo*-**3**] (mM)	[*exo*-**3**] (mM)	[**2'**] (mM)	[*endo*-**3'**] (mM)	[*exo*-**3'**] (mM)
1f	66	88	0	19	0	0	1
1g	73	87	0	15	0	0	1.5

Local Equilibrium Distributions

Diene	[**1**] (mM)	[**2**] (mM)	[*endo*-**3**] (mM)	[*exo*-**3**] (mM)	[**2'**] (mM)	[*endo*-**3'**] (mM)	[*exo*-**3'**] (mM)
1f	75	97	3.4	6.7	0.31	3.1×10^{-3}	0.69
1g	79	93	2.1	7.2	0.55	$<1.0 \times 10^{-3}$	0.95

Diene	Nonequilibrium distribution			K_h(mM^{-1})	Estimated equilibrium distribution			Released energy (J/L)
	[**DIC**] (mM)	[D_2O] (mM)	[**DIU**] (mM)		[**DIC**] (mM)	[D_2O] (mM)	[**DIU**] (mM)	
1f	150	7800	0	2.2×10^{10}	8.9×10^{-13}	7650	150	1.3×10^{4}
1g	140	7800	0	2.2×10^{10}	8.3×10^{-13}	7660	140	1.2×10^{4}

Diene	**1**, **2**, *endo*-**3**, *exo*-**3**		**2'**, *endo*-**3'**, *exo*-**3'**	
	Stored energy (J/L)	Efficiency (%)	Stored energy (J/L)	Efficiency (%)
1f	31	0.24	0.96	7.5×10^{-3}
1g	15	0.12	1.8	1.5×10^{-2}

Following a similar procedure, the stored energy after the second fuel addition was calculated (Table S9). This time, the differences between the stored energy after the second and the first fuel addition were also calculated. Thermodynamic efficiencies were calculated for this net increase in the stored energy, by dividing these increases by the energy released from the second batch of the fuel.

Tables S9. Nonequilibrium distributions after the second fueling obtained from the fueling experiments (Section **5e**), corresponding local equilibrium distributions, energy released from the fuel hydration reaction, and increase in stored energy compared to the first fuel addition and thermodynamic efficiency. Thermodynamic efficiency was not calculated for the case when the stored energy decreased after the second fuel addition. R = 8.314 J/mol·K and T = 40° C.

Nonequilibrium Distributions

Diene	[**1**] (mM)	[**2**] (mM)	[*endo*-**3**] (mM)	[*exo*-**3**] (mM)	[**2'**] (mM)	[*endo*-**3'**] (mM)	[*exo*-**3'**] (mM)
1f	73	94	0	23	0	0	0.6
1g	68	85	0	20	0	0	1.8

Local Equilibrium Distributions

Diene	[**1**] (mM)	[**2**] (mM)	[*endo*-**3**] (mM)	[*exo*-**3**] (mM)	[**2'**] (mM)	[*endo*-**3'**] (mM)	[*exo*-**3'**] (mM)
1f	84	105	4.0	8.1	0.17	2.0×10^{-3}	0.43
1g	79	95	2.1	7.4	0.66	$<1.0 \times 10^{-3}$	1.1

Diene	Nonequilibrium distribution			K_h(mM^{-1})	Estimated equilibrium distribution			Released energy (J/L)
	[**DIC**] (mM)	[D_2O] (mM)	[**DIU**] (mM)		[**DIC**] (mM)	[D_2O] (mM)	[**DIU**] (mM)	
1f	150	7470	150	2.2×10^{10}	1.8×10^{-12}	7320	290	1.2×10^{4}
1g	140	7500	140	2.2×10^{10}	1.7×10^{-12}	7360	270	1.1×10^{4}

Diene	**1**, **2**, *endo*-**3**, *exo*-**3**		**2'**, *endo*-**3'**, *exo*-**3'**	
	Increase in stored energy (J/L)	Efficiency (%)	Increase in stored energy (J/L)	Efficiency (%)
1f	6.8	5.7×10^{-2}	−0.43	-
1g	13.3	0.12	0.35	3.1×10^{-3}

c. Fueling with 3 equivalents of DIC over 3 cycles

The stored energy and corresponding thermodynamic efficiency after each fuel addition in the multiple fuel addition experiments (1.0 eq. × 3) were calculated in the same way as the Section **8b** (Tables S10, Tables S11, Tables S12). For diene **1h**, the calculation was done only for the first fueling cycle because the second and third fuel additions showed almost identical responses to the first.

Tables S10. Nonequilibrium distributions after the first fueling obtained from the fueling experiments (5f), corresponding local equilibrium distributions, energy released from the fuel hydration reaction, and stored energy and thermodynamic efficiency. R = 8.314 J/mol·K and T = 40° C.

Nonequilibrium Distributions

Diene	[**1**] (mM)	[**2**] (mM)	[*endo*-**3**] (mM)	[*exo*-**3**] (mM)	[**2'**] (mM)	[*endo*-**3'**] (mM)	[*exo*-**3'**] (mM)
1f	71	82	0	15	0	0	1.6
1g	85	84	0	13	0	0	1.9
1h	47	105	3	21	0	0	2.8

Local Equilibrium Distributions

Diene	[**1**] (mM)	[**2**] (mM)	[*endo*-**3**] (mM)	[*exo*-**3**] (mM)	[**2'**] (mM)	[*endo*-**3'**] (mM)	[*exo*-**3'**] (mM)
1f	77	88	3.1	6.2	0.48	4.9×10^{-3}	1.1
1g	89	87	2.2	7.6	0.64	$<1.0 \times 10^{-3}$	1.3
1h	54	112	3.6	14	0.61	$<1.0 \times 10^{-3}$	2.2

Diene	Nonequilibrium distribution			K_h(mM^{-1})	Estimated equilibrium distribution			Released energy (J/L)
	[**DIC**] (mM)	[D_2O] (mM)	[**DIU**] (mM)		[**DIC**] (mM)	[D_2O] (mM)	[**DIU**] (mM)	
1f, **1g**	94	7860	0	2.2×10^{10}	5.5×10^{-13}	7770	94	8.1×10^{3}
1h	98	8170	0	2.2×10^{10}	5.5×10^{-13}	8070	98	8.4×10^{3}

Diene	**1**, **2**, *endo*-**3**, *exo*-**3**		**2'**, *endo*-**3'**, *exo*-**3'**	
	Stored energy (J/L)	Efficiency (%)	Stored energy (J/L)	Efficiency (%)
1f	21	0.26	1.5	1.9×10^{-2}
1g	10	0.13	2.0	2.5×10^{-2}
1h	6.2	7.4×10^{-2}	1.8	2.1×10^{-2}

Tables S11. Nonequilibrium distributions after the second fueling obtained from the fueling experiments (5f), corresponding local equilibrium distributions, energy released from the fuel hydration reaction, and increase in stored energy compared to the first fuel addition and thermodynamic efficiency. Thermodynamic efficiency was not calculated for the case when the stored energy decreased after the second fuel addition. R = 8.314 J/mol·K and T = 40° C.

Nonequilibrium Distributions

Diene	[**1**] (mM)	[**2**] (mM)	[*endo*-**3**] (mM)	[*exo*-**3**] (mM)	[**2'**] (mM)	[*endo*-**3'**] (mM)	[*exo*-**3'**] (mM)
1f	63	84	0	18	0.5	0	1
1g	87	86	0	17	0	0	1.7

Local Equilibrium Distributions

Diene	[**1**] (mM)	[**2**] (mM)	[*endo*-**3**] (mM)	[*exo*-**3**] (mM)	[**2'**] (mM)	[*endo*-**3'**] (mM)	[*exo*-**3'**] (mM)
1f	72	93	3.0	6.1	0.47	4.5×10^{-3}	1.0
1g	94	92	2.4	8.5	0.55	$<1.0 \times 10^{-3}$	1.1

Diene	Nonequilibrium distribution			K_h(mM^{-1})	Estimated equilibrium distribution			Released energy (J/L)
	[**DIC**] (mM)	[D_2O] (mM)	[**DIU**] (mM)		[**DIC**] (mM)	[D_2O] (mM)	[**DIU**] (mM)	
1f, **1g**	93	7650	93	2.2×10^{10}	1.1×10^{-12}	7560	190	7.6×10^{3}

Diene	**1**, **2**, *endo*-**3**, *exo*-**3**		**2'**, *endo*-**3'**, *exo*-**3'**	
	Increase in stored energy (J/L)	Efficiency (%)	Increase in stored energy (J/L)	Efficiency (%)
1f	9.5	0.13	−1.5	-
1g	5.9	7.8×10^{-2}	−0.29	-

Tables S12. Nonequilibrium distributions after the third fueling obtained from the fueling experiments (Section **5f**), corresponding local equilibrium distributions, energy released from the fuel hydration reaction, and increase in stored energy compared to the second fuel addition and thermodynamic efficiency. Thermodynamic efficiency was not calculated for the case when the stored energy decreased after the third fuel addition. R = 8.314 J/mol·K and T = 40° C.

Nonequilibrium Distributions

Diene	[**1**] (mM)	[**2**] (mM)	[*endo*-**3**] (mM)	[*exo*-**3**] (mM)	[**2'**] (mM)	[*endo*-**3'**] (mM)	[*exo*-**3'**] (mM)
1f	67	80	0	19	0	0	1.2
1g	79	82	0	18	0	0	1.5

Local Equilibrium Distributions

Diene	[**1**] (mM)	[**2**] (mM)	[*endo*-**3**] (mM)	[*exo*-**3**] (mM)	[**2'**] (mM)	[*endo*-**3'**] (mM)	[*exo*-**3'**] (mM)
1f	77	90	3.1	6.3	0.36	3.8×10^{-3}	0.84
1g	88	90	2.3	7.7	0.51	$<1.0 \times 10^{-3}$	0.99

Diene	Nonequilibrium distribution			K_h(mM^{-1})	Estimated equilibrium distribution			Released energy (J/L)
	[**DIC**] (mM)	[D_2O] (mM)	[**DIU**] (mM)		[**DIC**] (mM)	[D_2O] (mM)	[**DIU**] (mM)	
1f, **1g**	92	7460	180	2.2×10^{10}	1.7×10^{-12}	7370	280	7.4×10^{3}

Diene	**1**, **2**, *endo*-**3**, *exo*-**3**		**2'**, *endo*-**3'**, *exo*-**3'**	
	Increase in stored energy (J/L)	Efficiency (%)	Increase in stored energy (J/L)	Efficiency (%)
1f	2.5	3.4×10^{-2}	1.1	1.5×10^{-2}
1g	4.8	6.4×10^{-2}	−0.12	-

9. DFT calculations

To gain deeper insight about the outcomes of the fueled operation, we conducted DFT calculations. It is known that the *exo*/*endo* selectivity of the Diels-Alder reactions of furan derivatives is thermodynamically controlled, in contrast to the kinetically controlled Diels-Alder reactions of cyclopentadiene derivatives.[12] Therefore, we only computed equilibrium geometries and corresponding energies of each molecule. When a molecule can take multiple conformers, only the conformer with the lowest Gibbs free energy is reported. The calculation was done for furan derivatives **1a**, **1d**, **1f** and **1h**, which are representative of different substitution patterns of furan.

The calculation was done in Spartan'20 under gas phase conditions. We first screened conformers with molecular mechanics calculation (MMFF) and optimized the structures of remaining conformers with the Hartree-Fock method calculation (HF/3-21G). These geometries were further subjected to the DFT calculation (ωB97X-D/6-31G*) to compute the total energy, and only the conformers with sufficiently low energy were subjected to final geometry optimization (ωB97X-D/6-31G*). For compound **1h**, **2**, **2'**, *exo*/*endo*-**3h** and *exo*/*endo*-**3h'**, only one geometry optimization (ωB97X-D/6-31G*) was performed. XYZ coordinates for all structures are listed in the Appendix.

The results of the DFT calculation were consistent with the *exo*/*endo* selectivity observed in equilibration experiments with furans **1** and dienophiles **2** or **2'** (Table 1 and Figure 3a in the main text, SI Section 4b): when the *exo*- adduct was favored in experiments, the calculated Gibbs free energy of the *exo*- adduct was lower than the *endo*- adduct (Figure S85–S88). In most cases, *exo*- adducts were favored over *endo*- adducts. This is because *exo*- adducts have less steric clashing between the substituents of a furan ring and the substituents of dienophiles (diacid or anhydride group). However, the adduct formation between furans with a urea group at the 2-position (**1a**, **1b** and **1c**) and maleic acid **2** showed inverted selectivity, favoring the *endo*- adducts. DFT calculation of *exo*/*endo*-**3a** suggested that this is due to a hydrogen bond between the carboxylic group and the urea group, which was present only in *endo*-**3a** (Figure S85). In *endo*-**3a'**, this hydrogen bond disappeared, which explains why the normal selectivity (favoring the *exo*- adduct) was recovered in this case. Interactions between the carboxyl/carbonyl group and the urea group were also present in *exo*-**3a** and *exo*/*endo*-**3a'**,[13] but these groups were poorly arranged for forming a hydrogen bond as in *endo*-**3a**, which makes these interactions weaker. A similar hydrogen bond was observed in *endo*-**3d** between the carboxylic group and the carbamate group, which made the calculated energy of *endo*-**3d** lower than *exo*-**3d** (Figure S86). However, the low yield and slow reaction kinetics of these adducts in the experimental investigation prevented their study under equilibrium conditions to assess selectivity between *exo*- and *endo*-**3d** experimentally. Thus, we could not compare the result of calculation with experimental observation in this case.

As regards to the yield of adduct formation, 3-substituted furans (**1f**, **1g**, **1h**) tend to have higher yields than 2-substituted furans (**1a**–**1e**) in equilibration experiments with maleic acid **2** or maleic anhydride **2'**. This is because substituents at the 3-position of furan have less steric clashing with substituents of the dienophiles when adducts are formed.[12]

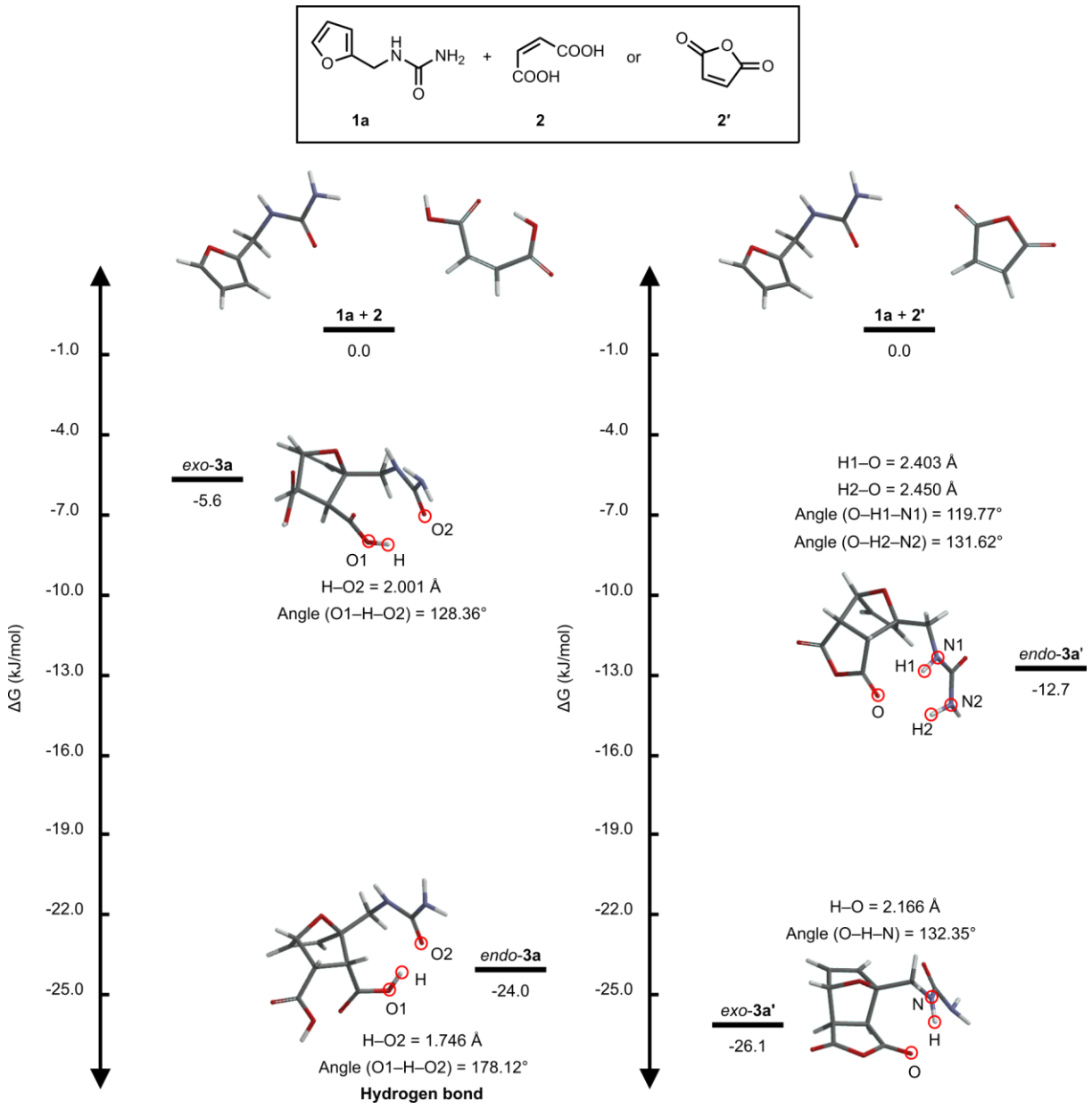

Figure S84. Calculated geometry and energy of **1a**, **2**, **2'** and adducts formed from them. Relative Gibbs free energy in comparison to the reactants are shown. Interacting moieties in adducts are highlighted with a red circle together with a relevant distance and an angle.

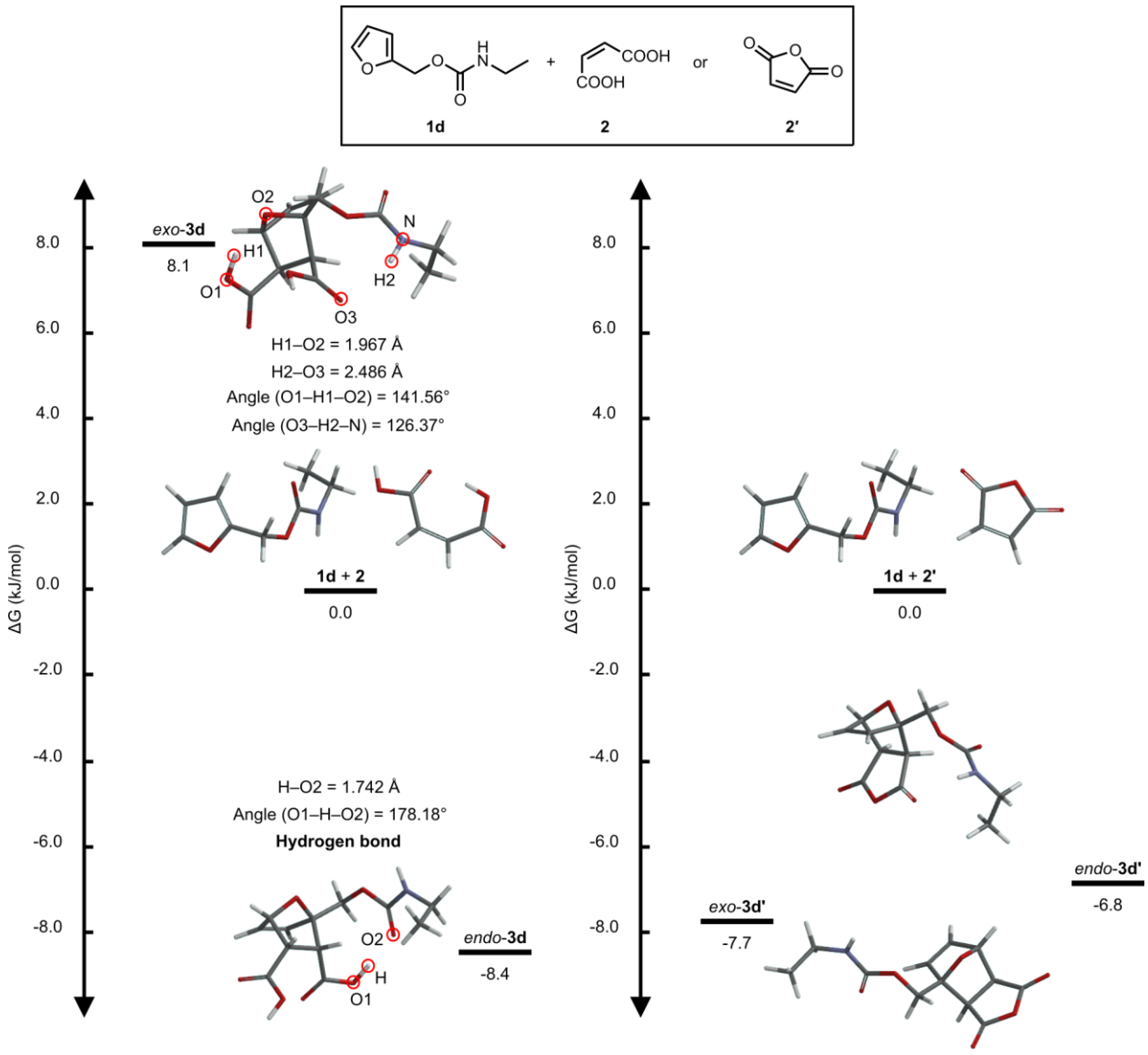

Figure S85. Calculated geometry and energy of **1d**, **2**, **2'** and adducts formed from them. Relative Gibbs free energy in comparison to the reactants are shown. Interacting moieties in adducts are highlighted with a red circle together with a relevant distance and an angle.

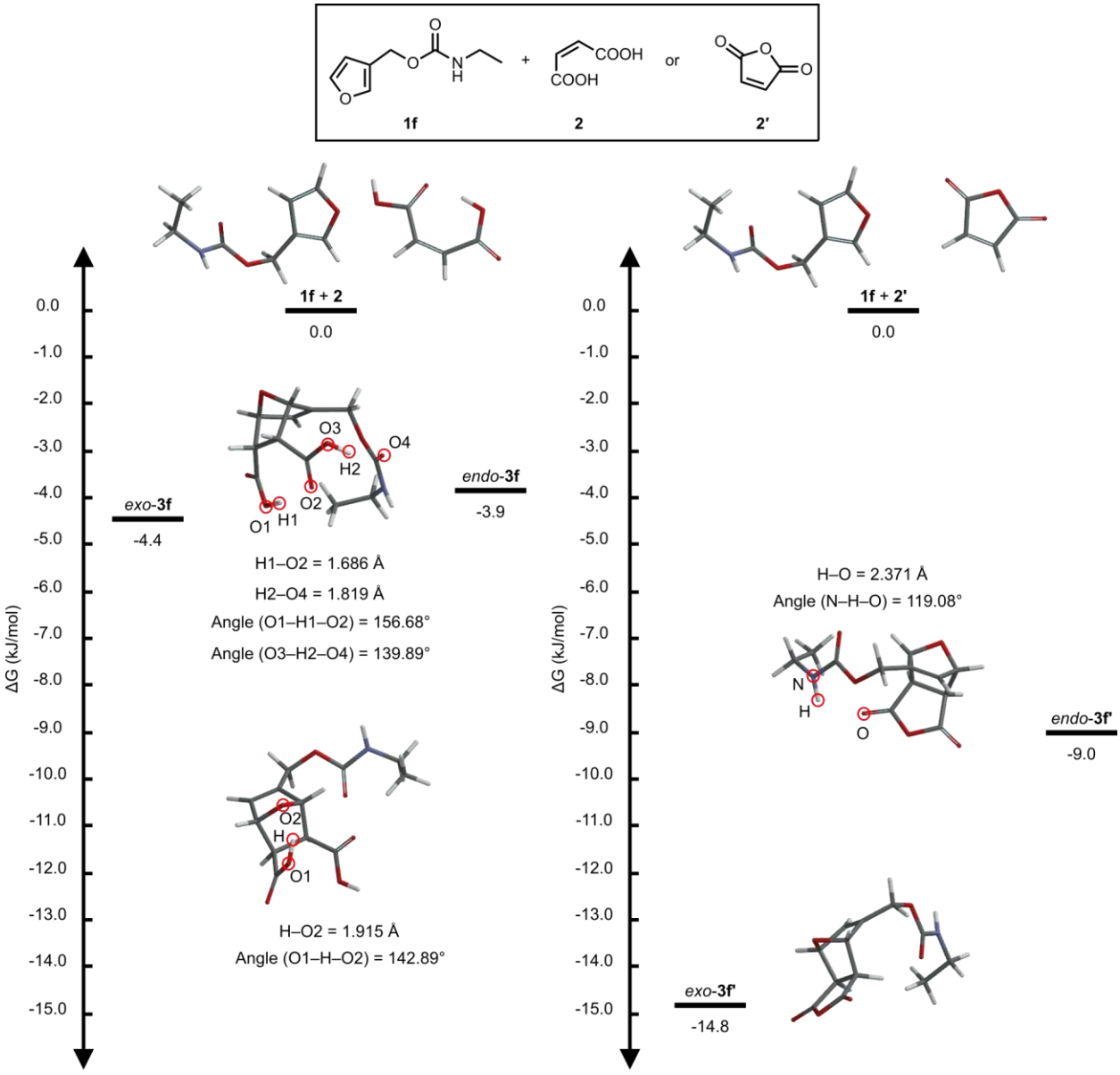

Figure S86. Calculated geometry and energy of **1f**, **2**, **2'** and adducts formed from them. Relative Gibbs free energy in comparison to the reactants are shown. Interacting moieties in adducts are highlighted with a red circle together with a relevant distance and an angle.

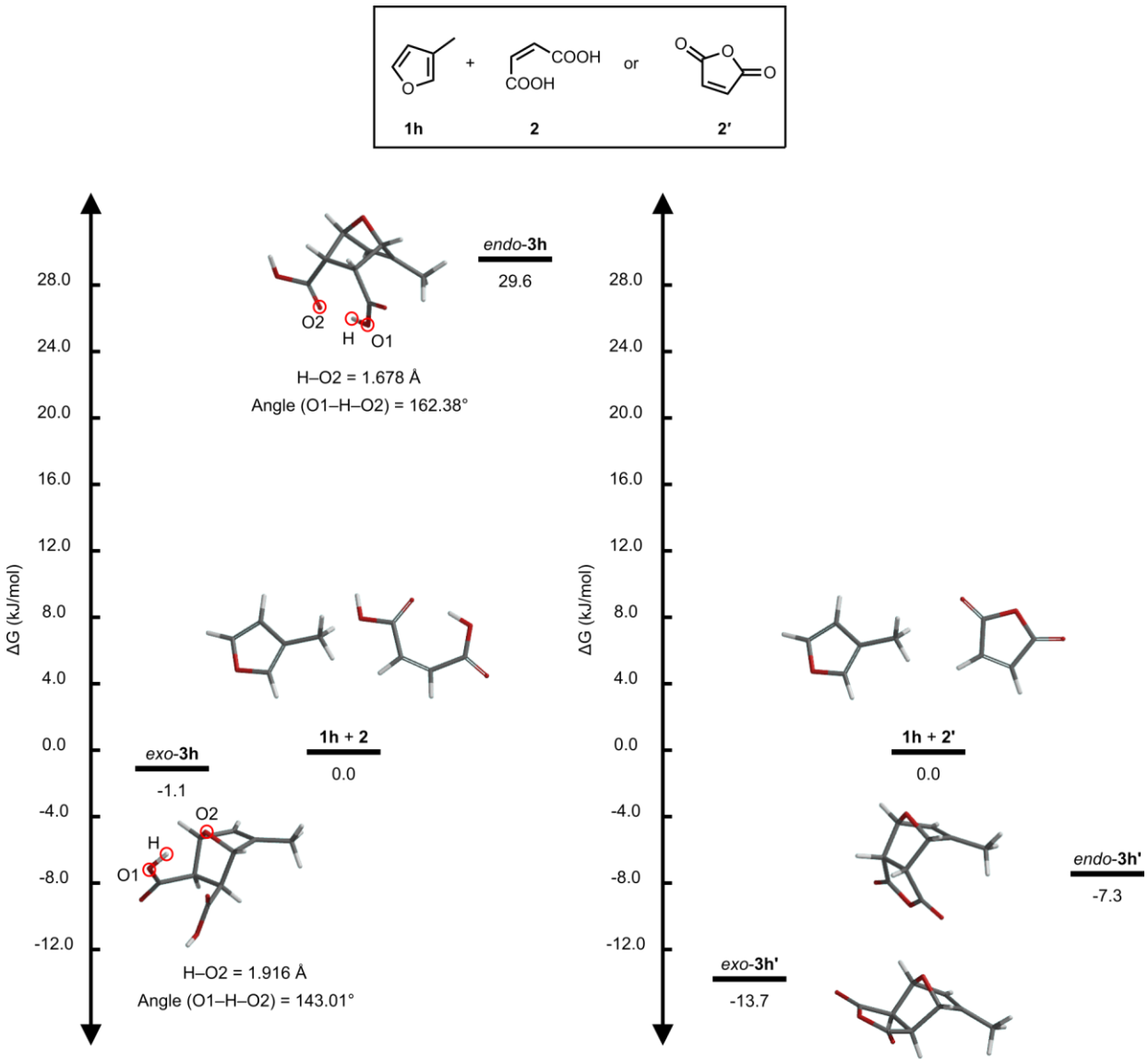

Figure S87. Calculated geometry and energy of **1h**, **2**, **2'** and adducts formed from them. Relative Gibbs free energy in comparison to the reactants are shown. Interacting moieties in adducts are highlighted with a red circle together with a relevant distance and an angle.

In experiments, we observed that the half-life of anhydride *exo*-**3h'** (20 h in the presence of 3 equivalents of DIC) was longer than that of anhydrides *exo*-**3f'** and *exo*-**3g'** (ca. 16 h), and that faster hydrolysis of *exo*-**3f'** and *exo*-**3g'** is due to an intramolecular effect between the carbamate group and the anhydride part (SI Section 7). To gain further insights into this effect from DFT calculations, we compared the charges at the carbon atoms of two carbonyl groups of the anhydride part in *exo*-**3f'** and *exo*-**3h'**, as well as the energy level of LUMO (Figure S89). We also did this comparison for *endo*-**3f'** and *endo*-**3h'**. In the case of *exo*-**3f'** and *exo*-**3h'**, we observed no significant difference in the charges at the reacting carbon atoms or the energy level of LUMO. This is because the carbamate group and the anhydride part in *exo*-**3f'** are too far apart to interact directly. Therefore, we think that the interaction between these groups is bridged by some other species in the system, most likely by a cluster of water molecules.[14] Note that this effect is not taken into consideration in our DFT calculation because it was done in gas phase conditions. On the other hand, in the case of *endo*-**3f'** and *endo*-**3h'**, one of the carbon atoms in *endo*-**3f'** in close proximity to the carbamate group had a larger positive charge than the corresponding carbon atom in *endo*-**3h'**. Also, *endo*-**3f'** had lower LUMO energy than *endo*-**3h'**. These indicate direct interaction between the carbamate group and the anhydride part in *endo*-**3f'**.

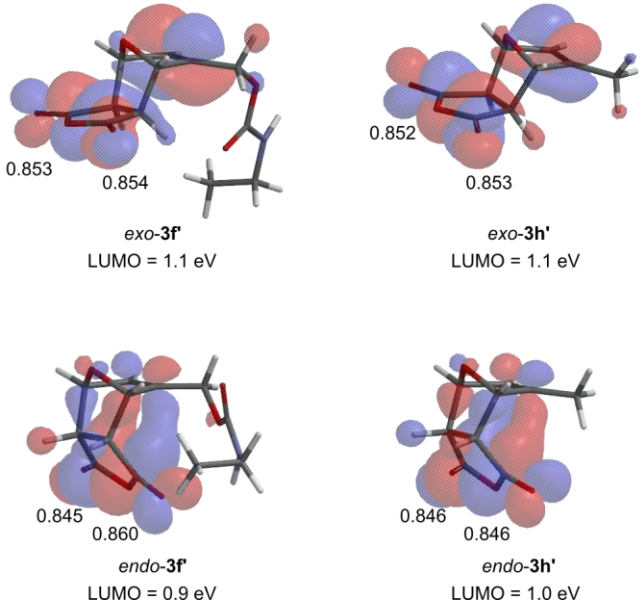

Figure S88. Distribution and energy level of LUMO, and natural charges at the carbon atoms of anhydride carbonyl groups of *exo*-**3f'**, *exo*-**3h'**, *endo*-**3f'** and *endo*-**3h'**.

10. References

[1] R. G. Fischer, J. E. Lancaster, A. Zweig. New Method for Selective Monofluorination of Aromatics Using Silver Difluoride, *J. Org. Chem.* **1980**, *45*, 3597–3603.

[2] K. Das, L. Gabrielli, L. J. Prins. Chemically Fueled Self-Assembly in Biology and Chemistry, *Angew. Chem. Int. Ed.* **2021**, 2–26.

[3] S. Corrà, M. T. Bakić, J. Groppi, M. Baroncini, S. Silvi, E. Penocchio, M. Esposito, A. Credi. Kinetic and energetic insights into the dissipative non-equilibrium operation of an autonomous light-powered supramolecular pump, *Nat. Nanotechnol.* **2022**, *17*, 746–751.

[4] L. Binks, S. Borsley, T. R. Gingrich, D. A. Leigh, E. Penocchio, B. M. W. Roberts. Chem, *Chem* **2023**, *9*, 2902–2917.

[5] T. Marchetti, L. Gabrielli, D. Frezzato, L. J. Prins. ATP Drives the Formation of a Catalytic Hydrazone using an Energy Ratchet Mechanism, *Angew. Chem. Int. Ed.* **2023**, e202307530.

[6] R. Rao, M. Esposito. Nonequilibrium thermodynamics of chemical reaction networks: Wisdom from stochastic thermodynamics, *Phys. Rev. X* **2016**, *6*, 1–23.

[7] S. Amano, M. Esposito, E. Kreidt, D. A. Leigh, E. Penocchio, B. M. W. Roberts. Information thermodynamics of a synthetic molecular motor, *Nat. Chem.* **2022**, *14*, 530–537.

[8] S. Di Noja, M. Garrido, L. Gualandi, G. Ragazzon. Control over Dethreading Kinetics Allows Evaluating the Entropy Stored in an Interlocked Molecular Machine Out-of-Equilibrium, *Chem. Eur. J.* **2023**, *29*, e202300295.

[9] C. Gao, A. Vargas Jentzsch, E. Moulin, N. Giuseppone. Light-Driven Molecular Whirligig, *J. Am. Chem. Soc.* **2022**, *144*, 9845–9852.

[10] E. Olivieri, J. M. Gallagher, A. Betts, T. W. Mrad, D. A. Leigh. Endergonic synthesis driven by chemical fuelling, *ChemRxiv* **2023**, DOI: 10.26434/chemrxiv-2023-6nqn3-v2.

[11] F. Tordini, A. Bencini, M. Bruschi, L. De Gioia, G. Zampella, P. Fantucci. Theoretical study of hydration of cyanamide and carbodiimide, *J. Phys. Chem. A* **2003**, *107*, 1188–1196.

[12] R. C. Cioc, M. Crockatt, J. C. van der Waal, P. C. A. Bruijnincx. The Interplay between Kinetics and Thermodynamics in Furan Diels–Alder Chemistry for Sustainable Chemicals Production, *Angew. Chem. Int. Ed.* **2022**, *61*, e20211472.

[13] T. T. Truong, H. T. Nguyen, M. N. Phan, L. T. T. Nguyen. Study of Diels-Alder reactions between furan and maleimide model compounds and the preparation of a healable thermo-reversible polyurethane, *J. Polym. Sci. Part A* **2018**, *56*, 1806–1814.

[14] J. Chen, P. H. L. Sit. *Chem. Phys.* **2015**, *457*, 87–97.

11. Appendix – Coordinates of computed structures

Maleic acid 2 minimized structure

C	0.424524	0.663322	0.985647
C	-0.606070	-0.162792	0.761378
H	0.504412	1.080955	1.984904
H	-1.289458	-0.363151	1.580871
C	1.561024	1.183551	0.134187
C	-0.953439	-0.868593	-0.489332
O	-0.354477	-0.830648	-1.551092
O	2.337997	1.948389	0.655116
O	1.686484	0.806678	-1.128539
H	0.975260	0.184453	-1.403024
O	-2.057008	-1.603713	-0.339319
H	-2.229249	-2.038452	-1.190798

Maleic anhydride 2' minimized structure

C	-0.134697	1.017170	-0.125541
C	-0.834264	-0.004686	-0.610219
H	-1.706972	-0.006856	-1.248691
H	-0.277609	2.080685	-0.258437
C	-0.207361	-1.265823	-0.117496
C	0.975936	0.462319	0.702106
O	0.875758	-0.915555	0.666475
O	-0.520229	-2.399351	-0.317649
O	1.829438	1.032095	1.309452

1a minimized structure

O	-0.512663	1.260658	1.591973
C	0.385753	0.829853	0.661204

C	0.497850	1.744831	-0.335705
C	-0.385878	2.819385	0.002278
C	-0.966603	2.468839	1.176965
H	-0.560471	3.728569	-0.554866
H	-1.685930	2.948061	1.822853
H	1.120229	1.642409	-1.212271
C	0.975488	-0.524401	0.872246
H	1.937734	-0.577006	0.362252
H	1.139796	-0.702126	1.938841
N	0.157464	-1.614097	0.351402
H	-0.749492	-1.711249	0.788284
C	0.194425	-1.844655	-1.012260
O	1.016319	-1.338144	-1.756401
N	-0.800751	-2.696900	-1.461476
H	-1.120497	-3.417027	-0.829274
H	-0.642773	-3.017001	-2.406044

***exo*-3a minimized structure**

C	-0.727517	1.010495	-0.026630
C	1.164296	0.868495	1.471802
C	0.023834	2.971440	0.849146
C	1.112405	2.005222	0.407204
C	-1.123149	2.348510	0.587326
C	-0.187177	0.149056	1.207602
H	1.180375	1.262719	2.492200
H	0.183051	3.912728	1.360395
H	2.081584	2.401547	0.113777
H	-0.872455	0.240107	2.050872
O	0.490987	1.336021	-0.681058

C	2.407250	0.013673	1.317053
C	-0.145422	-1.302738	0.799239
O	0.748955	-1.850451	0.196438
O	3.261622	0.156927	0.479037
O	2.496182	-0.884369	2.314535
H	3.279994	-1.424747	2.127461
O	-1.317865	-1.880633	1.092402
H	-1.471591	-2.596610	0.442853
H	-2.136107	2.647419	0.829029
C	-1.697286	0.375775	-1.026247
H	-2.447846	-0.233739	-0.519059
H	-2.213694	1.184022	-1.556795
N	-1.003225	-0.459206	-1.979616
H	-0.173154	-0.044867	-2.379043
C	-1.140700	-1.817758	-2.042529
O	-2.036327	-2.437634	-1.470419
N	-0.220437	-2.445476	-2.857380
H	0.713844	-2.058805	-2.871698
H	-0.230428	-3.447122	-2.727898

***endo*-3a minimized structure**

H	-1.984429	-1.686703	1.970365
C	-1.471721	-1.363501	1.066367
C	0.493023	-0.425708	0.037869
C	-1.611273	-1.012007	-1.166246
C	-0.939436	0.105762	-0.384448
C	-1.943599	-1.927102	-0.259458
C	0.083491	-1.466833	1.115810
H	1.043494	0.390234	0.510399

H	-2.334911	-2.922638	-0.410005
H	0.423218	-1.092299	2.086679
O	-1.619277	0.044778	0.867570
C	0.614455	-2.875556	0.991386
C	1.272110	-0.929857	-1.169205
O	-0.060216	-3.864969	0.837251
O	1.307593	-2.088930	-1.503528
O	1.940852	-2.915544	1.198617
H	2.213749	-3.834572	1.049378
O	1.860483	0.019003	-1.898620
H	1.773611	0.913680	-1.493105
H	-1.662032	-1.078106	-2.245658
C	-1.017747	1.503430	-0.966725
H	-2.060781	1.714957	-1.219627
H	-0.430289	1.560724	-1.885385
N	-0.552740	2.533050	-0.059237
H	-1.085376	2.635731	0.792914
C	0.750449	2.939656	-0.045569
O	1.606077	2.518556	-0.826852
N	1.062794	3.857401	0.925790
H	0.346061	4.486282	1.256012
H	1.982369	4.261080	0.827260

exo-3a' minimized structure

H	-0.972966	3.033301	-1.588521
C	-0.449912	2.166585	-1.189173
C	-0.327389	-0.217749	-0.989180
C	1.240761	1.358001	0.085081
C	-0.103832	0.672894	0.301228

C	1.020263	2.296142	-0.832927
C	-0.583567	0.860061	-2.048754
H	1.723237	2.967176	-1.309894
O	-1.029177	1.727477	0.034297
H	0.070555	0.852244	-2.921673
H	0.504376	-0.898067	-1.173545
C	-2.018693	0.633219	-2.472894
C	-1.626561	-0.992852	-0.935176
O	-2.546654	-0.449070	-1.786858
O	-2.671702	1.247805	-3.257429
O	-1.893776	-1.950913	-0.263123
H	2.152362	1.046479	0.578344
C	-0.384431	0.015850	1.647795
H	-1.467525	-0.034650	1.786648
H	0.034127	0.634791	2.443650
N	0.148044	-1.322549	1.763915
H	-0.379693	-2.040941	1.283168
C	1.477451	-1.531241	2.031657
O	2.266466	-0.630428	2.281953
N	1.864770	-2.858028	1.967837
H	1.178545	-3.565182	2.190050
H	2.774920	-3.020358	2.373523

***endo*-3a' minimized structure**

H	0.558262	3.195062	-1.575613
C	0.434676	2.204125	-1.145688
C	-1.043489	0.369310	-0.709702
C	1.348881	0.504767	0.041195
C	-0.073701	0.871847	0.446009

C	1.669631	1.345230	-0.940905
C	-0.654548	1.307800	-1.850282
H	-2.081565	0.460425	-0.381986
H	2.566150	1.378143	-1.545993
H	-1.471917	1.920473	-2.233248
O	-0.118331	2.268804	0.163059
C	-0.131678	0.388208	-2.929843
C	-0.789917	-1.016135	-1.254745
O	-0.243586	-0.931966	-2.506437
O	0.328711	0.655269	-3.995325
O	-1.004586	-2.078529	-0.739530
H	1.922639	-0.302232	0.478367
C	-0.523214	0.535852	1.857900
H	-1.466849	1.049640	2.067474
H	0.227313	0.876879	2.572642
N	-0.695170	-0.888720	2.034604
H	-1.434305	-1.324886	1.501647
C	0.400520	-1.682149	2.319344
O	1.438930	-1.235213	2.783080
N	0.194634	-3.025843	2.085936
H	-0.402144	-3.279340	1.309461
H	1.044656	-3.566821	2.148581

1d minimized structure

O	-0.448749	3.051629	0.771732
C	-0.846792	1.770387	1.007966
C	-0.130132	1.243006	2.036320
C	0.768606	2.268222	2.467407
C	0.526191	3.335865	1.664328

H	1.495423	2.214667	3.265146
H	0.938578	4.331260	1.607423
H	-0.228460	0.237054	2.416623
C	-1.888177	1.212084	0.106123
H	-2.546293	0.541623	0.660586
H	-2.468163	2.019522	-0.342729
O	-1.324685	0.501163	-1.007117
C	-0.926393	-0.763915	-0.732049
O	-1.095877	-1.327113	0.332290
N	-0.341205	-1.317087	-1.825850
H	-0.110327	-0.688699	-2.579988
C	0.352278	-2.589076	-1.731451
H	0.361363	-3.042714	-2.727728
H	-0.244031	-3.232361	-1.080438
C	1.771700	-2.463084	-1.182868
H	2.250517	-3.446559	-1.131566
H	1.747335	-2.038477	-0.175016
H	2.387293	-1.817398	-1.819146

***exo*-3d minimized structure**

C	0.084651	0.406348	-1.416776
C	2.323444	0.517323	-0.505172
C	1.100929	2.441185	-1.529309
C	1.999277	1.266720	-1.841607
C	-0.091045	1.911829	-1.269393
C	0.897942	-0.019018	-0.124505
H	2.703132	1.180104	0.271939
H	1.421116	3.472255	-1.455971
H	2.854239	1.437206	-2.494631

H	0.522736	0.511930	0.750610
O	1.091662	0.328993	-2.434915
C	3.410895	-0.540476	-0.723948
C	0.811890	-1.485090	0.242857
O	0.552590	-1.894616	1.350360
O	4.286920	-0.733231	0.078227
O	3.372175	-1.198513	-1.890551
H	2.518538	-1.021176	-2.329241
O	1.046149	-2.302542	-0.795397
H	0.990272	-3.212194	-0.461328
H	-1.004510	2.372389	-0.919031
C	-1.131300	-0.435598	-1.799058
H	-1.890551	0.184050	-2.280452
H	-0.812663	-1.228605	-2.475194
O	-1.680654	-1.107535	-0.673192
C	-2.316093	-0.319439	0.238462
O	-2.648272	0.829934	0.022390
N	-2.513874	-1.010764	1.385121
H	-1.928283	-1.828040	1.496068
C	-2.897869	-0.301114	2.596902
H	-3.298990	-1.042297	3.294033
H	-3.710220	0.379945	2.334155
C	-1.734239	0.463511	3.224041
H	-0.890900	-0.206483	3.419683
H	-2.039956	0.926966	4.167436
H	-1.399139	1.256044	2.547386

***endo*-3d minimized structure**

H	-3.580585	-1.061142	-0.695339

C	-2.555068	-0.921353	-1.031275
C	-0.203110	-0.870937	-0.522610
C	-1.189452	-0.357559	-2.748787
C	-0.842203	0.283126	-1.410452
C	-2.256545	-1.114113	-2.505006
C	-1.480609	-1.695620	-0.208910
H	0.191454	-0.437586	0.398594
H	-2.741706	-1.830664	-3.151544
H	-1.707593	-1.565437	0.853833
O	-2.117603	0.417643	-0.801657
C	-1.461463	-3.183592	-0.465589
C	0.915156	-1.590778	-1.267108
O	-2.179952	-3.764746	-1.242589
O	0.760327	-2.628692	-1.861947
O	-0.626172	-3.814421	0.376543
H	-0.634594	-4.750184	0.120506
O	2.087247	-0.953383	-1.286993
H	2.073647	-0.137995	-0.737732
H	-0.584064	-0.309473	-3.645119
C	-0.120762	1.609228	-1.482254
H	-0.704404	2.293745	-2.099531
H	0.873443	1.480397	-1.917525
O	-0.027190	2.251980	-0.210202
C	1.081727	2.057106	0.519222
O	2.016925	1.330956	0.197672
N	1.044964	2.778222	1.656170
H	0.185891	3.267420	1.857140
C	2.032118	2.588620	2.708801
H	2.070218	3.513460	3.291056

H	3.002584	2.462747	2.224093
C	1.724347	1.390601	3.602707
H	0.744365	1.496662	4.079479
H	2.479545	1.299051	4.389670
H	1.729116	0.466713	3.016681

***exo*-3d' minimized structure**

C	-0.317234	-1.991324	-2.244194
C	-0.826330	-2.534795	0.033030
C	-1.180633	-0.316542	-0.985656
C	-0.118312	-1.158375	-0.285572
C	-1.293211	-0.828799	-2.208197
C	-0.961604	-3.126802	-1.375322
H	0.081719	-2.316386	-3.203255
H	-1.747224	-2.408425	0.603105
H	-1.740169	0.473882	-0.503458
H	-1.989972	-0.568462	-2.994596
C	-0.078985	-4.357097	-1.352263
O	0.487102	-4.507060	-0.103511
C	0.093652	-3.503016	0.750391
O	0.150921	-5.119163	-2.240427
O	0.471586	-3.461838	1.882832
O	0.718177	-1.554990	-1.372260
C	0.661154	-0.538094	0.852370
H	0.016579	-0.441665	1.728727
H	1.519762	-1.162284	1.100950
O	1.191411	0.729908	0.489451
C	0.425169	1.808091	0.789076
N	1.047725	2.942531	0.397458

H	1.992830	2.860143	0.057109
C	0.481206	4.250415	0.676435
H	0.876306	4.946976	-0.069239
H	-0.597518	4.175968	0.517367
O	-0.669397	1.751632	1.319517
C	0.768105	4.744419	2.091604
H	0.335790	4.053920	2.821256
H	1.844550	4.817616	2.276864
H	0.325833	5.734051	2.246982
H	-1.968989	-3.394436	-1.696575

endo-3d' minimized structure

C	1.573862	2.537802	-1.627760
C	0.965623	0.380687	-0.780496
C	-0.515082	2.379405	-0.756810
C	0.568776	1.672223	0.045491
C	0.112584	2.917963	-1.801379
C	1.719833	1.003135	-1.956246
H	2.330067	3.177789	-2.075860
H	1.543377	-0.302437	-0.155381
H	-1.574909	2.330812	-0.543207
H	-0.307176	3.427259	-2.659368
H	2.773466	0.730053	-2.020233
C	0.974322	0.536102	-3.183712
O	-0.112709	-0.225594	-2.798805
C	-0.191390	-0.347862	-1.426666
O	1.204758	0.758016	-4.333255
O	-1.089389	-0.946528	-0.913785
O	1.709437	2.485429	-0.213736

C	0.376673	1.492519	1.536091
H	0.114812	2.450547	1.989967
H	1.295009	1.107755	1.984300
O	-0.705891	0.610013	1.787810
C	-0.371662	-0.687499	2.044351
N	-1.486253	-1.414019	2.282171
H	-2.352986	-1.000035	1.971935
O	0.772037	-1.098988	2.088950
C	-1.412455	-2.863038	2.391586
H	-2.308139	-3.192386	2.927341
H	-0.550415	-3.094150	3.022012
C	-1.289930	-3.572698	1.046855
H	-0.370713	-3.265534	0.542151
H	-2.131608	-3.328918	0.391960
H	-1.263930	-4.657822	1.193728

1f minimized structure

O	1.400167	0.743669	3.642936
C	0.663807	1.605185	2.907311
C	-0.161528	0.938934	2.058945
C	0.091469	-0.457513	2.290887
C	1.042725	-0.507670	3.253579
H	0.830980	2.654451	3.097526
H	-0.385037	-1.284081	1.784674
H	1.551305	-1.314916	3.757247
C	-1.122056	1.551932	1.093542
H	-1.239271	2.618445	1.296008
H	-2.097166	1.063151	1.146998
O	-0.647919	1.494172	-0.260927

C	-0.873772	0.329305	-0.908935
O	-1.491015	-0.612449	-0.448209
N	-0.337311	0.376633	-2.155140
H	0.279154	1.148354	-2.356019
C	-0.292963	-0.806976	-2.993671
H	-1.251828	-1.318554	-2.882147
H	-0.213041	-0.473355	-4.032965
C	0.849660	-1.755883	-2.640358
H	0.842821	-2.627570	-3.303503
H	0.739044	-2.105105	-1.609577
H	1.821776	-1.260158	-2.738201

exo-3f minimized structure

C	0.389448	0.355354	-1.694292
C	2.589594	-0.269421	-0.940764
C	1.628996	2.044874	-0.830495
C	2.391369	1.083325	-1.716360
C	0.372925	1.597260	-0.813217
C	1.098157	-0.749077	-0.862705
H	3.032496	-0.134126	0.044724
H	-0.526788	0.048458	-2.190068
H	2.069889	2.856687	-0.265306
H	3.277790	1.457480	-2.227506
H	0.744938	-0.755903	0.170340
O	1.390522	0.689402	-2.661758
C	-0.781473	2.027752	0.035442
H	-0.727960	1.552890	1.020054
H	-0.784013	3.111872	0.162600
C	3.520586	-1.187523	-1.729278

C	0.827166	-2.128932	-1.421588
O	0.139379	-2.374073	-2.384831
O	4.507994	-1.686736	-1.259085
O	3.177610	-1.383861	-3.014249
H	2.393981	-0.839458	-3.231577
O	1.436925	-3.075271	-0.696571
H	1.252880	-3.926563	-1.125594
O	-2.036643	1.710708	-0.563861
C	-2.438761	0.424734	-0.390065
O	-1.819753	-0.398436	0.259765
N	-3.607810	0.203792	-1.032211
H	-3.934578	0.935740	-1.644981
C	-4.122756	-1.147100	-1.200722
H	-5.205809	-1.070898	-1.336239
H	-3.944513	-1.677264	-0.262533
C	-3.474651	-1.891407	-2.364940
H	-3.646671	-1.367582	-3.311643
H	-3.896210	-2.898006	-2.454671
H	-2.395276	-1.986649	-2.212867

***endo*-3f minimized structure**

H	-2.274000	2.091182	2.197515
C	-1.342586	1.858901	1.689900
C	0.928496	1.096517	1.819959
C	-0.201141	1.830598	-0.277218
C	0.569752	2.357460	0.935474
C	-1.404110	1.518654	0.212910
C	-0.489318	0.735858	2.373392
H	1.566449	1.438622	2.641531

H	1.403276	3.033900	0.758357
H	-2.227353	1.015653	-0.277452
H	-0.479969	0.936296	3.450623
O	-0.440257	2.959083	1.714119
C	-1.227581	-0.605069	2.255294
C	1.739884	0.120510	1.008211
O	-2.436634	-0.595120	2.233716
O	1.572770	-1.085203	0.930697
O	-0.549540	-1.744950	2.315191
H	0.368142	-1.606334	1.988670
O	2.688085	0.747090	0.324990
H	2.934024	0.180232	-0.444615
C	0.354858	1.598444	-1.652005
H	-0.138495	2.250326	-2.377528
H	1.429390	1.781273	-1.690294
O	0.085371	0.258830	-2.091964
C	1.114823	-0.604333	-2.192086
O	2.297912	-0.296625	-2.080713
N	0.686867	-1.851250	-2.473147
H	1.422366	-2.540694	-2.439266
C	-0.698500	-2.302107	-2.374575
H	-0.745977	-3.272637	-2.876574
H	-1.321689	-1.612536	-2.948922
C	-1.198975	-2.406772	-0.937505
H	-1.187301	-1.425404	-0.458206
H	-0.572459	-3.078479	-0.344146
H	-2.226583	-2.781914	-0.914332

***exo*-3f' minimized structure**

C	-0.471313	-1.186778	-2.153934
C	-1.918017	0.215223	-0.874583
C	-0.748891	-1.757222	0.023418
C	-2.014499	-1.343004	-0.702614
C	0.225059	-1.649505	-0.880649
C	-0.801987	0.326492	-1.918807
H	-0.015395	-1.417140	-3.115931
H	-0.662172	-1.939664	1.087579
H	-2.974463	-1.712430	-0.345295
C	-1.484162	0.922782	-3.129192
O	-2.818435	1.150663	-2.855869
C	-3.141936	0.768285	-1.573533
O	-1.014260	1.171925	-4.197032
O	-4.252182	0.873278	-1.147051
O	-1.759215	-1.773497	-2.035295
C	1.707264	-1.716914	-0.710684
H	2.198034	-1.050899	-1.427793
H	2.081290	-2.732165	-0.867385
O	2.112553	-1.381868	0.614369
C	1.990503	-0.065186	0.921061
N	2.314073	0.150984	2.216381
H	2.475120	-0.658340	2.796863
O	1.652574	0.795521	0.129154
C	2.128318	1.457348	2.826811
H	2.491394	2.206660	2.117963
H	2.772289	1.499898	3.709929
C	0.675652	1.743403	3.196116
H	0.051548	1.719444	2.297927
H	0.294687	1.002459	3.908027

H	0.583851	2.735619	3.650259
H	0.073480	0.906797	-1.627551
H	-1.750762	0.737829	0.067339

***endo*-3f' minimized structure**

C	1.307792	-0.704936	-0.365338
C	0.537817	-2.873268	0.301423
C	1.988545	-1.396497	1.687632
C	2.026724	-2.457607	0.602860
C	1.537365	-0.295387	1.086123
C	0.029147	-1.635639	-0.442945
H	2.203856	-1.557109	2.736255
C	-1.209914	-1.228224	0.320938
O	-1.313883	-1.979448	1.471139
C	-0.346848	-2.968357	1.523594
O	2.309136	-1.695383	-0.563466
C	1.264596	1.063548	1.644431
H	1.294893	1.050405	2.735611
H	1.997555	1.782137	1.264056
O	-0.046108	1.499122	1.290155
C	-0.142931	2.209872	0.131584
N	-1.437797	2.504124	-0.124930
H	-2.106794	1.922446	0.360747
O	0.814165	2.530857	-0.548572
C	-1.813916	3.002613	-1.439527
H	-2.824041	3.411726	-1.350547
H	-1.143637	3.831142	-1.680464
C	-1.752352	1.935420	-2.531154
H	-2.379829	1.077354	-2.272822

H	-2.092564	2.345286	-3.487758
H	-0.721924	1.589582	-2.655070
H	2.722657	-3.284782	0.716052
H	-0.223463	-1.802685	-1.490260
H	1.356861	0.078101	-1.117512
O	-0.285631	-3.729897	2.439431
O	-2.046445	-0.424372	0.031490
H	0.496967	-3.800145	-0.273156

1h minimized structure

O	-0.848986	-1.107741	1.475649
C	0.244044	-1.093235	0.671234
C	0.231758	-0.016346	-0.155726
C	-0.975529	0.693471	0.171395
C	-1.579065	-0.013498	1.157928
H	0.936617	-1.910657	0.803367
H	-1.333588	1.609265	-0.278008
H	-2.492080	0.120796	1.716971
C	1.252219	0.354753	-1.185922
H	2.070538	-0.370946	-1.209875
H	1.684363	1.340131	-0.979610
H	0.809709	0.394008	-2.187404

***exo*-3h minimized structure**

C	-1.039503	0.101067	-0.388832
C	1.326967	0.008383	0.072085
C	-0.075934	2.080706	0.129305
C	0.747159	1.192829	-0.777419
C	-1.203554	1.410325	0.370213

C	-0.008075	-0.743492	0.417143
H	1.854292	0.342166	0.964183
H	-1.931744	-0.436965	-0.702161
H	0.250488	3.026307	0.543785
H	1.459080	1.670613	-1.449624
H	-0.189960	-0.699360	1.494790
O	-0.262064	0.497748	-1.523904
C	-2.357952	1.718339	1.260904
H	-2.466829	0.952495	2.039413
H	-3.295762	1.731565	0.693465
H	-2.235577	2.687369	1.751404
C	2.320926	-0.799245	-0.760243
C	-0.040985	-2.204926	0.017572
O	-0.769252	-2.685015	-0.816675
O	3.440195	-1.042550	-0.395117
O	1.868487	-1.203711	-1.959224
H	0.968094	-0.849772	-2.107797
O	0.837997	-2.922313	0.731580
H	0.803505	-3.832563	0.395155

***endo*-3h minimized structure**

H	-2.462275	0.387402	1.213634
C	-1.526504	0.437032	0.657117
C	0.873690	0.732316	0.683279
C	-0.515407	0.416019	-1.375592
C	-0.011970	1.468373	-0.396930
C	-1.462226	-0.236381	-0.696397
C	-0.245108	-0.006330	1.489221
H	1.290367	1.503888	1.331361

H	0.451862	2.365623	-0.803300
H	-2.016833	-1.117822	-0.991153
H	-0.311700	0.487948	2.463826
O	-1.170248	1.774543	0.366426
C	-0.252100	-1.500471	1.700967
C	2.100694	0.117715	0.000684
O	0.157620	-2.329465	0.917461
O	3.038517	0.843469	-0.228494
O	-0.866426	-1.925119	2.813596
H	-1.141760	-1.178682	3.361993
O	2.077419	-1.135941	-0.433102
H	1.289298	-1.624092	-0.100439
C	0.059322	0.174523	-2.729345
H	1.114452	-0.112274	-2.658232
H	0.006507	1.082971	-3.340197
H	-0.477192	-0.625246	-3.246383

exo-3h' minimized structure

H	-1.304563	2.235750	-0.237522
C	-0.658493	1.362361	-0.172246
C	-0.459595	-1.002478	0.132529
C	1.461446	0.530788	-0.149486
C	0.516160	-0.043171	0.900074
C	0.715914	1.413752	-0.816770
C	-1.314465	0.012462	-0.638676
H	0.945533	-0.455967	1.812744
H	0.977148	1.987335	-1.697439
O	-0.351827	1.045285	1.181685
H	-1.351560	-0.095465	-1.722880

H	0.060388	-1.759906	-0.455773
C	-2.700917	-0.146105	-0.047326
C	-1.432902	-1.658825	1.089856
O	-2.688666	-1.114835	0.933470
O	-3.695722	0.450674	-0.326398
O	-1.212036	-2.508822	1.897660
C	2.850033	0.040262	-0.379547
H	2.848727	-1.030064	-0.622624
H	3.463861	0.161396	0.520481
H	3.331537	0.575571	-1.201813

endo-3h' minimized structure

H	-1.704774	2.222980	0.398911
C	-1.039112	1.362637	0.396025
C	-0.785186	-1.008303	0.624253
C	1.104759	0.605267	0.279350
C	0.232978	-0.043601	1.349961
C	0.295565	1.486574	-0.313669
C	-1.706081	0.005507	-0.057999
H	-1.277615	-1.659692	1.347284
H	0.728524	-0.473365	2.218318
H	0.490802	2.100860	-1.183630
H	-2.748989	-0.033734	0.258066
O	-0.650184	1.005452	1.718801
C	-1.589060	-0.308429	-1.531520
C	-0.209749	-1.822981	-0.512101
O	-0.708830	-1.360951	-1.712070
O	-2.126524	0.217818	-2.457363
O	0.584802	-2.714406	-0.468685

C	2.502810	0.191032	-0.031951
H	2.543597	-0.872211	-0.294731
H	3.152998	0.332108	0.839227
H	2.909269	0.767437	-0.866478